estec

European Space Research
and Technology Centre
Keplerlaan 1
2201 AZ Noordwijk
The Netherlands
T +31 (0)71 565 6565
F +31 (0)71 565 6040
www.esa.int

DOCUMENT

LOFT Payload Definition Document

Prepared by	**LOFT Consortium**
Reference	**SRE-PA/2011.088/**
Issue	**2**
Revision	**4**
Date of Issue	**09/10/2012**
Status	**Update for instrument AO**
Document Type	**Payload Definition Document**
Distribution	**Open**

European Space Agency
Agence spatiale européenne

APPROVAL

Title: LOFT Payload Definition Document	
Issue 2	**Revision** 4
Author: LOFT Consortium	**09/10/2012**
Approved by	**Date**
A.D. Short, M. Ayre (Editors)	09/10/2012

CHANGE LOG

Reason for change	Issue	Revision	Date
PDD provided to ESA by LST	Draft (0)	0.5	14 August 2011
PDD issued by ESA as part of LOFT ITT	1	1.0	12 October 2011
PDD issued by ESA at time of industry KO	1	1.2	7 February 2012
PDD updated following MTR	2	2.1	29 June 2012
Revision to PDD updated following MTR	2	2.2	04 July 2012
Revision in preparation for instrument AO	2	3	19/09/2012
Revision to update LAD mass budget	2	4	09/10/2012

CHANGE RECORD

Issue 2	**Revision** 4		
Reason for change	**Date**	**Pages**	**Paragraph(s)**
Editorial changes following ESA review	12/10/11	throughout	throughout
Minor corrections and typos	07/02/12	throughout	throughout
Complete revision by consortium following MTR	29/06/12	throughout	throughout
Revision to PDD updated following MTR	04/07/2012	throughout	throughout
Made AD2 (technical note on response stability transformation into pointing stability an applicable document. Changed table 2-1 to reflect latest information from payload consortium (APE applies to instrument boresights, removed RPE requirement as now covered by response stability). Table 2-2 LAD requirements updated to reflect latest information from payload consortium (changes to energy range, resolution, FoV, background knowledge, redundancy.	19/09/2012		

Table 2-3 WFM requirements updated to reflect latest information from payload consortium. Changes to energy range, resolution, redundancy. Changes made throughout to remove TBCs where appropriate. Changes to text on collimator design. Removed section reporting thermal modelling results from the CDF (outdated and not really relevant). TBD number of temperature sensors as part of the LAD module added. Removed figure 3-32 (was consortium-specific, should not make any reference to consortium structure in PDD). Elaborated on Orbital Phases definition to include night-time operations in eclipse when the solar illumination constraint is removed. Placeholder inserted to account for degraded energy resolution temperature requirements. Removed bold-face requirements. Corrected Table 3-13 caption. Updated Table4-2, instrument performance specification. Slight changes to WFM instrument architecture section 4.2.3.1 Changed LAD operating temperatures information to reflect latest discussions with the PI – VERY IMPORTANT. **V2.4 changes** Updated LAD mass budget to account for tripling of collimator thickness. Also provide predicted LAD mass budget if the preferred alternative collimator technology (Tantalum) is chosen. Clarified WFM camera boresight orientations and rotations around boresight.			

Removed 5 degree oversizing of sunshade (sunshade must function in nominal pointing conditions, where APE is of order 1 arcminute, so 5 degrees is much too large).			

Table of contents:

1 INTRODUCTION

1.1 Scope

This Payload Definition Document describes the consolidated instrument designs of the Large Area Detector (LAD) and the Wide Field Monitor (WFM) proposed for LOFT. The current issue (2.0) describes the status of the instruments at the time of the Mid-Term Review (MTR) of the LOFT mission study phase.

1.2 Applicable Documents

[AD 1] LOFT Science Requirements Document (SciRD), SRE-SA/LOFT/2011-001, Issue 1, Rev.4, 29/06/2012.

[AD 2] LOFT_LAD_RespStab_20120322 “pointing stability”.

1.3 Reference Documents

1.3.1 LAD Section Reference Documents

[RD 1] LOFTM3 Proposal, 03/12/2010.

[RD 2] LOFT_WFM_TB_20110728, “LOFT Wide Field Monitor Thermal Blanket”, By J. Alvarez et al., 28 July 201.

[RD 3] AMICSA2010 proceeding paper: “STARX32: A Complete On-Chip X-Ray Spectroscopy Readout System with Imaging Capability”, by P. Bastia et al.

[RD 4] LOFT_SysN_NIEL_20120508 “Radiation damage of the LOFT SDDs and its effects on the energy resolution”, by E. Del Monte et al., 08/05/2012.

[RD 5] LOFT_LAD_TMT_20110809 “LOFT Deployed Array Optical Alignment Thermal and Mechanical Tolerances”, by B. Winter, 09/08/2011 .

[RD 6] LOFT-WFM_TechN_20120518 “LOFT WFM technical note”.

[RD 7] LOFT_WFM_Simul_20110815, “Preliminary Wide Field Monitor Simulations”, by J.J.M. in ‘t Zand, Ed.0, Rev. 0.1, 05/08/2011.

[RD 8] LOFT-WFM_MechDsg_20110729, “LOFT Wide Field Monitor Mechanical Design”, by J. L. Gálvez et al., Issue 1.0, 29/07/2011.

[RD 9] K40_bkg, “LAD background due to 40K activity in the collimators”, by Riccardo Campana, 14/11/2011.

[RD 10] LOFT_CDF_external_final_presentation, “LOFT external final presentation of the CDF study”, by C. Corral Van Damme, 7/10/2011.

[RD 11] LOFT_Additional_Thermal_Cases, “LOFT additional thermal cases”, by C. Corral Van Damme, 17/1/2012.

[RD 12] MSSL-LOFT-AN-11001 “LOFT LAD Harness & PSU Evaluation Analysis”, M,R, Hailey draft C 17apr2012.

[RD 13] Soeren Brant presentation 29nov2011.

[RD 14] LOFT_LAD_DDV_20120518 “LOFT Large Area Detector Design, Development and Verification plan”.

[RD 15] LOFT_SysN_SDD_TDP_20120516 “Design Development and Validation report LOFT-LAD and WFM Silicon Drift Detectors: current status and development plan".

[RD 16] LOFT_SysN_ASIC_TDP_20120502 "LOFT-LAD ASIC: Development plan’.

[RD 17] LOFT_SysN_FEE_TDP_AIV_20120511 “LOFT System Notes LOFT-LAD FEE development and AIV plan’.

[RD 18] LOFT-LAD_RespStab-20120322 “LOFT Large Area Detector Response Stability”.

[RD 19] Calibration accuracy of the deadtime, M. vd Klis.

1.4 WFM Section Reference Documents

[RD 20] LOFTM3 Proposal, 03/12/2010.

[RD 21] LOFT_WFM_Thermal Blanket, “LOFT Wide Field Monitor Thermal Blanket”, by J. Alvarez, M. Hernanz, 10/10/2011.

[RD 22] AMICSA2010 proceeding paper: “STARX32: A Complete On-Chip X-Ray Spectroscopy Readout System with Imaging Capability”, by P. Bastia et al.

[RD 23] LOFT_SysN_NIEL_20110804 “Radiation damage of the LOFT SDDs and its effects on the energy resolution”, by E. Del Monte et al., 08/05/2012.

[RD 24] LOFT_WFM_LBAS_20120515, “LOFT Wide Field Monitor LOFT Burst Alert System”, by S. Brandt, 2012-05-15 issue 2.0.

[RD 25] LOFT_WFM_Redundancy_20120515, “LOFT Wide Field Monitor Redundancy”, by S. Brandt, 2012-05-16.

[RD 26] LOFT_WFM_DTC_20120516, “LOFT Wide Field Monitor Data modes”, compression and telemetry, by S. Brandt, 2012-05-16.

[RD 27] LOFT-WFM-MechDsg-20110729, “LOFT Wide Field Monitor Mechanical Design”, by J. L. Gálvez et al., 29/07/2011.

[RD 28] LOFT_WFM_E2E-20120516, “LOFT Wide Field Monitor End-to-end model”, by I.Donnarumma, et al. 2012-05-16.

[RD 29] LOFT_CDF external final presentation, “LOFT external final presentation of the CDF study”, by C. Corral Van Damme, 7/10/2011.

[RD 30] LOFT_Additional_Thermal_Cases, “LOFT additional thermal cases”, by C. Corral Van Damme, 17/1/2012.

[RD 31] LOFT_LAD_TechN_20120203, “LOFT LAD Instrument technical note”, by Tom Kennedy, 03/02/2012.

[RD 32] LOFT_WFM_CAL_20120515, "LOFT Wide Field Monitor Calibration", by C.Budtz-Jørgensen, Y. Evangelista, R.Campana, I.Donnarumma, 2012-05-12.

[RD 33] LOFT_WFM_VHF_20120516, "LOFT Wide Field Monitor VHF ground segment description", by D. Götz, 2012-06-16 issue 2.0.

[RD 34] LOFT_WFM_Simul_20120515, "LOFT Wide Field Monitor Preliminary Simulations", by J. in't Zand, 2012-05-15 issue 3.0.

[RD 35] LOFT_LAD_TMest_20120509, "LOFT Large Area Detector Telemetry estimate", by J. Wilms, C. Tenzer, 2012-05-09.

[RD 36] LOFT_WFM_Be_20120504, "LOFT Wide Field Monitor Be shielding against orbital debris" by E. Del Monte, 2012-05-04.

[RD 37] LOFT_SysN_WFMsel_20120430, "LOFT System Notes WFM selection procedure and results" by J. W. den Herder, C. Budtz-Jørgensen, 2012-04-30.

[RD 38] LOFT_SysN_RadDam_20120430, "LOFT System Notes Radiation Damage measurements of the ALICE-type SDD, by E. Del Monte, P. Azzarello,A. Rashevsky, N. Zampa, G. Zampa, 2012-04-30.

[RD 39] LOFT_WFM_RelCal_20120507, "LOFT Wide Field Monitor Relative calibrations requirements" by S. Brandt, WFM team, 2012-05-07.

[RD 40] LOFT_WFM_ImgSysRot_20120425, "LOFT Wide Field Monitor Images Systematic and Rotations" by S. Brandt, 2012-04-25.

[RD 41] LOFT_LAD_BkgMdl_20111130, "LOFT Large Area Detector Background Models" by R. Campana, 2011-11-30.

[RD 42] LOFT_LAD_SupCLL_20120312, "LOFT Large Area Detector A LAD design with MCP + Super-Collimator" by S. Brandt, R. Campana, 2012-03-12 issue 2.0.

[RD 43] LOFT_CDF_v9.3, "CDF Study Report LOFT Large Observatory for X-Ray Timing" by N. Rando (ESA), 2011-10.

[RD 44] LOFT_WFM_MaOpFr_20110922, “LOFT Wide Field Monitor Mask Open Fraction”, by S. Brandt, 2011-09-22 issue 1.0.

1.5 Acronyms

8PSK	Eight Phase-Shift Keying
A&A	Astronomy and Astrophysics Journal
A/D	Analogue to Digital
ABT	Absolute Time Events
AD	Applicable Document
ADC	Analogue to Digital Converter
AGILE	Astro-rivelatore Gamma a Immagini Leggero
AGN	Active Galactic Nuclei
AIV	Assembly Integration and Verification
ALICE	A Large Ion Collider Experiment (at CERN)
AMA	Pointing knowledge for each axis averaged over full orbit
AO	Atomic Oxygen
AOCS	Attitude and Orbit Control system
APD	Absolute Pointing Drift
APE	Absolute Pointing Error
ASI	Agenzia Spaziale Italiana
ASIC	Application Specific Integrated Circuit
BAT	Burst Alert Telescope (on Swift satellite)
BB	Breadboard
BEE	Back End Electronics
BeppoSAX	Satellite per Astronomia X (Beppo Occhialini)
BOL	Beginning Of Life
CBE	Current Best Estimate
CERN	European Centre for Nuclear Research
CFRP	Carbon Fibre Reinforced Plastic
CMN	Common Mode Noise
CN	Common Mode Noise
CONF	Configuration
CRFP	Carbon Fibre Reinforced Plastic
CSIC	Consejo Superior de Investigaciones Científicas
CTE	Coefficient of Thermal Expansion
CTS	Counts
CVS	Concurrent Version Software
CXB	Cosmic diffuse X-ray Background
DC/DC	Direct Current to Direct Current (conversion)
DH	Data Handling
DHU	Data Handling Unit

DM	Development Model
DMM	Design Maturity Margin
DP	Detector Panel
DSSD	Double Sided Strip Detector
DTU	Technical University of Denmark
ECSS	European Cooperation for Space Standardization
EDAC	Error Detection And Correction
EDS	Event Data System
EEPROM	Electrically Erasable Programmable Read Only Memory
EGSE	Electronic Ground Support Equipment
EM	Engineering Model
EMC	Electro Magnetic Compatibility
ENC	Equivalent Noise Charge
EOL	End-Of-Life
EOS	Equation Of State
EPS	Electric Power System
ESD	Electrostatic Discharge
eV	Electron Volt
FB CTRL	Feedback Control
FEE	Front-End Electronics
FIFO	First-in First-out buffer
FM	Flight Model
FOV	Field of View
FPGA	Field Programmable Gate Array
FS	Flight Spare
FWHM	Full Width at Half Maximum
FWZR	Full Width at Zero Response
GEANT	CERN detector development tool
GNU	Gnu's Not Unix
GPS	Global Positioning System
GRB	Gamma-Ray Burst
GSE	Ground Support Equipment
GSO	Global Seismic Oscillations
HETE	High Energy Transient Experiment
HK	Housekeeping
HRC	High Resolution Imager
HTRS	High Time Resolution Spectrometer (on IXO/Athena)
HTRS	Heaters
HV	High Voltage

HVU	High Voltage Unit
ID	Identification number
IEEC	Institute of Space Sciences (under CSIC)
INFN	Instituto Nazionale di Fisica Nucleare
INTEGRAL	International Gamma Ray Laboratory
IR	Infrared light
IROS	Iterative Removal Of Sources
ITS	Inner Tracking System
IXO	International X-ray Observatory (defunct – now ESA 'Athena')
LAD	Large Area Detector
LEO	Low Earth Orbit
LHC	Large Hadron Collider (at CERN)
LIGO	Laser Interferometer Gravitational-Wave Observatory
LOFT	Large Observatory For x-ray Timing
LSST	LOFT Science Study Team
LV	Low Voltage
LVDS	Low Voltage Differential Signal
M3	ESAs 3rd call for ideas for medium sized mission
MBEE	Module Back-End Electronics
MCP	Micro Channel Plate
MGSE	Mechanical Ground Support Equipment
MIP	Minimum Ionizing Particles
MIRAS	Microwave Infrared Radiometer with Aperture Synthesis
MIXS	Mercury Imaging X-ray Spectrometer (BepiColombo instrument)
MLI	Multi Layer Insulation
MOC	Mission Operations Centre
M-R	Neutron star Mass/Radius relation
MSSL	Mullard Space Science Laboratory
MTR	Mid-Term Review
MV	Medium Voltage
N/A	Not applicable
NIEL	Non-Ionizing Energy Loss
NIM	Nuclear Instruments and Methods
NIR	Near InfraRed
NOP	Non Operational
OAR	Open Area Ratio
OBDH	On-Board Data Handling system
OGSE	Optics Ground Support Equipment
OP	Output

OTF	On-Target Flag
PA	Product Assurance
PBEE	Panel Back-End Electronics
PCA	Proportional Counter Array (on RXTE)
PCB	Printed Circuit Board
PDHU	Payload Data Handling Unit
PET	Positron-Electron Tomography
PLM	Payload Module
PPS	Pulse per Second
PROM	Programmable Read Only Memory
PSU	Power Supply Unit
PWR	Power
QE	Quantum Efficiency
QM	Qualification Model
QPO	Quasi Periodic Oscillation
QPSK	Quadrature Phase-Shift Keying
R&D	Research and Development
RCS	Reaction Control System
RMS	Root Mean Square
ROM	Read Only Memory
ROSAT	Röntgen Satellite (German X-ray satellite)
RPE	Relative Pointing Error
RS	Reed-Solomon encoding
RTEMS	Real Time Executive for Multiprocessor Systems
RTN	Return
RXTE	Rossi X-ray Timing Explorer
S/C	Spacecraft
SAA	South Atlantic Anomaly
SAA	Solar Aspect Angle
SAGA	South Atlantic Geomagnetic Anomaly
SAR	Synthetic Aperture Radar
SDD	Silicon Drift Detector
SiC	Silicon Carbide
SMOS	Soil Moisture and Ocean Salinity (ESA satellite)
SOC	Scientific Operations Center
SPIE	International Society for Optical Engineering
SRON	Space Research Organization Nederland
STM	Structural/Thermal Model
SVN (svn)	Subversion (version control system)

TAS-I	Thales Alenia Space - Italy
TBC	To Be Confirmed
TBD	To Be Defined
TBW	To Be Written
TC	Telecommand
TCS	Thermal Control System
TM	Telemetry
ToA	Time Of arrival
TRL	Technology Readiness Level
TT&C	Telemetry and Telecommunication system
UCL	University College London
UT	Universal Time
UV	Ultra Violet light
V	Visible light
VIRGO	French Italian Gravitational-Wave Observatory
Vis	Visible light
WFM	Wide Field Monitor
XMM	X-ray Multi Mirror Mission

2 LOFT PAYLOAD REQUIREMENTS

Item	Requirement	goal
Net observing time core science	20.2 Msec	26.2 Msec
Additional open observing time observatory science	20 Msec	26 Msec
Calibration time	5%	2%
minimum science observing times	1 minute (1 source during 2 weeks per year) 10 minutes (10 sources during 2 weeks per year)	
Accessible sky fraction (daytime) within Nominal Field of Regard	>35 %	50%
Accessible sky fraction (daytime) within Degraded Field of Regard	>50 %	75%
Galactic centre visibility	>35%	>65%
Mission duration	4 year	5 year
APE (satellite, 3 axis +)	1 arcmin	0.5 arcmin
Pointing knowledge for each axis over the full orbit (AMA, 3σ, 10 Hz)	<20 arcsec	<5 arcsec
ToO (following alert of SOC)	<12 hours for triggers during SOC working hours, <24 hrs otherwise	< 8 hours for triggers during SOC working hours
Orbit	LEO, <600 km, < 5 deg	LEO, 550 km, <2 deg
Slews per orbit (average)	0.5	0.5
Slews per orbit (at least)	2	2
Instrument data rate (typical)[1)]	LAD: 300 kbps (~ 150 mCrab) + WFM 100 kbps	
Instrument data rate (sustained)	LAD: 1000 kbps (~500 mCrab) + WFM 100 kbps	LAD: ~1 Crab
data transfer per orbit	6.7 Gbit/orbit	14 Gbit/orbit

Table 2-1: Overview of LOFT system requirements

1. The WFM should always be less than 10% of the total bandwidth. For a total of 6.68 Gbit/orbit this corresponds to 113 kbps (~100 minute orbit).

Item	Requirement	Goal
Effective area	4 m^2 @ 2 keV	5 m^2 @ 2 keV
	8 m^2 @ 5 keV	9.6m^2 @ 5 keV
	10 m^2 @ 8 keV	12 m^2 @ 8 keV
	1 m^2 @ 30 keV	1.2 m^2 @ 30 keV
Calibration accuracy area	15%	10%
Energy range	2 – 30keV nominal	1.5 – 30 keV nominal
	30-80 keV extended (for monitoring events outside LAD FoV)	30-80 keV extended
Energy resolution (FWHM, EoL)	260 eV @ 6 keV	200 eV @ 6 keV
	200 eV @ 6 keV (singles, 40%)	160 eV @ 6 keV (singles, 40%)
Energy resolution (degraded performance can be allowed in ~$^1/_3$ of cases TBC)	400 eV @ 6 keV	300 eV @ 6 keV
knowledge energy scale	10^{-2}	0.8 10^{-2}
Collimated FoV (FWHM)	0.9-1.1 degree	0.45-0.55 degree(*)
Transparency of collimator	<1% at 30 keV	0.5% at 30 keV
Response stability	<0.01 Hz: <2% per decade	1% per decade
(frequency-dependent, see relevant Tech Note)	0.01 -1 Hz: <0.2% per decade	0.05% per decade
	1-1200 Hz: <0.02% per octave	0.005% per octave
	>2000 Hz: Lower is better	Lower is better
	10-2000 Hz: <0.0002% nearly periodic	<0.00005% nearly periodic
Time resolution	10 µs	7 µs
Absolute time accuracy	1 µs	1 µs
Dead time	< 1% @ 1 Crab,	< 0.5% @ 1 Crab,
Calibration knowledge deadtime		Less than the statistical precision of power spectrum for 1 day at 15 Crab up to F_{Ny} = 10 kHz (see [RD 19])
Background	< 10 mCrab	< 5 mCrab
Background knowledge	1% at 5-10 keV	<0.25% (AGN reverberation mapping studies)
Max flux (continuous, rebinned in energy >30 keV)	> 500 mCrab	>750 mCrab
Max flux (continuous, re-binned)	15 Crab	30 Crab
On-board memory (transmitted over more orbits)	15 Crab, 300 minutes (full event info)	30 Crab, 300 minutes (full event info)
Redundancy	Loss of <25% of the area due to single point failure	<17%

(*)note that the smaller FoV, which is a design parameter, improves the background but can only be realized if the pointing goal is reached (as they are dependent on each other)

Table 2-2: Overview of LAD requirements

Item	Requirement	Goal
Location accuracy	1 arcmin	0.5 arcmin
Angular resolution	5 arcmin	3 arcmin
Sensitivity (5 σ)	1 Crab (1 s) 5 mCrab (50 ks)	0.2 Crab (1s) 2 mCrab (50 ks)
Calibration accuracy (sensitivity)	20 %	15 %
Field of view	1 pi steradian around the LAD pointing	1.5 pi steradian around LAD pointing including anti-solar direction
Energy range	2 – 50 keV primary 50-80 keV extended (for monitoring source contamination)	1.5 – 50 keV primary 50-80 keV extended
Energy resolution (FWHM)	500 eV @ 6 keV	300 eV @ 6 keV
Energy scale knowledge	4%	1%
Number of energy bands for compressed images	>=8	>=16
Time resolution	300 sec for normal data 10 μsec for event data	150 sec for normal data 5 μsec for event data
Absolute time calibration	1 μsec	1 μsec
duration for rate triggers	0.1 sec - 100 sec	1 msec - 100 sec
Rate meter data	16 msec	8 msec
Availability of 10 sigma transient event position Availability of 10 sigma Transient event time		< 1 minute (75% of cases) < 30 sec (7% of cases)
Availability of triggered WFM data	3 hours	1.5 hours
Onboard memory	5 min @ 100 Crab	10 min @ 100 Crab
Broadcast	<30 sec after the event for 75% of the events (TBC)	<20 sec after the event for 75% of the events (TBC) Also the position <2 min after the event (TBC)
Redundancy	No full loss of FoV due to single point failure	

Table 2-3: Overview of WFM requirements

3 THE LAD INSTRUMENT

3.1 Introduction

In the following, the baseline design of the LAD is described and the corresponding resources, in terms of mass, envelope, power and data rate are quantified. Such estimates play an important role in the context of the definition of the LOFT mission as they strongly influence the spacecraft requirements and corresponding resources. Under or over estimating the required resources would in fact lead to inaccurate choices at system level, thus significantly increasing the development risks and/or the cost at completion. A summary of the baseline instruments' characteristics is given in Table 3-1.

Instrument Characteristic	LAD
Detector type	Si Drift Detector
Mass [CBE, kg]	584(1,2)
Peak Power [CBE, W]	713 (average& peak)
Detector Operating T [°C]	<-32 (at 600km, 5 degrees inclination orbit; temperature requirement is relaxed at lower altitude/inclinations.)
Overall detector size	18 m^2
Energy range [keV]	2-80 (30-80 coarse energy binning)
Energy resolution [FWHM]	<260 eV @ 6 keV
Pixel size	0.97 mm x 35 mm
Field of View	60 x 60 $arcmin^2$
Angular Resolution	N/A
Typ/Max data rate [kbps]	200/1000(4,5)

(1) excluding deployment, hinges, panel structure and panel harness
(2) including digital electronics
(3) secondary power
(4) 100 mCrab/500 mCrab
(5) after compression

Table 3-1: Summary of LAD characteristics

3.2 Sky visibility

Note: The convention describing the FoR of the LOFT LAD-instrument is as follows. The LAD FoR is determined by two Solar Aspect Angles (SAA) of the sunlight on the plane of the LAD instrument. The canonical position of the LOFT SC is defined such that the SAA on the LAD is 90^o , i.e. the sun-line is parallel to the plane of the LAD instrument, and the two bounding angles of the FoR are specified with respect to this canonical position.

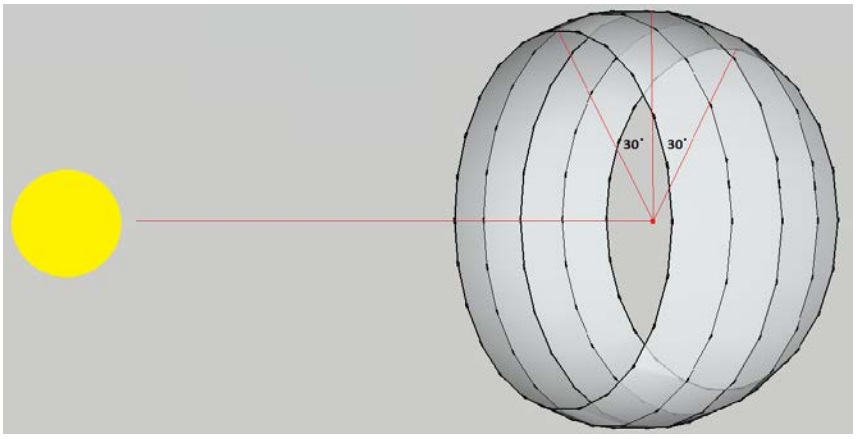

Figure 3-1: Example LAD FoR of 90°±30°

The FoR of the LAD is then defined as the segment of the sky that is bound by these two angles. The percentage coverage of the FoR is then given simply by sin(angle_1)+sin(angle_2)/2.

The requirement for sky availability for the LAD is 50%, with a goal of 75% (at the degraded energy resolution of 400 eV). The way to achieve this whilst minimising the solar illumination of either the upper or lower surfaces of the LAD is to target a spherical segment centred on a great circle orthogonal to the sun-line, i.e. with the LAD panels able to point perpendicular to the Sun-Earth line +/- 30°. However, other combinations of angles are also possible, and may be preferable in combination with an asymmetry in the LAD Module thermal design (e.g. illumination of the lower surface of the LAD Module could be preferable). For science reasons, there is a strong wish to increase the sky fraction towards the goal of 75%, in particular in the Galactic Centre direction. The factors affecting this trade-off are:

- Detector temperature: Increasing the range of angles increases the solar illumination of the panels (upper or lower surface), and so increases the LAD temperature; this in turn increases the LAD SDD dark current which degrades the spectral resolution.
- Increasing the angle in the negative sense (i.e. pointing closer towards the sun) increases the WFM temperature, degrading WFM spectral resolution (although adding a sunshield could mitigate this effect, at least for moderate increases in angle). Conversely, increasing the angle in the negative sense (pointing further away from the sun) decreases the WFM temperature.
- The effect of solar aspect angle (SAA) on the LAD panel temperature has been modelled at the M3 proposal stage (see [RD 1]), and the effect on the LAD panel temperature and WFM temperature by the ESA-CDF [RD 10].
- Solar array: Increasing the range of angles decreases the illumination of the solar array, if it is fixed. An increase in the panel area will be required, or a mechanism to orient the array. If the range of angles is asymmetric, the array's fixed orientation (or mean position if rotatable) can be set to maximise the time-averaged solar illumination.

The maximum temperature for the LAD at the end of the Nominal Operations Phase is driven by the requirement for an energy resolution of <260eV @ 6 keV. The energy resolution is determined by the combination of detector readout noise and dark current. The resolution is dominated by the dark current, which increases during the mission due to radiation damage of the detectors, dominated by passages through the South Atlantic Geomagnetic Anomaly (SAGA). [RD 4] shows that a less inclined or lower orbit allows a higher detector temperature because radiation damage is reduced by less SAGA-interaction. A less inclined or lower orbit cannot be achieved within the mass constraints of a VEGA launch, but can be achieved with a Soyuz launch (the lower inclination and altitude increase the S/C mass, as more fuel is required for initial orbit reorientation and periodic orbit maintenance manoeuvres, [RD 10]).

As an example, [RD 13] shows that increasing the range of SAAs to $+30^{o}/-50^{o}$ increases the sky coverage from 50 to 63%. This represents a factor 1.27 in sky coverage, and 1.33 for galactic centre coverage. The increase in solar array area required is 13% for a fixed array. [RD 11] shows that the -50^{o} SAA case increases the LAD temperature to -26.6: -24.9C (-30^{o} gives -36.6: -35.3C).

Note: at the beginning of the mission, because the detectors are yet to have accumulated radiation damage, their temperature requirements are relaxed compared to the end of the mission. However, this effect is very slight for lower orbits, in which the damage to the detectors is very limited.

3.3 LAD instrument description

3.3.1 Overview

The study of the energy-resolved timing properties of the X-ray emission of cosmic sources requires the accurate measurement of the time-of-arrival (TOA) and energy of the largest number of photons from the target source. The unambiguous identification of the target source in this type of experiment (e.g., the PCA on-board RXTE, Jahoda et al. ApJS 163 401 2006) is most effectively achieved by narrowing the field of view by means of an aperture collimator, down to a level (typically ≤1°) large enough to allow for pointing uncertainties yet small enough to reduce the aperture background (cosmic diffuse X-ray background) and the risk of source confusion (i.e. two or more sources simultaneously in the field of view). Alternative techniques would offer a much smaller effective area (X-ray optics) or much worse source-to-background ratio (coded masks).

In this type of instrument, the knowledge of the impact point of the photon on the detector array is not needed (if not for the use of proper detector calibration data), so there is no need for position sensitive detectors. Instead, detector read-out segmentation is useful/necessary to reduce the effects of pile-up and dead time. As we show below, the development of a 10 m^2–class experiment is now made possible by the recent advancements in the field of large-area silicon detectors, which are able to time tag an X-ray photon with an accuracy <10 μs and an energy resolution of ~250 eV (FWHM, Full Width at Half Maximum), and capillary-plate X-ray collimators. The key feature of the LOFT design is the low mass per unit area enabled by the solid-state detectors and capillary plate collimators.

The Large Area Detector (LAD) of LOFT is designed as a classical collimated experiment. A set of Detector Panels (the payload consortium baseline is 6, but other numbers of panels can also be considered) are tiled with 2016 Silicon Drift Detectors (SDDs), electrically and mechanically organized in groups of 16, referred to as Modules. Each of the 6 Panels hosts 21 Modules, each one in turn composed of 16 SDDs.

The SDDs are 450 μm thick and operate in the energy range 2-80 keV. The field of view of the LAD is limited to ~60arc min by X-ray collimators Micro-Channel Plates. A ~6 mm thick sheet of Lead glass is perforated by a huge number of micro-pores, ~100μm diameter, ~20 μm wall thickness. The stopping power of Pb in the glass makes the MCPs effective in collimating X-rays below 30 keV (the energy range from 30 to 80 keV is used only for exceedingly bright events from outside the instrument field of view, shining through the collimator walls).

3.3.1.1 The large-area Silicon Drift Detector

The primary enabling technology for the LAD is the large-area Silicon Drift Detectors (SDDs) developed for the Inner Tracking System (ITS) in the ALICE experiment of the Large Hadron Collider (LHC) at CERN, by one of the scientific institutes in the LOFT Consortium – INFN Trieste, Italy – in co-operation with Canberra Inc. (Vacchi et al. 1991 NIM A306 187; Rashevsky et al. 2002 NIM A485 54).

The key properties of the Si drift detectors (Gatti & Rehak 1984 NIM A225 608) are their capability to read-out a large photon collecting area with a small set of low-capacitance (thus low-noise) anodes and their very small weight (~1 kg m^{-2}). The working principle is shown in Figure 3-1: the cloud of electrons generated by the interaction of an X-ray photon is drifted towards the read-out anodes, driven by a constant electric field sustained by a progressively decreasing negative voltage applied to a series of cathodes, down to the anodes at ~0 V. The diffusion in Si causes the electron cloud to expand by a factor depending on the square root of the drift time. The charge distribution over the collecting anodes then depends on the absorption point in the detector. The conceptual structure of the large-area SDD is shown in Figure 3-2.

In ALICE 260 SDDs, a total area of 1.37 m^2, have been in operation (successfully) since 2008. These detectors were produced on 5-inch diameter, 300 μm thick Si wafers and have a monolithic active area of 53 cm^2 each, with an anode pitch of 294 μm. The LAD detector design is an optimisation of the ALICE detector: 6", 450 μm thick wafers will be used to produce 76 cm^2 monolithic SDDs (Figure 3-2: 108.52 mm x 70.00 mm active area, 120.84 mm x 72.50 mm geometric area). The anode pitch is increased to 970 μm (this value updates the 854 μm in the proposal, as a result of an optimization analysis) to reduce the power consumption while optimising energy resolution (corresponding to an elemental area of 0.970 mm x 35 mm = 0.3395 cm^2).

The Si tile is electrically divided in two halves, with 2 series of 112 read-out anodes at two edges and the highest voltage along its symmetry axis. The drift length is 35 mm. A drift field of 370 V/cm (1300 V maximum voltage), gives a drift velocity of ~5 mm/μs and a

maximum drift time of ~7 μs, the highest detector contribution to the uncertainty in the determination of the absolute TOA of the photon, 30% smaller than the scientific requirement. The maximum size of the charge cloud reaching the anodes (depending mostly on the drift distance, not on the photon energy) is ~1 mm (corresponding to an event absorbed at the bottom of the drift channel).

Depending on the relative size and position of the Gaussian-shaped charge cloud when reaching the anode pattern, the event charge may be collected by 1 or 2 anodes. Based on this, we define the event *multiplicity* as single (approximately 45% of the total), when the full charge of the event is collected by a single anode, and double (~55% of the total) when the charge is shared on two neighbouring anodes. Since in the two options the same charge compares to the noise of one or two anodes, the single events display higher spectroscopic quality and can be selected for observations requiring higher spectral performance. They correspond to about half of the LAD area. In general, single events correspond to photons absorbed at a relatively small distance from the collecting anodes and in a drift position relatively "centered" with the anode (a photon detected even very close to the anode but in a position that is in between the two drift channels will share its charge over the two anodes anyway).

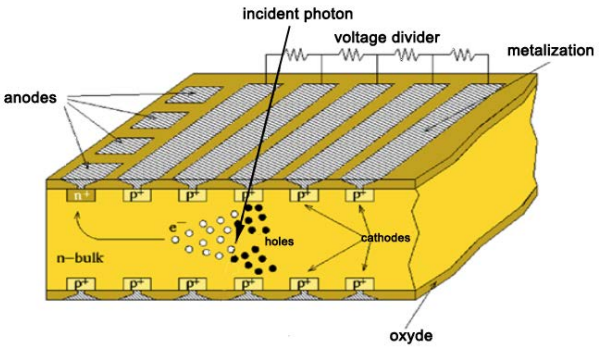

Figure 3-2: The electrical structure and working principle of an SDD

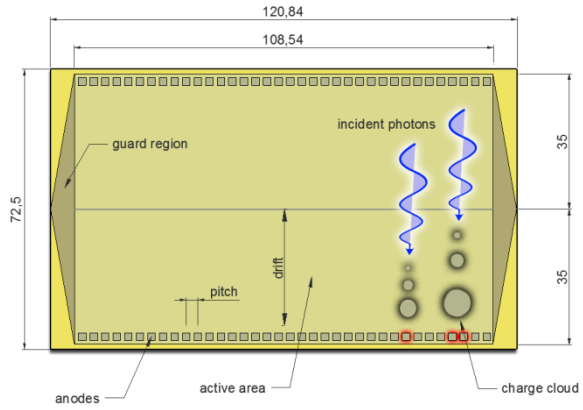

Figure 3-3: Size and functional drawing of a single SDD

The large-area SDDs were originally designed for particle tracking, that is high energy events. Over the last few years R&D work has been carried out to characterise and optimise the same detector design for detection of soft X-rays. The preliminary results obtained with a spare detector of ALICE (300 μm thick, 294 μm anode pitch, no design optimization), with a bread-board read-out based on discrete electronics, show high spectral performance already at room temperature, as shown in Figure 3-3. The very first results obtained with this prototype in terms of X-ray spectral and position resolution are published in Zampa et al. 2011 (NIM A 633, 15) and Campana et al. 2011 (NIM A 633, 22). These papers primarily describe the methods, while the performances presented there are very preliminary and do not include a number of improvements actually foreseen in the LOFT detectors and already implemented in the lab.

Since the anode capacitance of the SDD is very small (~50 fF), the main source of noise for these detectors is represented by the leakage current of the volume corresponding to the drift channel. The results obtained in the lab at room temperature can be largely improved by lowering the operating temperature, achieving much smaller values of the leakage current, as shown in Figure 3-4, enabling much higher spectral resolution (Figure 3-5). However, when operated in space, Silicon detectors suffer by a number of effects due to the radiation environment (Total Dose, Non-Ionizing Energy Losses, ...) usually causing a severe increase in the leakage current. The case for LOFT has been studied, as reported in the technical note [RD 4]. Our study shows that in the LOFT orbit the radiation environment is very favourable. However, despite the very low particle flux (lower than 10^8 cm^{-2} in the worst case), NIEL events are still expected to cause a significant increase in the detector leakage current. The amount of the increase strongly depends on the parameters of the orbit (mostly inclination and altitude), as the particles causing the effect are the low energy protons trapped in the south Atlantic anomaly. However, our analysis shows that operating the detectors at temperature of -5°C (TBC) meets the scientific requirements on spectral resolution at the end of the Nominal Operations Phase duration of 4 years in the worst case orbit (600 km and ~5° inclination). Lower altitude and/or inclination would allow to meet the requirements at higher temperature (or to achieve better spectral performance at lower temperatures.

Additional information about the detector performance and development may be found in the relevant Technology Development Plan [RD 15].

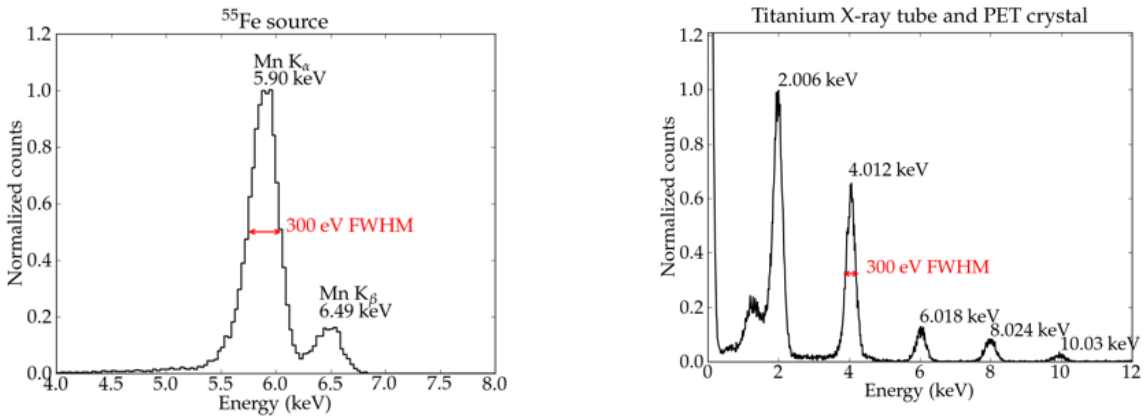

Figure 3-4: Energy spectra measured using a spare ALICE detector equipped with discrete read-out electronics, at room temperature. The FWHM energy resolution was measured as ~300 eV at 5.9 keV. The minimum line energy is ~1.5 keV (the spurious Al k-fluorescence from the detector box)

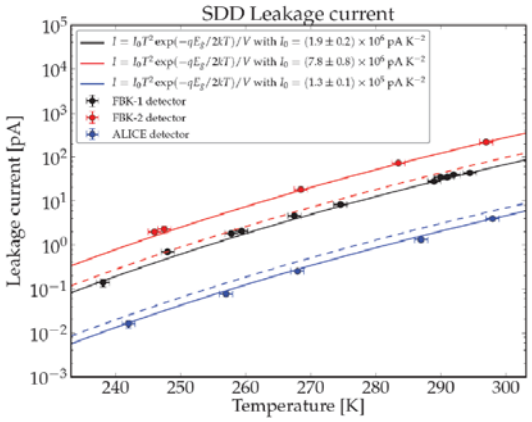

Figure 3-5: Measured decrease of the SDD leakage current with decreasing temperature, between -30°C and +25°C, using both ALICE and FBK prototypes. The leakage current decreases with temperature as ~$2^{(\Delta T/7°C)}$. The current FBK prototypes have a worse substrate leakage current (see SDD TDP for details)

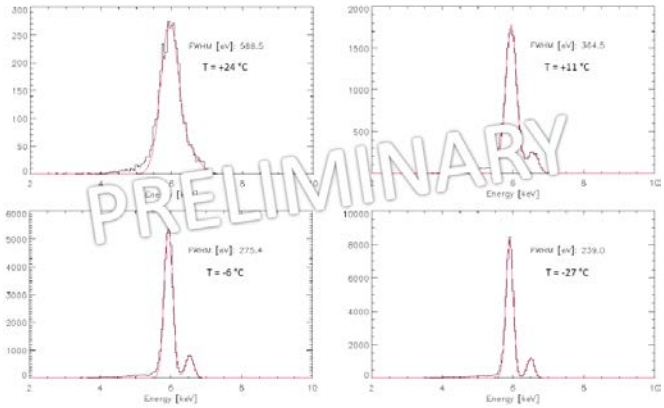

Figure 3-6: Energy resolution for a Fe55 source (lines at 5.9 and 6.4 keV) as measured in the lab as a function of temperature using an "FBK-2" detector prototype equipped with discrete read-out electronics. Here "single-events" spectra are shown

3.3.1.1.1 Energy resolution breakdown

The overall energy resolution of the LOFT/LAD detector is affected by various sources of noise and systematics. The reconstruction of the energy of an incoming photon depends on the following factors:

1. Fano noise
2. Electronic noise
3. Charge reconstruction (number of anodes, common-mode noise subtraction)
4. ADC quantization noise

Moreover, the integration of signals from the ~5×10^5 LAD channels give rise to other sources of uncertainty:

5. Gain spread
6. Offset spread.

In the following we discuss in more detail each of these contributions.

3.3.1.1.1.1 Fano noise

When a photon of energy E is absorbed by the Silicon bulk, it produces on average one electron-hole pair every 3.6 eV deposited. The dispersion around this number is reduced w.r.t. the Poissonian value by the so-called Fano factor *f*, that for Silicon is about 0.12:

$$\sigma_F^2 = ef \times \left(\frac{E}{E_I} \right) \quad \text{[Coulomb}^2\text{]}$$

where E_I = 3.6 eV/electron, and E is expressed in eV. For a 5.9 keV photon, the Fano noise is equal to about 118 eV FWHM. The Fano noise can be considered as the limiting factor for the energy resolution of a solid-state detector.

3.3.1.1.1.2 Electronic noise

In general, the electronic noise for a single channel is given by the following formula:

$$\sigma_{ENC}^2 = i_n^2 T_{sh} F_i + \frac{C^2 e_n^2 F_V}{T_{sh}} + C^2 A_f F_{fv} \quad \text{[Coulomb}^2\text{]}$$

where:

- F_i (parallel), F_v (series) and F_{vf} (flicker, 1/f) are numerical coefficients that depend only on the particular type of shaper used (CR-RC^n, semi-gaussian, etc).
- i_n^2 is the power spectral density of the parallel (current) noise, in particular of the leakage current (and therefore is temperature-dependent).
- e_n^2 is the power spectral density of series (voltage) noise, mainly due to the first transistor.
- A_f is the power spectral density for the 1/f noise.
- C is the total input capacitance.
- T_{sh} is the shaper time constant.

The leakage current, and therefore the energy resolution, also depends on the radiation damage on the detector, quantified by the NIEL. The increase in leakage current is proportional to the equivalent 1 MeV neutron fluence. Assuming the LOFT baseline orbit (600 km, 5° inclination), after 4+1 years the increase in leakage current due to the radiation damage is 58400 pA/cm^{3}at 20 °C. For more details see the [RD 4].

3.3.1.1.1.3 Charge reconstruction

The electron cloud produced by the absorption of an incoming photon spreads to a size proportional to the square root of the distance from the anodes. In general the signal will be integrated by one or more anodes. Moreover, the signal is affected by a varying baseline due to the common-mode noise: this baseline can be evaluated by reading out the channels without signal. More precisely, if we have a signal spread over N anodes, and we use M channels to measure the baseline, the resulting energy resolution is (taking into account also the Fano noise):

$$\sigma^2 = \sum_{i=1}^{N} \sigma_{ENC,i}^2 + \frac{N^2}{M^2} \sum_{j=1}^{M} \sigma_{ENC,j}^2 + \sigma_f^2 = N\sigma_{ENC}^2 + \frac{N^2}{M^2} M\sigma_{ENC}^2 + \sigma_f^2 = N\left(1 + \frac{N}{M}\right)\sigma_{ENC}^2 + \sigma_f^2$$

where we also assumed that all channels are equally noisy, i.e. $\sigma_{ENC,\,i} = \sigma_{ENC}$ for all *i*.

The energy resolution, therefore, is proportional to the number of anodes over which the signal spreads, and inversely proportional to the number of channels used to evaluate the

common-mode noise, as shown in the following figure. At least 10 channels have to be used to determine the CMN in order to not affect the energy resolution significantly Figure 3-7).

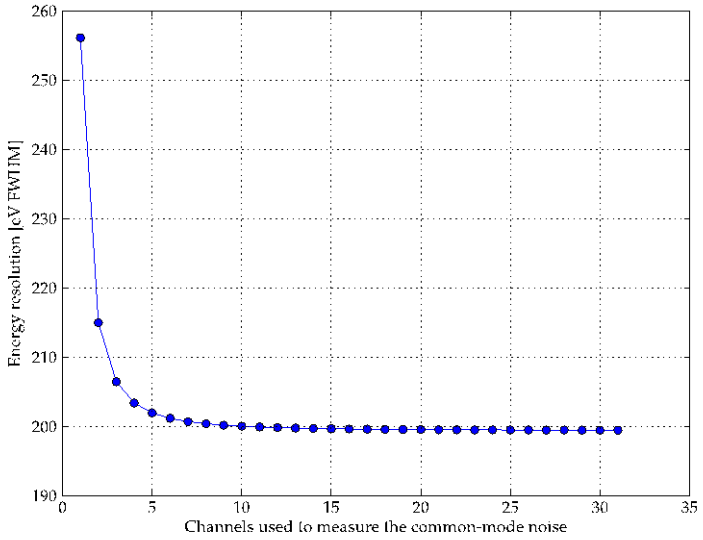

Figure 3-7: Overall energy resolution for one-anode events (N=1) vs. the number M of channels in which the CMN is measured. Here an energy of 6 keV and single-anode electronic noise of 19 e- have been assumed

3.3.1.1.1.4 ADC noise

The quantization introduced by the ADC has an effect on the energy resolution. If we have n bits, the whole dynamic range (ΔE keV from E_{min} to E_{max}) is divided into $\Delta E/2^n$ levels. For each of these levels, we can consider an uniform probability distribution, and therefore the standard deviation is $\Delta E/(2^n\sqrt{12})$. Assuming an ADC with 11 bits of resolution (2048 levels), and a dynamic range ΔE = 100keV, each level is ~50eV wide. The corresponding error is therefore Δ_{ADC}~33eV FWHM.

3.3.1.1.1.5 Gain and offset spread

Another source of uncertainty to be taken into account is due to the residual spread in the knowledge of the gain for the various channels. The overall gain spread is the cumulative effect of the dispersion in the ADC stability, in the accuracy of the feedback and test capacitance values, and in the accuracy and stability of the test voltage calibrator:

$$\frac{\Delta Gain}{Gain} = \sqrt{\left(\frac{\Delta ADC}{ADC}\right)^2 + \left(\frac{\Delta Cfeed}{Cfeed}\right)^2 + \left(\frac{\Delta Ctest}{Ctest}\right)^2 + \left(\frac{\Delta Vt}{Vt}\right)^2}$$

The residual spread on the gain values after the electronic calibration depends on the electronic noise of the test circuit. As an example, for SuperAGILE (calibration with 4 amplitudes and 200 pulses) the residual spread was 1%. The spreading of the offset values must be considered in addition to the gain spread.

The requirement for the LAD energy resolution is 200 eV FWHM over single-anode events at 6 keV and at end of life (4+1 years). In order to establish the maximum allowable residual gain and offset spread (over all the 451584 LAD channels) compatible with this requirement, in function of the electronic noise value (and therefore in function of the operating temperature and radiation damage), numerical simulations have been performed and shown in Figure 3-8.

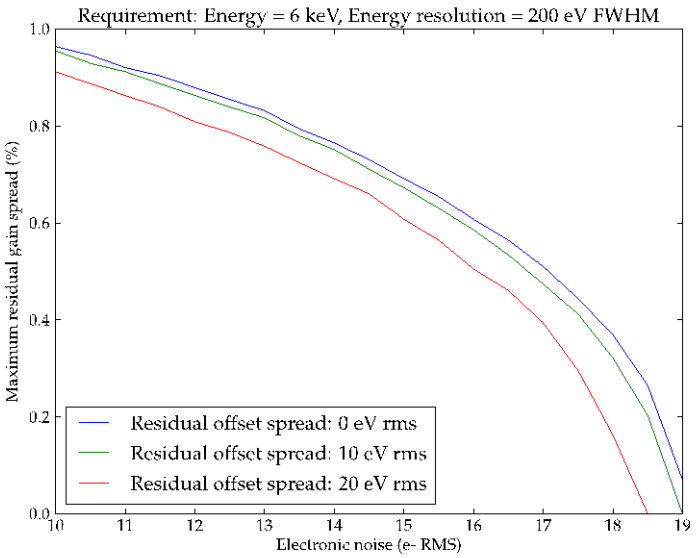

Figure 3-8: Maximum allowable residual gain and offset spread, as a function of the input electronic noise, compatible with the requirement of 200 eV FWHM resolution at 6 keV

It is evident that, in order to not affect the energy resolution at 6 keV for an input electronic noise of e.g. 17 e^- rms., the residual gain spread after correction should be lower than ~0.4% r.m.s. and the residual offset spread lower than 20 eV rms.

In the following Table we show the energy resolution breakdown for the requirement value of 200 eV FWHM @ 6 keV, assuming an input electronic noise of 17 e- rms. and assuming to use >10 channels to measure the common-mode noise.

Energy	Fano noise	Electronic noise	ADC noise	Total before gain and offset spread	Residual Gain Spread	Residual Offset Spread	Total after residual gain and offset spread
6 keV	118 eV FWHM	144 eV FWHM	33 eV FWHM	189 eV FWHM	0.4% rms	20 eV rms	200 eV FWHM

Table 3-2: Energy resolution breakdown for the LAD requirement of 200 eV FWHM @ 6keV

3.3.1.2 The Collimator

The other innovative element of the LOFT/LAD design is the low-mass capillary plate X-ray collimator. This is foreseen to be based on the technology of microchannel plates (MCPs), drawing on the heritage of EXOSAT (1983-6) whose MEDA and GSPC detectors were collimated in this way and on the much more recent development of microchannel plate X-ray optics for the BepiColombo Mercury Imaging X-ray Spectrometer (MIXS)

experiment (GW Fraser et al., Planetary and Space Science 58 (2010) 79). In particular, the collimator channel of this instrument (MIXS-C) provides a secure, high TRL basis for the LAD collimator design. The MCP optic production process, furthermore, has been demonstrated to be flexible with regard to channel pore size (10-100 microns square) and channel aspect ratio (10:1 - 500:1).

The originally-proposed LAD collimator parameters have evolved during the study phase to date, including (i) the field-of-view (ii) the required transparency of the collimator at high (> 30keV) X-ray energies and (iii) the requirement for a "flat-top" component of the basic triangular collimator response function, describing X-ray transmission versus off-axis angle. The study has been informed by analytical and Monte Carlo (GEANT4) modelling, by specific X-ray measurements on thick MCPs in the University of Leicester 27m long X-ray test beamline and discussions with the technology provider, Photonis (Brive-la-Gaillarde, France).

The key technical findings informing the new collimator baseline design include:

- There is no requirement to develop a new micro-channel plate glass with higher lead oxide fraction (~37%) than the present standard lead silicate glass, since the stopping power of the collimator can be simply controlled by changing the channel septal thickness (noting that this involves a trade-off with OAR and/or collimator thickness).
- There is no requirement to use radioisotope-free glass in the collimator manufacture, since the count rate due to 40K betas and gammas is estimated to be well below other background sources.
- An extended flat-top response is incompatible with the required effective area, whether the flat-top is realised by spherical slumping of the MCP, by coating of the channel walls with a high-Z metal such as gold or iridium, or deliberate plate-to-plate misalignment. The stability of the LAD response will instead be achieved by the combination of the 'flattened' collimator response and AOCS parameters.

The key elements of the design are summarised in Table 3-3. Figure 3-9 shows a scanning electron microscope image of a MIXS-C format plate; the side length of the channels is 20 microns, the wall thickness, 6 microns.

To further raise collimator TRL will require the procurement from Photonis of a test block of the LAD-specific area (8 x 11 cm^2, rather than the 4 x 4 cm^2 of MIXS-C), with the larger pores (100 rather than 20 µm) and thicker walls (20 rather than 6 µm). The block will yield up to 16 representative LAD collimator plates for X-ray and environmental tests.

The baseline LAD collimator element is a self-supporting single tile, 11 cm x 8 cm size. An 80 nm, self-standing Aluminium film will be placed on the MCP front side (including holes), at production level. In addition to the MSSL heritage in MCP charged particle detectors, Leicester has been using similar large structure in spring-mounted photon counting detectors - up to 10 x 10 sq.cm and indeed 16 x 5 sq.cm. Additional technical details on the MCP collimator technology development are given in [RD 14].

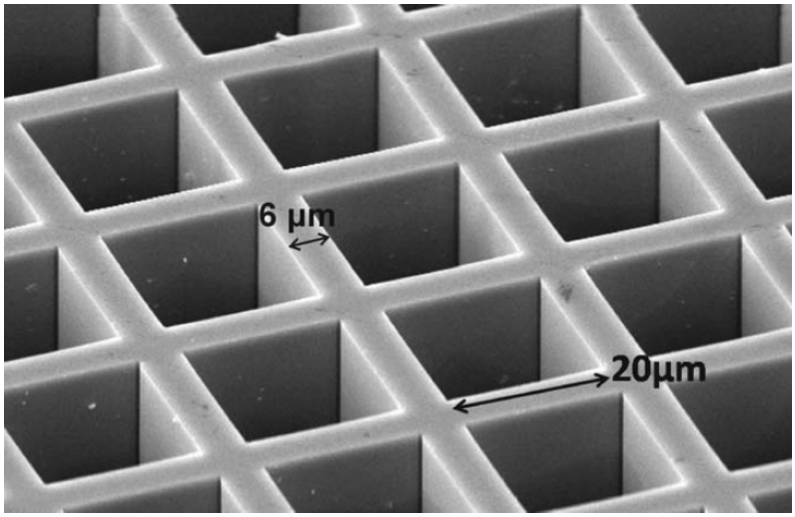

Figure 3-9: High resolution image of MCP surface

Parameter	Value	Comment
Pore size (microns)	100	Demonstrated in 40x40mm format
Septal thickness (microns)	20	Demonstrated in 40x40mm format
Channel aspect ratio	60:1	Demonstrated (MIXS-C is 55:1 with different pore size)
Channel length	6 mm	Demonstrated with smaller pores (expected to be easier)
Open area fraction	70%	
Spherical slumping	None	
Channel coating	None	
Leakage	Acceptable to 30 keV	By calculation
Flat top	Determined by reflectivity;less than 5 arcminutes at 30 keV	Pore misalignments and reflectivity lead to rounding of the top of the transmission curve.

Table 3-3: MCP requirements

The X-ray study of a 5 mm thick (channel aspect ratio 250:1) is described in Figure 3-10: the measured X-ray transmission of 5mm thick, 20 µm square-pore test collimator piece. The channel aspect ratio is 250:1, rather than the 60:1 required for LAD. The pore wall is 6 µm instead of the 20 µm baselined for the LAD. The four X-ray energy regimes are all produced by a Mo anode; right-to-left, the configurations are:

- 0.9-2.4 keV Mo L line plus continuum
- keV filtered Mo L line
- 30 keV endpoint continuum
- 20 keV endpoint continuum.

The red line indicates the expected off-axis collimator response at high energies (i.e. independent of reflection or leakage). The broken lines then indicate the 13.75 arcmin FWHM of the triangular collimator response function. The data shows an angle-independent leakage fraction of about 9% of peak transmission at 30 keV, and less than 1% at 20 keV. Thus, the measured high energy leakage is about a factor of ~2 less than that predicted for a single 6 micron thick septum. The rapid onset of transparency above 20 keV for such collimator material is therefore confirmed. A wall thickness of 20 microns, however, from Figure 3-10, should produce acceptably low high-energy leakage up to 30 keV.

The narrow-band 2.3 keV data set extends only to about 30 arcmin. The implied product of energy and critical angle is therefore only ~0.5 x 2.3 =1.15 degrees x keV, or just less than half the 2.4 degrees x keV assumed hitherto. In other words, MCPs thicker than used for MIXS-C may exhibit significantly higher levels of surface roughness, owing to the much longer etch times required, with consequent benefit in reduced "large angle" susceptibility to the soft X-ray background.

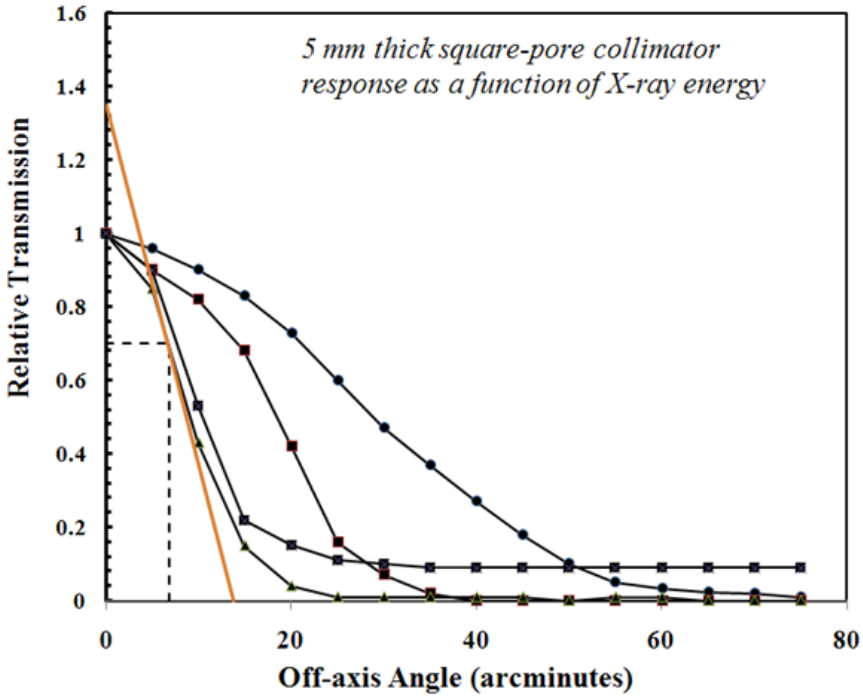

Figure 3-10: 5mm thick square port collimator response

3.3.2 Background due to ^{40}K activity

The naturally occurring potassium element contains approximately 0.0117% of the radioactive isotope ^{40}K, leading to a total activity for natural potassium of A_k ~30 Bq/g = 0.81 nCi/g. An analysis has been performed [RD 9] in order to identify the effects of this radiation in terms of LOFT-LAD background. A conservative estimate of the background contribution due to the radioactivity of the potassium contained in the glass of the collimators, assuming a 15 m^2 MCP capillary surface, with 4 mm thickness (to be updated to the current 6 mm baseline), and using a lead glass with 5% potassium content, to be in

the range 100-200 *cts/s*, corresponding to a fraction of about 3%-6% of the overall LAD background. This background is almost flat, as shown in Figure 3-11, therefore we have a similar count rate (160 *cts/s)* for the ^{40}K contribution to the background in the extended LAD band from 30 to 80 KeV.

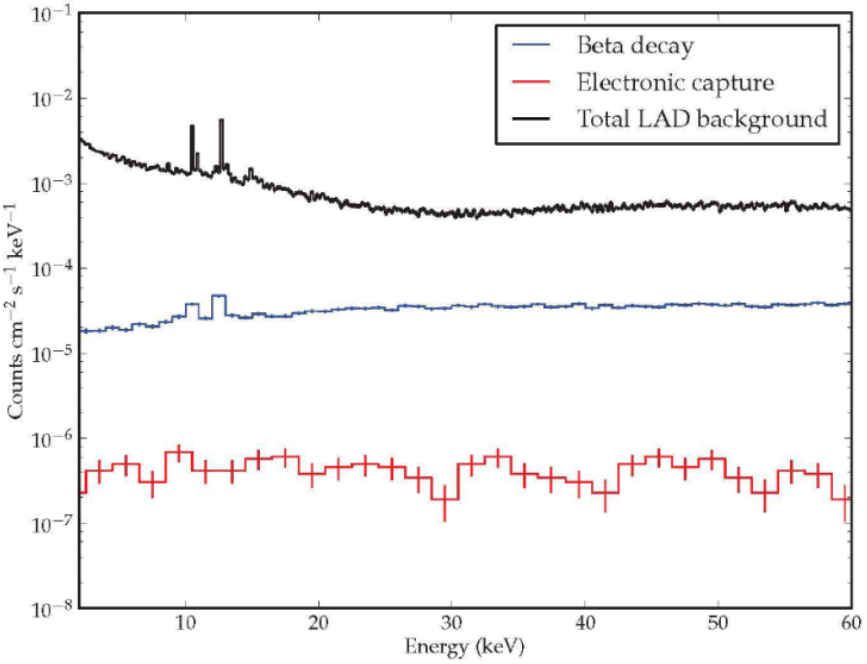

Figure 3-11: LAD background due to the 40K activity in the collimator glass

3.3.3 Instrument performance specifications

Table 3-4 provides a summary of the current performance specifications of the LOFT/LAD design.

Parameter	Value
Energy range	2-80 keV (30-80 keV larger energy binning)
Effective Area	10 m^2 (@8 keV)
Field of View	≤1^o
Energy resolution	≤260 eV at 6 keV (EOL)
Time resolution	~7 μs
Dead-time	<1% for 1 Crab source
Background	~10 mCrab
Maximum average source fux	500 mCrab
Maximum peak source flux	15 Crab

Table 3-4: Current LAD performance specifications

3.3.4 Instrument configuration

In the current, consortium design, the LAD experiment is composed of 6 independent and identical detector panels. Such a design satisfies the scientific requirements of LOFT in terms of effective area within the envelope of a Soyuz launcher and it will be considered as a baseline in the present document. The baseline configuration is certainly not considered a constraint, as alternative configurations that satisfy the same requirements and optimize the overall resources can certainly be considered, especially as the Soyuz launcher offers additional space (e.g. for panel length).

The basic LAD detection element is composed of SDD+FEE+Collimator, hereafter referred to as Detector. The assembly philosophy employs a hierarchical approach: Detector, Module, Detector Panel, LAD Assembly. The LAD Assembly is composed of 6 Detector Panels, one Detector Panel is composed of 21 Modules. Each Module includes 16 Detectors. The read-out electronics is organized as follows. Each Detector is equipped with its own Front-End Electronics (FEE). The FEEs of the 16 Detectors in a Module converge into a single Module Back End Electronics (MBEE). One Panel Back-End Electronics (PBEE) for each Detector Panel is in charge of interfacing in parallel the 21 MBEE included in a PBEE, making the Module the basic redundant unit. A block diagram of the LAD organization is shown in Figure 3-12.

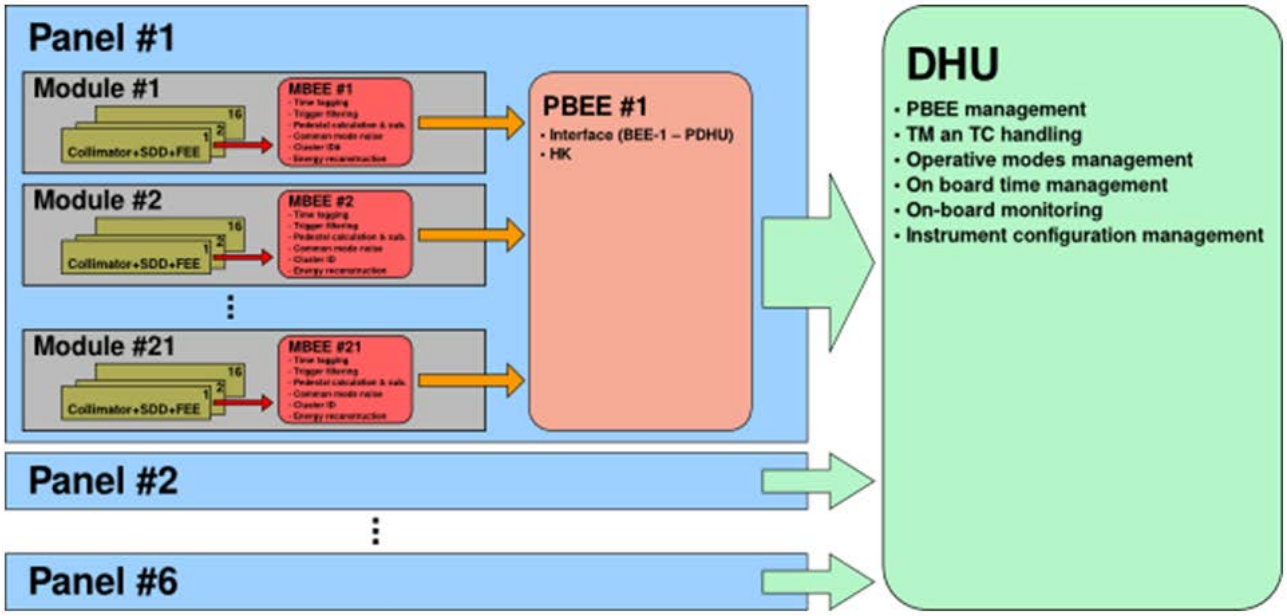

Figure 3-12: a block diagram showing the organization and structure of the LAD

The current design envisages a set of 6 co-aligned Detector Panels connected by mechanised hinges to a satellite structure, the optical bench hosting the WFM or the spacecraft bus itself. The panels are folded down during launch and deployed when in orbit. Figure 3-13 shows the organization of the detectors in the Module and in the Panel. Figure 3-14 shows a the proposal baseline, with the 6 Detector Panels deployed from the central Optical Bench housing upon which is mounted the WFM.

Figure 3-13: Left: Front-side view of a Module (based on the 6 panel design), showing the mounting of collimator, SDD and the FEE; MBEE (not shown) is on the backside, internal to the Module box. Right: An example LOFT Detector Panel with assembled Modules and interfaces to the deployment mechanism (managed by industry)

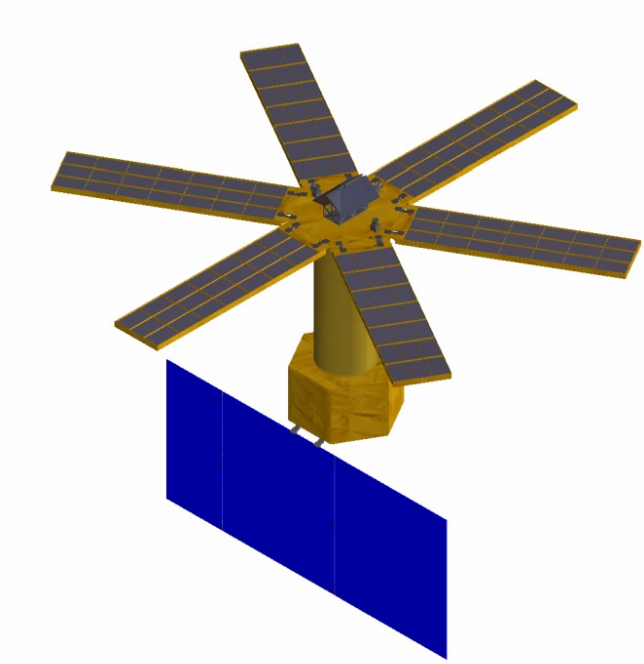

Figure 3-14: The deployed LAD, in the baseline instrument consortium configuration

3.3.5 Instrument optical design

3.3.5.1 Baffle

No baffling is required. Shielding against diffuse X-ray background will be provided by the collimator (front) and a metal shield (back). UV/Visible light will be shielded by a metal deposition on the top of the collimator and by a thermal screen (see below).

3.3.5.2 Filters

Shielding against UV/Visible/IR light is required. A thermal screen filter will contribute (together with the MCP collimator optical properties, see below) to a high level of rejection of UV/V/IR but be transparent to low energy (2 keV) X-rays. The filter was preliminarily identified in the proposal as 1 μm thick Polyimide covered with 0.04 μm Aluminium on both sides (0.08 μm total). This is based on the design by LUXEL of the self-standing filters flown in the Chandra HRC (0.6 μm Polyimide covered with 0.08 μm Aluminium, 10 cm x

10 cm surface, self-standing). For the LAD, each filter can be mounted either above or below each collimator, either at tile level or at detector size. In both cases the size of the individual filter is smaller than that of Chandra. The soft X-ray transparency is >90% at 2 keV and the optical transmission is $<10^{-6}$.

The filter design and position (it could be located in-between the MCP collimator and the SDD) are TBC pending the consolidation of the LAD Module thermal analysis. For example a switch to a single-sided polyimide filter, with bare Kapton as the outer layer, could improve the thermal performance of the Module.

3.3.6 Instrument unit mechanical design

In this section we provide a description of the LAD mechanical design in terms of 6 identical Detector Panels. However, as stated above, alternative designs able to deploy the same (or greater) effective area in orbit and operate it at the required temperature are worth considering as well.

3.3.6.1 Detector Panel

The detector panel will be provided by Industry. However, some minimal description of the panel is provided in order to provide context. The detector panel is a structure that will hold the detector modules. It will provide, via hinges, for the deployment of the array as a whole and, via its stiffness and construction, alignment and alignment stability for all the modules. Via its structure the various harnesses will run between the PLM and each module.

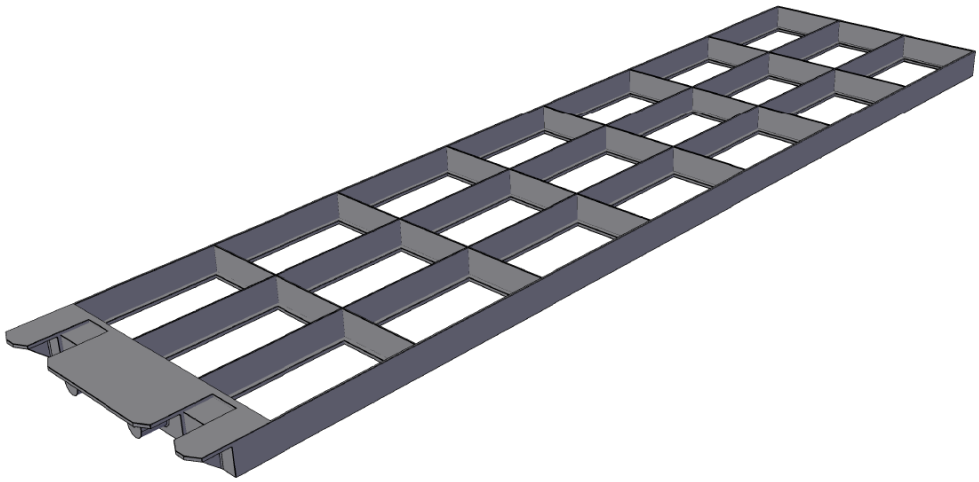

Figure 3-15: Mechanical structure of one Detector Panel in the consortium 6 panel baseline

A set of 21 (TBC) Modules will be integrated into a Detector Panel (Figure 3-15). This is a mechanical frame providing support and alignment interfaces for the individual Modules, for the Panel Back-End Electronics (PBEE) box (although there are good arguments for maintaining the PBEE on the Detector Panel, the location of the PBEE box may be also shifted to the spacecraft structure, if this is necessary) and enabling the electrical connection and routing between the MBEEs and the single PBEE in each DP. The DP will

have mechanical and alignment interfaces with the deployment mechanism. In order to fulfil the alignment requirements, the mechanical interface of the *Modules* with the DP structure will be of isostatic type (e.g., Collon et al. 2010 SPIE Proc. 7732 77321F).

3.3.6.2 Module

A design option for a module, containing 16 SDDs, is shown in Figure 3-16. In order to minimise alignment errors for the micropore optics, all optics for the module are held in one large frame; shown in the example as 2 MCP tiles per SDD within the module as a worst case; the current baseline is that this will be a single tile. (It is important to emphasise here that the "optical" element for the LAD is the collimator and not the detector, which is only required to collect all the photons transmitted by the collimator).

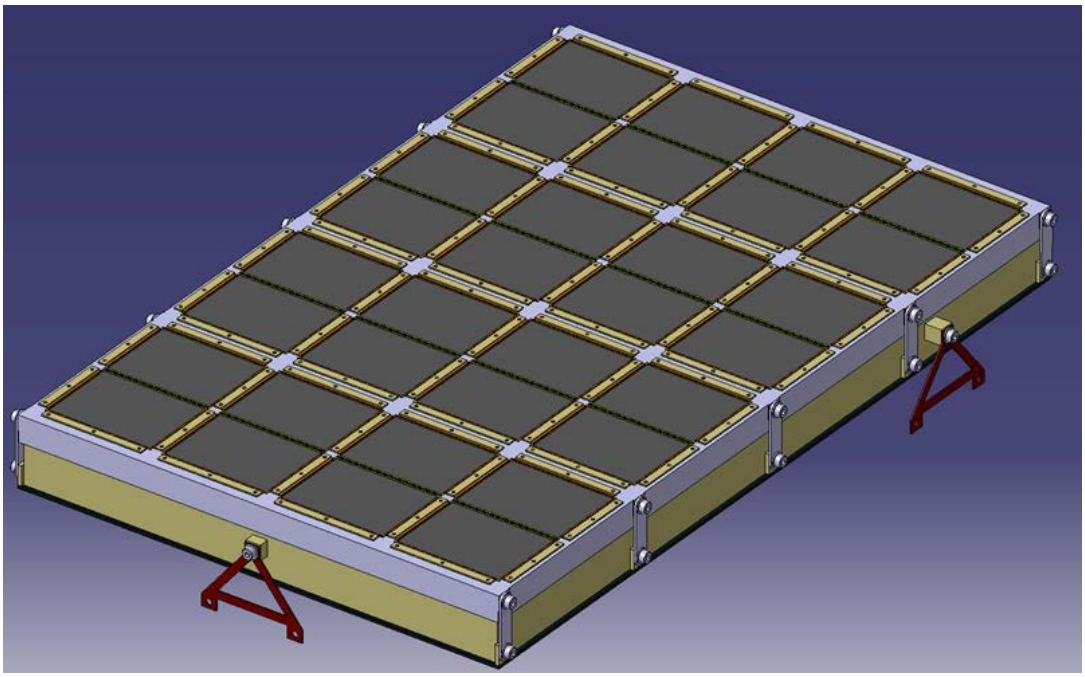

Figure 3-16: Detector module

The module consists of an aluminium box, (shown in blue, Figure 3-17) holding a PCB which contains all 16 SDDs in a 4 by 4 grid. On the top of the box the collimator tiles are held in a titanium frame.

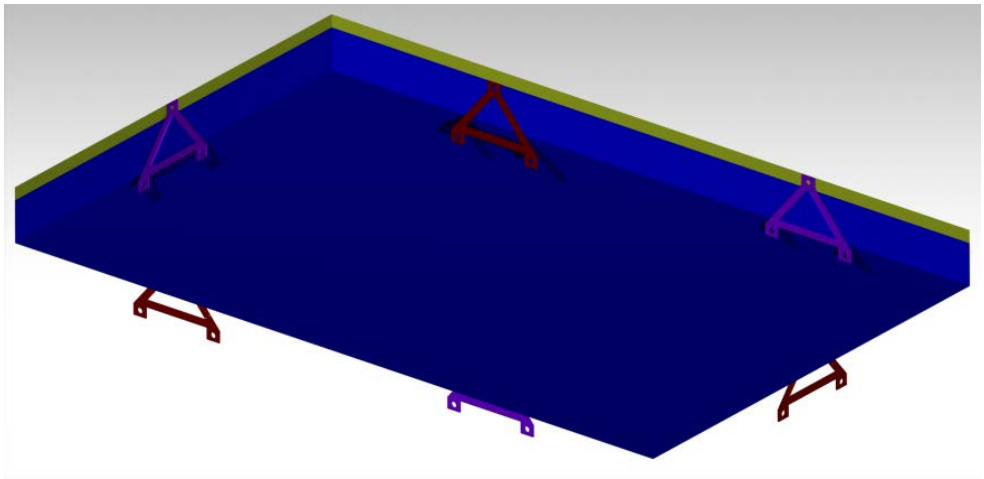

Figure 3-17: Bottom view of the module (based on outdated design with 6 kinematic mounts)

The exploded view (Figure 3-18) show the different parts and their location within the box (note. the collimator tile drawing is not updated here). One advantage of a single tile collimator is that it can be clamped rather than bonded to the frame, which allows the frame to be made from Aluminium, reducing mass and simplifying manufacture and alignment.

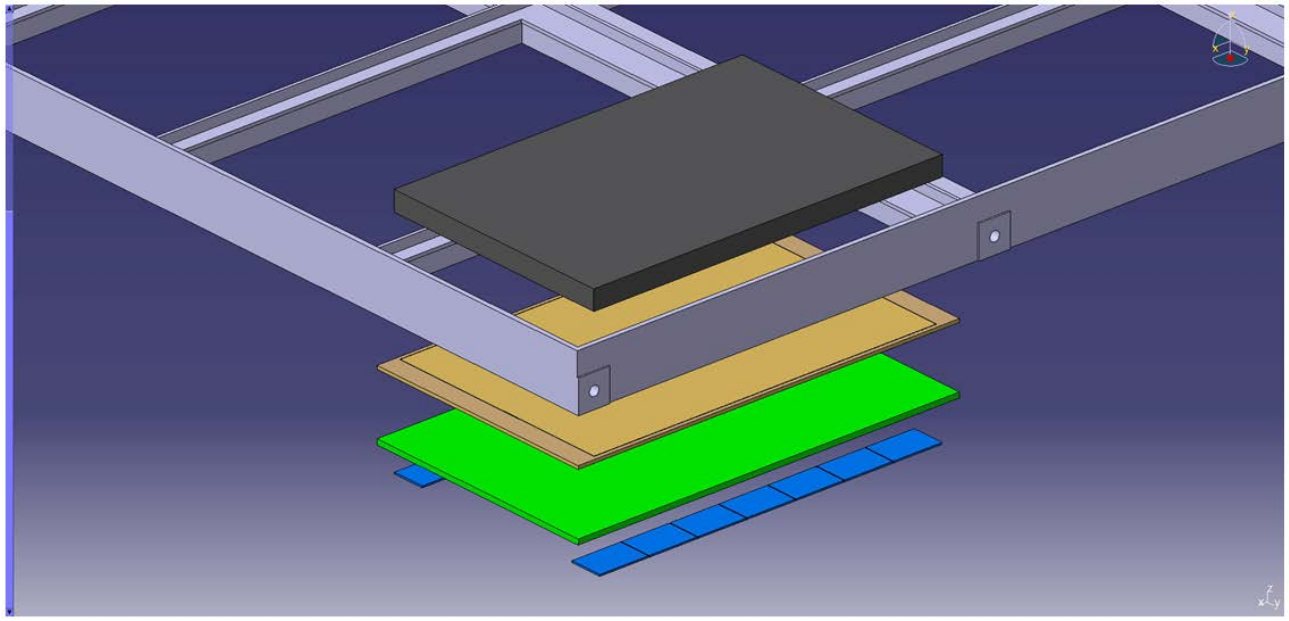

Figure 3-18: Exploded view of one detector unit and the collimator frame (collimator tile=grey, SDD=brown, FEE=green, ASIC=blue

A study of the LAD background components (at the time of the MTR) has shown that a high level of control of the LAD background systematic can be achieved if a detector surface equivalent to 1 Module (for the entire LAD instrument, incurring an acceptable A_eff loss of less than 1%) is equipped with a “blocked collimator”, which is a Pb glass tile with the same material and the same stopping power (mass and g cm^{-2}) as the collimator, in order to monitor the non-aperture background (>90% of the LAD background) continuously. As a baseline the 16 blocked detectors will be placed in a single Module, becoming a “blocked

module". Future simulations will clarify whether this is an optimal solution, or the blocked detectors are better distributed over different Detector Panels, but always adding up at 16 detectors. The thermo-mechanical properties of these blocked collimators will be nearly identical to those of the real collimators.

3.3.6.3 Detector

Each Silicon Drift Detector will be equipped with its own read-out electronics. The SDD is back-illuminated, in order to minimize the electrical contacts on the X-ray entrance window. On the front side of the SDD the Si tile will be glued to the PCB hosting the front-end electronics (ASICs and front-end components). The size of the PCB is slightly smaller than the size of the Si tile, so that the input pads of the ASICs, hosted at the edge of the PCB, directly face the anode pads of the SDD, minimizing the length of the wire bonding (which is a noise-sensitive element). The high voltage connection is also on the same (front) side. Instead, the medium voltage (powering the last section of the drift field and the pull-up cathodes) needs to be brought to the X-ray entrance side. This is done through a wrap-around cable. The working principle and dimensions of each Si tile are given in Figure 3-18 : 72.5 mm x 120.84 mm (including an active area of 108.54 mm x 70.0 mm). The thickness of the SDD is 0.45 mm. The FEE board is slightly smaller than the SDD tile to favour the wire-bonding connection to the SDD anode pads. Its dimensions are 66.0 mm x 120.84 mm, with a 2 mm thickness.

The backside of the detector needs to be shielded against photons from the diffuse X-ray background impinging from the bottom. A 500 μm thick Pb shield can solve this issue. The exact placement of such a shield (whether in the detector assembly or in the Module box) is still the subject of a trade-off study. The Pb shield should be located below any low-Z layer in the assembly (e.g., the Al box or the FEE board), in order to reduce the Pb fluorescence reaching the detector (a result of the reprocessing of high energy photons).

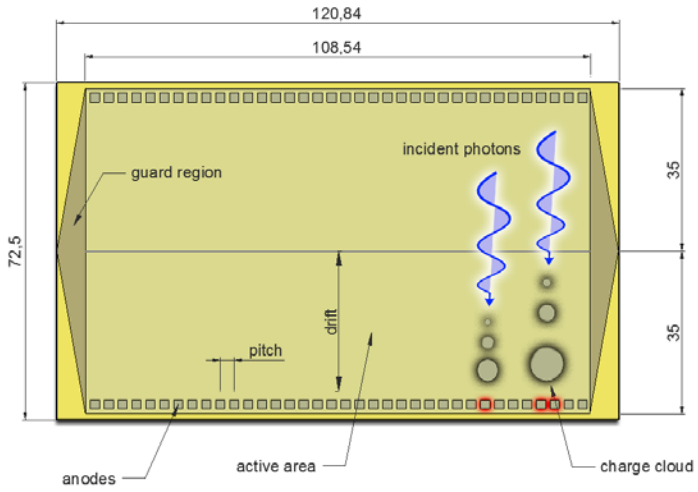

Figure 3-19: Dimensions and working principle of one Silicon Drift Detector

An updated mounting concept for the SDD is shown in Figure 3-20. The updated design is more resilient to CTE differences between the SDD PCBs and the detector module.

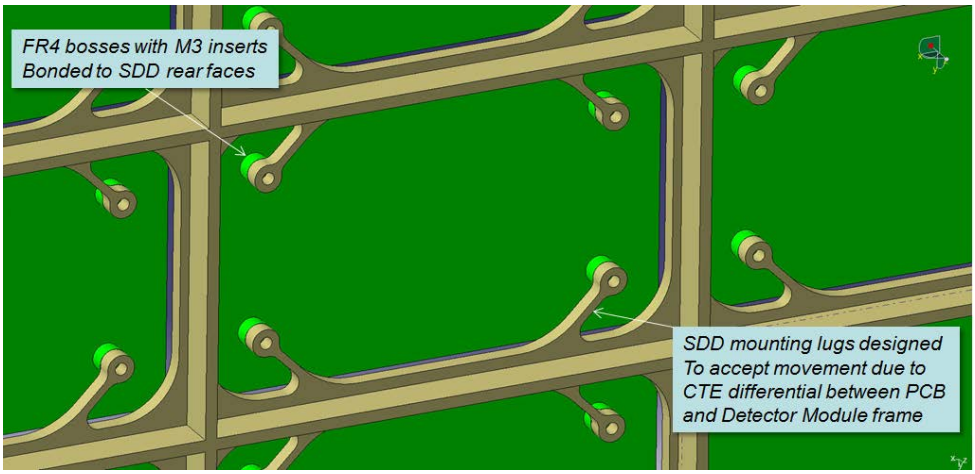

Figure 3-20: SDD/FEE mounting concept

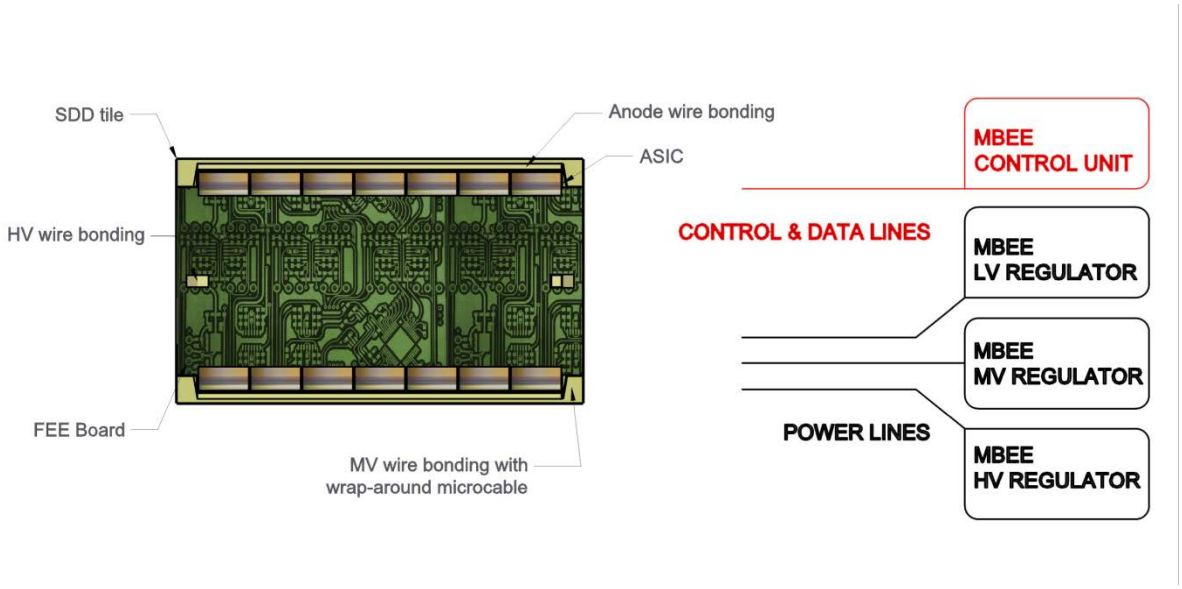

Figure 3-21: The back side of the LOFT detector, showing the front-end electronics and connections

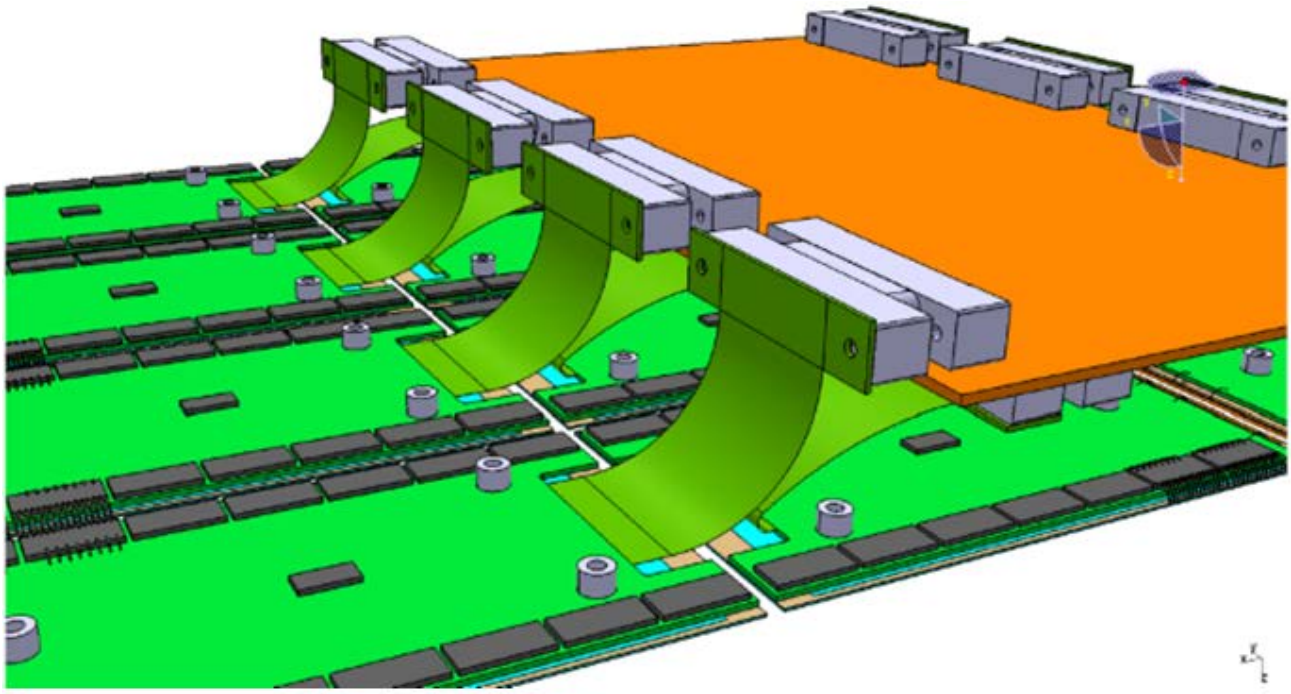

Figure 3-22: LOFT-LAD FEE (showing ASICS) to MBEE interfacing concept; separate connectors interface each FEE to the common MBEE - connectors are located to aid AIV

3.3.6.4 Collimator

The baseline collimator design has been improved. This design has several key advantages, including:

- Improvement in size: 8 x 11cm^2 (was 4 x 4 cm^2)
- Good TRL (provided by relevant heritage)
- Established manufacturing facility in Europe (Photonis, Brive-la-Gaillarde).

The revised design solution offers alternative mounting concepts, including clamping or gluing (will be the subject of a further review, prior to the end of phase review).

3.3.6.4.1 Collimator mounting concepts

The updated collimator mounting concept is summarised in Figure 3-23; showing 2 collimators per detector, i.e. the worst case scenario. The current baseline is a single collimator; which will actually be less demanding in terms of both manufacture and alignment.

A cut-through image of the collimator fixing is provided, also in Figure 3-23 (right image). This image shows the location/function of the beryllium copper springs, which are used to secure the MPO in place while also preventing damage to the sides of the optics. With such a clamping arrangement, the collimator frame can be made of Aluminium, which provides (with respect to the Ti-frame design with bonded MCPs) advantages in mass and a CTE which is matched to the Module structure which is also Aluminium. A complete module collimator is shown in Figure 3-24.

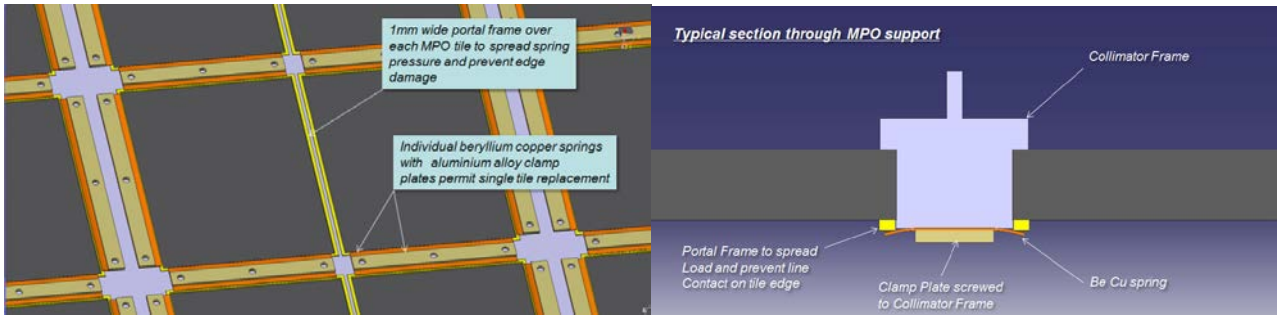

Figure 3-23: Collimator mounting concept; (left: zoomed in view showing the individual collimators, right: cut-though)

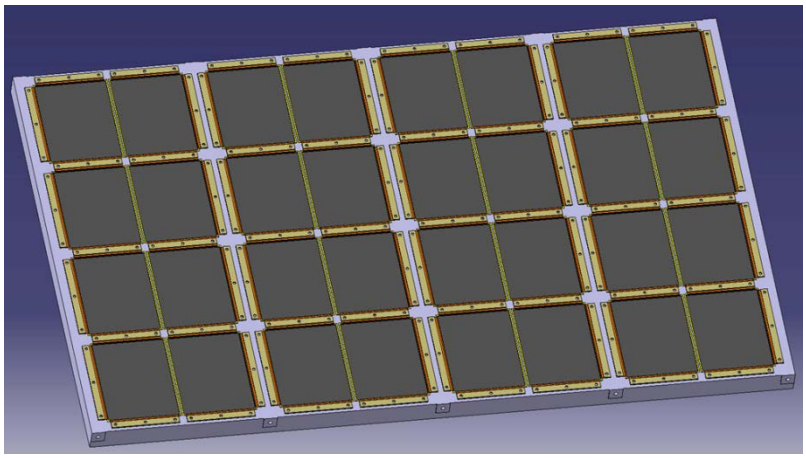

Figure 3-24: Complete module collimator configuration

3.3.6.5 LAD effective area breakdown

In the following we show the approach to derive the value of the effective area of the LAD at 8 keV.

In the payload consortium baseline (similar to ESA CDF), each LAD panel has external dimensions of 3.598 x 0.966 x 0.1 m^3, thus the total surface (considering 6 panels) is 6 x (3.598 x 0.966) m^2 = *20.85 m^2*. This number represents the total *LAD surface envelope (including detectors and mechanics).*

Each Panel hosts 21 (3 x 7) Modules, each one with external dimensions of 51.2 x 32.0 cm^2. A module accommodates 16 (4 x 4) SDD tiles, each one with external dimensions of 12.084 x 7.25 cm^2 = 87.609 cm^2. In the following we will call this area the *SDD geometrical area*. The overall *LAD geometrical area* can be calculated considering that the LAD is composed by 16 SDD tiles (1 Module) x 21 Module (1 Panel) x 6 Panels (LAD) = 2016 SDDs, which corresponds to 2016 x 87.609 = 176619.7 cm^2 = *17.66 m^2* (LAD *Geometrical Area*).

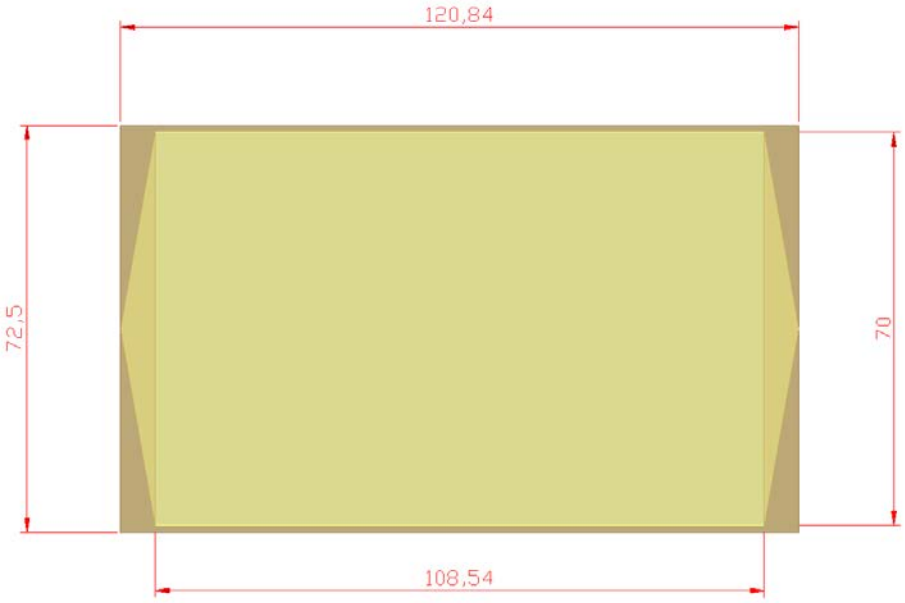

Figure 3-25: LOFT/LAD Silicon Drift Detector, the total geometrical area is 12.084 x 7.25 = 87.609 cm^2, the active area (green region) is 10.854 x 7.0 = 75.98 cm^2

As shown in Figure 3-25, each SDD has an *active area* of 10.854 x 7.0 = 75.978 cm^2, which corresponds to a total *LAD active area* of 2016 x 75.978 cm^2 = *15.32 m^2*. We can translate the *LAD active area* into the instrument *sensitive area* by taking into account:

- The MCP collimator Open Area Ratio (OAR, 70%)
- The efficiency of the 450 µm thick Silicon detector in the LAD energy band, including the Si quantum efficiency, as well as the absorption by the dead-layers on the SDD surface and by the LAD optical-thermal filter (97%)
- The area reduction due to the misalignments internal to a Module (1%)
- The area reduction due to the blocked collimator (0.8%).

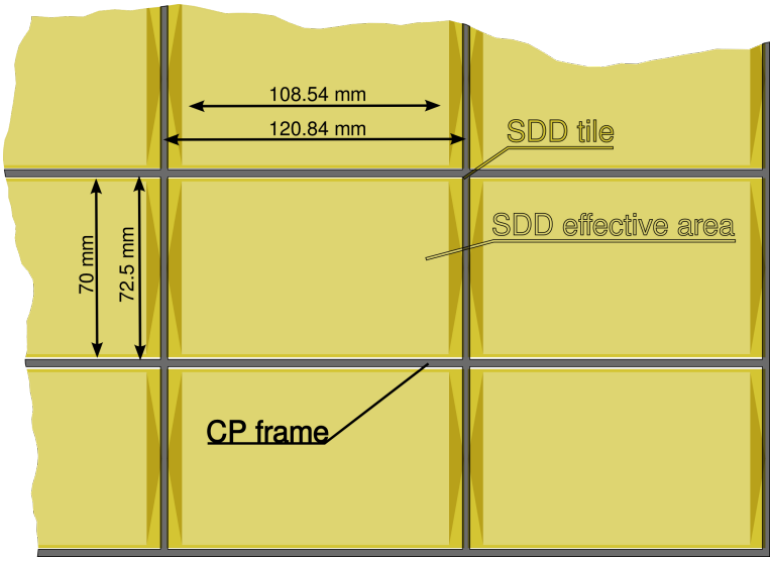

Figure 3-26: Baseline mounting of the MCP collimator on one SDD tile (yellow: SDD; grey: MCP tile)

At 8 keV, the QE of a 450 μm thick Silicon detector is 1, but the dead layers on the surface (e.g. the cathodes etc.) and the absorption by the optical-thermal filter decreases this value down to 0.971. Taking into account an OAR of 0.7 for the MCP and the 0.97% area loss due to the internal misalignment of the Module (35 arcsec over a 60' field of view). The resulting *LAD effective area* is:

$$2016 \times [\ 0.7 \times 75.978 \times 0.971 \times 0.9903 \times 0.992\ ] = 10.23\ m^2$$

In Table 3-5 we summarise the LAD characteristic areas at 8keV. This calculation takes into account the X-ray transparency of the thermal screen (see Section 3.3.5.2). An additional loss in effective area due to Module-Module or Panel-Panel misalignment is not accounted for here; a maximum mechanical misalignment of any Module with respect to the AOCS reference frame of 2.5' is sufficient to limit the loss in A_eff of these misalignments to 5%.

Item	Value [m^2]	Note
Surface	20.85	overall LAD surface (includes detectors and mechanical frames)
Geometrical Area	17.66	total surface of the Silicon tiles
Active Area	15.32	total sensitive area of the Silicon tiles
Effective Area (@ 8 keV)	10.25	total effective area of the LAD instrument

Table 3-5: LAD characteristic quantities

3.3.6.6 Background

Table 3-5 provides the background requirement as <10 mCrab, with a goal of <5 mCrab. The background has been assessed by means of Geant Montecarlo simulations, including both particle and X-ray background (diffuse and Earth albedo), as well as internal radioactivity of K40 contaminating the MCP glass. Results show that the dominant background sources are expected to be the cosmic diffuse X-ray background (CXB) and albedo X-rays from the Earth's atmosphere leaking through the collimator. Particle background can be reduced significantly by rejecting events above the LAD energy range, and events across multiple anodes. The overall background rate is equivalent to ~10-15mCrab. However, the background with respect to a 10 mCrab source varies spectrally, as shown in Figure 3-31a. Below 10 keV (which is the most important energy range for science) the background is significantly smaller than the required 10 mCrab, whereas above ~10 keV, the 10 mCrab countrate falls off more steeply than the background (which is dominated as stated above by diffuse CXB and Earth albedo X-rays).

A specific working group worked to study the background level and expected variability, primarily to determine and minimize the residual systematic uncertainty to be expected after background modelling and subtraction. The outcome of the working group was presented at the Tuebingen consortium meeting and will shortly be reported in a Technical Note. Two main proposals have come from these studies aimed at improving the control on the instrumental background:

- Include a “blocked collimator” in one (or more) module: the same glass optical thickness (mass and stopping power), but with no aperture, to monitor the internal background continuously
- Extend the energy range of the WFM up to 80 keV, to monitor the potentially contaminating point-like sources for the LAD.

Both these proposals have been indeed baselined. Based on the aforementioned analysis, the residual systematic uncertainty on the LAD background is now expected to be <0.25%.

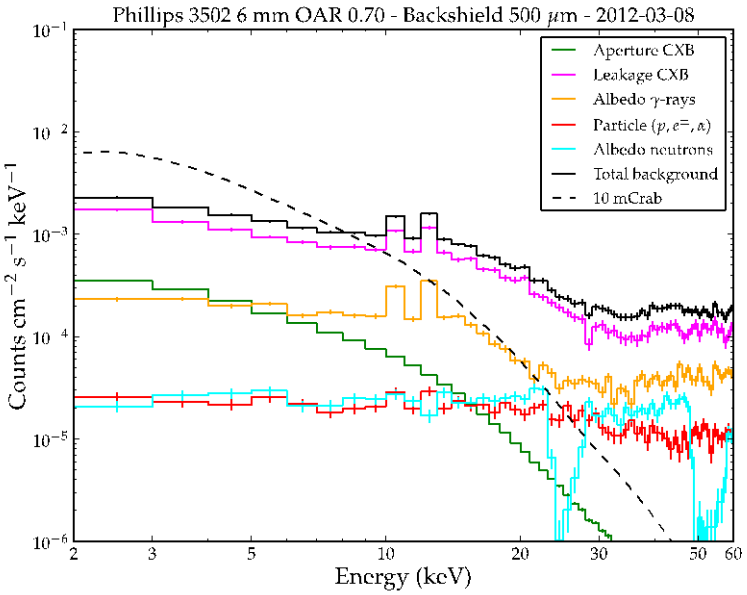

Figure 3-31a: LAD background components compared to a 10 mCrab spectrum(dashed)

3.3.7 Instrument unit thermal design

Considering the large extension of the experiment and the power limitations, the thermal control has to be passive. The required operating temperature of the LAD detectors is -32°C or below in the worst-case orbit. The temperature stability (for a steady-state attitude) is required to be within 5°C on the orbital time scale and similarly over the observation timescale.

Note: of course changes in attitude will lead to larger temperature transients – these will incur periods where scientific performance requirements are not met, which have to be considered in the overall observation availability of the spacecraft.

The structure of the LAD experiment is favourable for a passive control. The power dissipation is uniformly distributed over the whole LAD area. At Module level, the power is mostly evenly absorbed by the FEE boards (60%) and the Module Back End Electronics (MBEE, 40%). The large surface of the LAD has a large radiative potential. The back side of the Module will be used as a radiator (for this reason the mechanical structure of the panel is a grid). The FEE boards will have a direct thermal path to the module box. The larger

radiating surface of the detector module with respect to the MBEE should favour a lower temperature for the SDD+FEE than for the MBEE, as desirable.

The front-side of the LAD will use both the micro-capillary plate's collimator and a thermal screen as thermal insulators. Concerning the former, deposition of an 80 nm thick self-supporting Aluminium layer on the channel entrances provides a low absorptivity, low emissivity (α and ε both ~0.1) thermal control surface. The field of view of the collimator will also be covered with a thermal screen. The latter was identified in the proposal as 1 μm thick Polyimide covered with 0.04μm Aluminium on both sides (0.08 μm total). This is based on the design by LUXEL of the self-standing filters flown in the Chandra HRC (0.6 μm Polyimide covered with 0.08 μm Aluminium, 10 cm x 10 cm surface, self-standing). For the LAD, each filter can be mounted above each collimator, at detector size. In this case the size of the individual filter is smaller than that of Chandra. The soft X-ray transparency is >90% at 2 keV and the optical transmission is $<10^{-6}$.The thermal analysis of the LAD, including the choice and the mounting of the thermal screen, will be carried out during the study. The sides of the panel as well as the areas outside the field of view will be shielded with a MLI, as required.

During the assessment study we will aim at configuring the thermal design to further refine the thermal requirements within the science constraints, e.g. goal of increasing the sky coverage. A schematic summarising the LOFT-LAD reduced thermal model is provided in Figure 3-27.

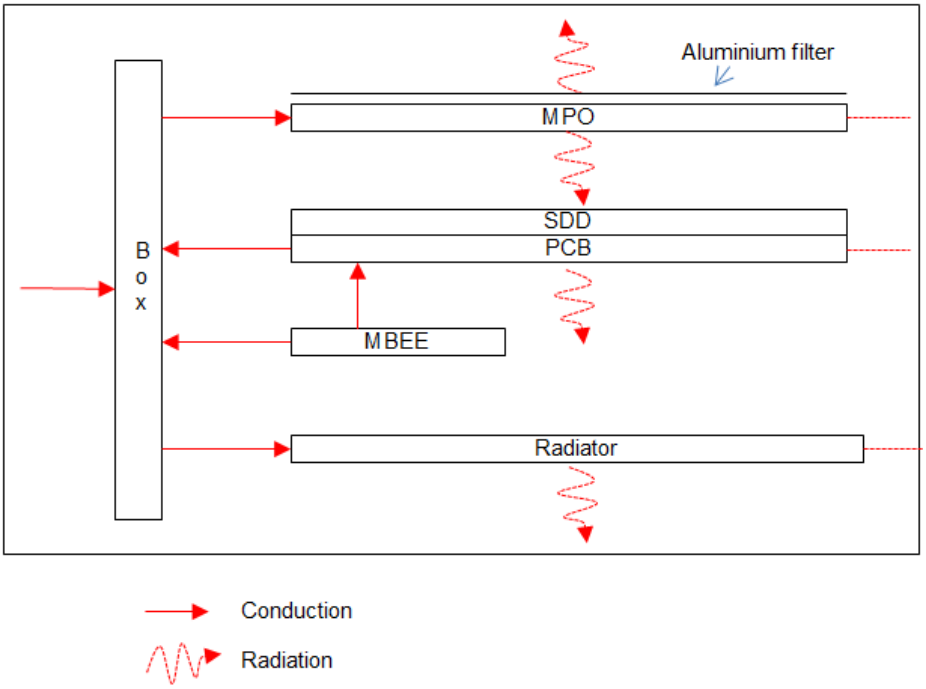

Figure 3-27: LOFT-LAD reduced thermal model schematic

3.3.8 Electrical design

3.3.8.1 Signal Processing

The LAD front-end read-out architecture is based on an ASIC whose main building blocks (both analogue and digital) will: discriminate good events above the noise level and collect, amplify and convert the analogue charge signals that are generated on the SDD anodes by the detection of an X-ray photon, into digital values. The ASIC is the core of the Front-End Electronics (FEE) which in turn takes care of the interface between the detector and the digital electronics. The signals will then be fed into the Module Back End Electronics (MBEE), from there to the Panel Back End Electronics (PBEE) and finally to the Data Handling unit (DHU). There are 16 anodes to each ASIC, 14 ASICs to readout each detector (7 on each side), 16 detectors per MBEE, 21 MBEEs per Panel and 6 PBEEs in total in the current design.

In the event of a signal charge above a pre-defined threshold on at least one anode, the LAD ASIC will store all anode charges in an analogue memory and send a trigger signal to the MBEE, waiting for validation of the signal from the MBEE (i.e. "A/D conversion" or "reset" via an MBEE command). Due to LAD SDD pitch size (about 1 mm), the charge generated by an X-ray photon event will typically affect only one or two anodes, which may in turn be connected to physically different ASICs. In such cases (i.e. a trigger generated by the first or last ASIC channel), the neighbouring ASIC will also be forced directly into the analogue storage of the charges via a dedicated line between the ASICs.

In addition to provide the full analogue signal processing chain, the main functions performed by the ASIC (Figure 3-28) are:

- trigger detection
- providing the trigger map of all triggered anodes
- A/D conversion.

When a trigger occurs in one of the channels in the FEE, a trigger signal is forwarded to the MBEE where a time tag is generated. The MBEE requests the trigger map from the ASIC and validates if only one or two adjacent anodes triggered. If the trigger map is invalid, i.e. more than two anodes triggered or the anodes are not adjacent, a command will be sent to the FEE to discard the event. A number of counters within the HK data at the MBEE keep track of the event types both accepted and rejected, as the control of the deadtime is a key feature for a timing experiment. If the event passes the selection criteria, the "A/D conversion" will be sent from the MBEE to the ASIC and the conversion will be carried out (inside the ASIC), providing an 11-bit output.

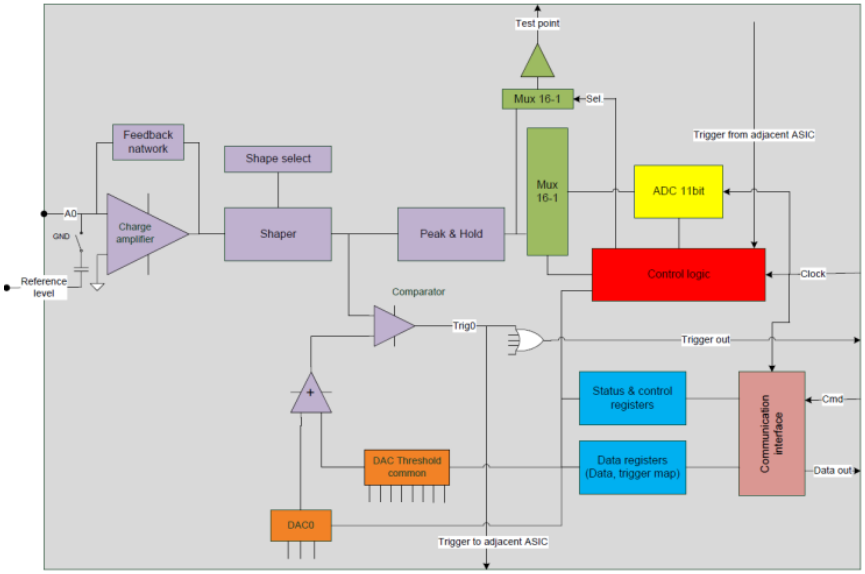

Figure 3-28: ASIC analogue section

Assuming a Wilkinson architecture (as derived from the STARX32 ASIC heritage), the time to complete the conversion is 102 µs (clock of 20 MHz) with a goal of 41 µs (clock of 50 MHz). For a 1 Crab source, the number of counts per detector side is 75 cts/s, thus the dead-time induced by the conversion will be below 0.7% (below 0.3% with 50 MHz clock). A trade-off study was performed on the dead-time and the decision was taken to prefer a slightly larger, but more consistent deadtime, which provides the advantage of a more precise dead-time knowledge. For this reason, all 7 ASICs on one side of the detector that are connected to one MBEE processing pipeline are on hold (inactive) during the short time (less than 2 us) until a triggered event is either acknowledged by the MBEE or discarded and also during the A/D conversion time. Although this increases slightly the deadtime, it allows a better control and homogeneity of the total dead-time / dead area for each event.
High energy events generated by Minimum Ionizing Particles will generally trigger more than two anodes and are therefore generally rejected before the A/D conversion. In cases where such an event only triggers one or two anodes, the data will be handled like a regular event and will be discarded after it passes through the processing pipeline of the MBEE - for being outside the valid event amplitude thresholds. As we are not expecting many events to fall into this category, these will not have a significant effect on the telemetry rate between FEE and MBEE.

Following the A/D conversion, the MBEE processing pipeline will be activated. The saved time tag will be added to the event package at the end of the processing pipeline. The time tag will be based on a 1 MHz clock provided by the DHU, synchronized once per second with the Pulse Per Second (PPS) received from the GPS. The MBEE will record the difference between the clock and the 1-s time elapse - on a one second basis/each second – to construct an On-board Time Correction. The main processing functions of the MBEE are:

- time tagging
- trigger validation and filtering

- pedestal subtraction
- common noise subtraction
- energy reconstruction
- event threshold application
- differential time calculation
- event reformatting
- Housekeeping data.

The MBEE is designed to process the events within a pipeline structure that handles the events from one side of a detector (7 ASICs). This pipeline is initiated 32 times within the MBEE FPGA (see section below) to allow processing of data from all 16 detectors simultaneously. All of the following steps of the pipeline are designed such that the processing time within each step is the same and shorter than the A/D conversion time of a following event. In this way, the data processing in the MBEE does not inflict additional dead-time and the pipeline is always ready for the next event.

The first step within each pipeline is the pedestal subtraction. A set of pedestal values (one for each anode) is stored within the MBEE. These values can be either uploaded from ground via telecommand or measured and adjusted on-board. After the subtraction of the pedestal value, the common noise (CN) is calculated and subtracted from the signal. The CN is a noise component common to all the channels connected to the same ASIC caused by the induced charge. This undesired baseline shift is composed of two effects: the CN produced by the detector and the CN introduced by the ASIC. Thus, the CN will be calculated independently for each event considering only the channels that are not affected by the charge cloud, i.e. the non-triggered anodes. Depending on the number of triggered anodes, the event will be graded as a type 1 or type 2 event (see Figure 3-39). The CN value is calculated by using a mean value algorithm on all un-triggered values.
After the CN subtraction, the energy of the event will be reconstructed. Each anode has an individual gain factor which is saved in a lookup table in the MBEE. These values are either uploaded from ground or can be automatically adjusted (see below) for use. The procedure of the energy reconstruction consists of the following steps:

1) Temperature adjustment of the gain: The gain calibration for each anode will be performed at a fixed temperature and a gain variability factor of 0.1% per degree is assumed (to be confirmed by on-ground calibrations). A linear correction E=E*(1-C*(T-T0)) is applied to the energy value of the event. For a realistic max 5^{o}C for T-T0, we obtain a correction factor C of 150 eV at 30 keV which is not negligible. A TBD number of temperature sensors (part of the payload) per detector module will monitor the temperature and the gain for each channel will be automatically adjusted according to the temperature readings.
2) Gain correction: The reconstructed energy of the event is the sum of the triggered channels, each multiplied by its individual, temperature corrected, gain factor.
3) Threshold Rejection: In each pipeline there are two values stored for an upper and lower energy threshold. High energy events, which only triggered one or two anodes and were therefore not rejected earlier, will show an energy above this threshold and will be discarded. Events which fall below the lower energy threshold after the subtraction of the CN and the pedestal noise will be also discarded, due to the fact

that most likely not the whole event was measured. Each discarded event will be counted in the housekeeping data, where the rates are monitored.

4) Energy Scaling: For a valid event the last step is the energy reconstruction into the final 9 bit energy word according to a pre-determined non-linear function. The energy resolution will have two energy regimes: 2 keV to 30 keV with 60 eV per digit and 30 keV to 80 keV with 2 keV per digit.

In the final event packet, the differential time is used instead of the absolute time for the time tags in order to reduce the amount of data to transfer to the PBEE and to the DHU. To calculate the differential time, the events are first stored within a common output buffer in the MBEE, taking all 16 detectors (32 pipelines) into account.

The events are reordered if necessary and the time difference between the individual events is calculated. An evaluation of the best calculation method will show if a negative differential time can be used, hence avoiding the reordering of the individual event packages. If the evaluated differential time is greater than the upper limit of the codable range, a dummy event will be generated to avoid loss of the relative time stamp. In addition, every 100 ms an Absolute Time Event will be generated to be able to resynchronize, if necessary. The final event-packet at the output of the MBEE is based on a 24 bit format.

Another important task of the MBEE is the creation and monitoring of the housekeeping data. Voltages, currents and temperatures. in each module are measured with a specific housekeeping board, which is located next to the signal processing board. These sensors monitor the health of the individual module and provide housekeeping data, which is sent directly to the PBEE where it is bundled to individual housekeeping packets. On MBEE level, the housekeeping consists of individual count rates of the valid and invalid events, time synchronizing discrepancies, and of the numerous temperatures, currents and voltages measured by the housekeeping board.

The Panel Back-End Electronics (PBEE) handles all events from the 21 individual modules of one of the six detector panels. It is the heart of the data acquisition and signal processing, located between the individual modules and the DHU on the satellite bus. The main tasks of the PBEE are:

- Interfacing the 21 MBEEs
- Collecting and buffering the event packets
- Reformatting the differential timestamp to reduce the number of dummy events.
- Reformatting the data to binned data depending on the observation mode
- Transferring the data to the DHU
- Collection of HK data and creation of HK packets.

For a 500 mCrab (15 Crab) source, the transmission rate from one MBEE to the PBEE will be 950 cts/s (28570 cts/s) or 23 kbps (886 kbps). With a total of 126 individual modules in LOFT it is therefore obvious that a very bright source exceeds the telemetry limit by far and data cannot be kept in the normal event-by-event mode. Depending on user selectable criteria, the DHU will automatically switch the PBEE into a different observation mode,

where the PBEE will reformat the data into the so-called binned data, i.e. generate spectra for individual adjustable time scales, where the number of energy bins and the integration time are flexibly adjustable. In this way, the data rate for brighter sources can be kept from exceeding the telemetry limit during longer observations and prevent an overflow of the mass memory.

For very low count rates, dummy time events from all 21 modules will dominate the data transferred from MBEE to PBEE. To reduce the overall telemetry, the PBEE generates differential timestamps for all the events from the 21 modules by calculating their absolute time and then creating a new differential time stamp.

The PBEE is also responsible to receive and monitor the HK data from the individual MBEEs. As the data gets sent to the PBEE, a housekeeping packet will be created every few seconds, including all health information of the individual detectors, rates of valid and invalid events.

There is no redundancy at the PBEE level. A cold redundant PBEE would mean doubling all the cabling on the panel. Although it is a critical point of failure for a whole detector panel, no redundancy is planned, as the loss of one of the six panels would not compromise the scientific goals of this mission. In the case of a SC design with less Detector Panels, segmentation of the PBEE may be necessary in order to maintain an appropriate level of graceful degradation in the event of a single PBEE failure.

The main functions of the DH are:

- Interfacing the PBEEs
- Interfacing the spacecraft OBDH
- Instrument configuration
- Control of mass memory
- Data processing compression
- HK collection
- Health monitoring/calibration.

The data handling electronics (or data handling unit - DHU) forms the ‘major’ controlling element of the instrument. It provides an interface to the spacecraft OBDH and also control of the LOFT instrument sub-systems. At the heart of the data handling unit is the processor (current baseline is a LEON), chosen for its additional flexibility - when compared to a hardware only architecture, i.e. a state-machine.

Software State	Description
Boot	This state is entered on power up and is running the bootstrap code from PROM. It is used to load, dump and run the main application code. The main application code can be loaded from the ground or be copied and run from EEPROM. Secondary rails and high voltages are off.
Safe	Safe is the first state entered when invoking the operational code. Initially only the DHU is on. All command and telemetry types are supported in the application code and the instrument can be safely powered off.

Idle	The idle software state is used whenever the instrument is not performing science or engineering tasks. It is important to note that even if the instrument is not acquiring data, the DHU should remain on in order to further process already acquired data and interact with the OBDH.
Science	The Science software manages the science operations. It provides full access to secondary rails.
Engineering	The engineering software manages the engineering support operations, including health check and limited calibration.

Table 3-6: Modes of the DHU

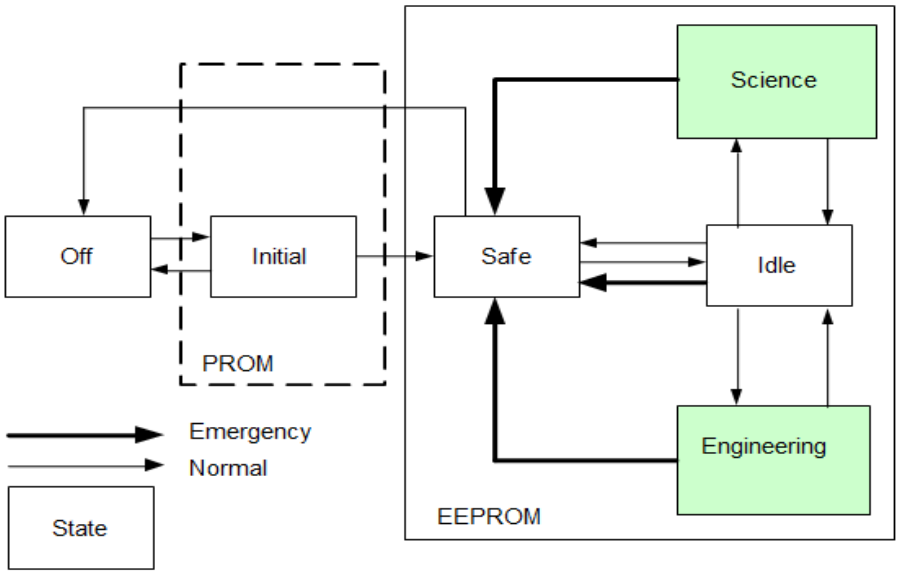

Figure 3-29: DHU modes and transitions

In addition to interfacing with the OBDH, the DHU is responsible for the following tasks:

- Instrument Configuration: At power on (or following reset) the DHU will configure the LAD to a pre-defined state. This will be through a combination of both hardware and software interactions: loading of tables, configuration of registers, etc. The proposed state transitions are shown in Figure 3-42 and the various modes of the DHU are summarised in Table 3-8.
- Health monitoring / instrument calibration: Support will be provided by the DHU for diagnostic operations; this includes:

    - Thermal control of the payload (if required)
    - Limited calibration procedures
    - Powering up/down and enabling/disabling selected subsystems for fault-checking.

- Command/data interface: The DHU will receive commands from the OBDH and act on them accordingly; mainly through software interaction. Commands will be stored on-board while waiting for their processing – various command priorities will be available. Time information will be created based on inputs from UT and GPS;

which in turn will be distributed via the PBEEs to the MBEEs and used for the synchronisation of telemetry.

- Housekeeping: The DHU will monitor housekeeping sensors in order to monitor configuration status and instrument health. Housekeeping will be polled on a regular basis; frequency is dependent on exact function. For example supply rail currents will require a relatively high polling frequency.

- Watchdog: a watchdog facility is included in order to guard instrument health. The watchdog must be polled on a regular basis (by the processor) in order to prevent it 'tripping': which would cause a reset of the instrument; and a return to basic mode (software).
- Data storage: Temporary data storage will be provided. This will be used to store 'raw' data in advance of its processing and also for its later compression (if required).
- Data compression: A dedicated data compression solution is currently baselined to be included in the DHU; this is in order to reserve processor resources for more appropriate tasks. The data compression device would be either ASIC or FPGA.
- Science data processing: The DHU will manage observation sequences and collect data in a pre-defined manner. The data will be processed in order to extract the required data product and also to reduce telemetry requirements. LOFT data processing is relatively flexible based on the use of an on board processor to allow for such cases.

The overall data flow is illustrated in
Figure 3-30. Monte Carlo studies show that for the majority of sources that will be observed with LOFT the generated data stay within the allocated telemetry limits. For a total of 6.68 Gbit/orbit this corresponds to 1113 kbps (~100 minute between ground contacts). The WFM should always be less than 10% of the total bandwidth, thus, the available rate for the LAD is ~ 1 Mbps. Strong sources with flux above a threshold of ~500 mCrab however generate data rates greater than the available rate. In these particular cases it is foreseen to store the excess data on board in a mass memory internal to the instrument and download it during following observations of weaker sources.

In order to size this internal mass memory, Monte Carlo simulations based on following exactly the RXTE source observing plans were performed and the detected rates were up-scaled to meet the LOFT detection parameters. The outcome of this simulation shows that following this observation plan, the mass memory would gradually fill up during the mission instead of being emptied now and then with observations producing less data. However, this result assumes taking all data in the event-by-event mode. One solution that will address this issue is therefore to observe brighter sources in the binned data mode, where customizable spectra (regarding the number of bins, and the integration time) are integrated already on board by the PBEE and single events are no longer transmitted. First simulation results show that a mass memory of 64 GB is sufficient (worst case) to ensure the storage and eventual download of all science data when switching to the binned data mode for sources above 500 mCrab.

More detailed follow-up simulations implementing a dedicated LOFT observation plan and with spectral and temporal resolution in the binned mode set according to realistic science goals for each observation will determine that threshold more precisely. Again note that this memory is located within the instrument DHUs and is not provided by the platform. Cold redundancy is planned for the DHU and PSU and it was accounted for in the mass budget.

Note: the PSU functionality is now baselined to be split between the PBEE/MBEE units; currently it is accounted for the mass budget of the LAD as a separate item, but this will be updated when the power switching architecture is finalised.

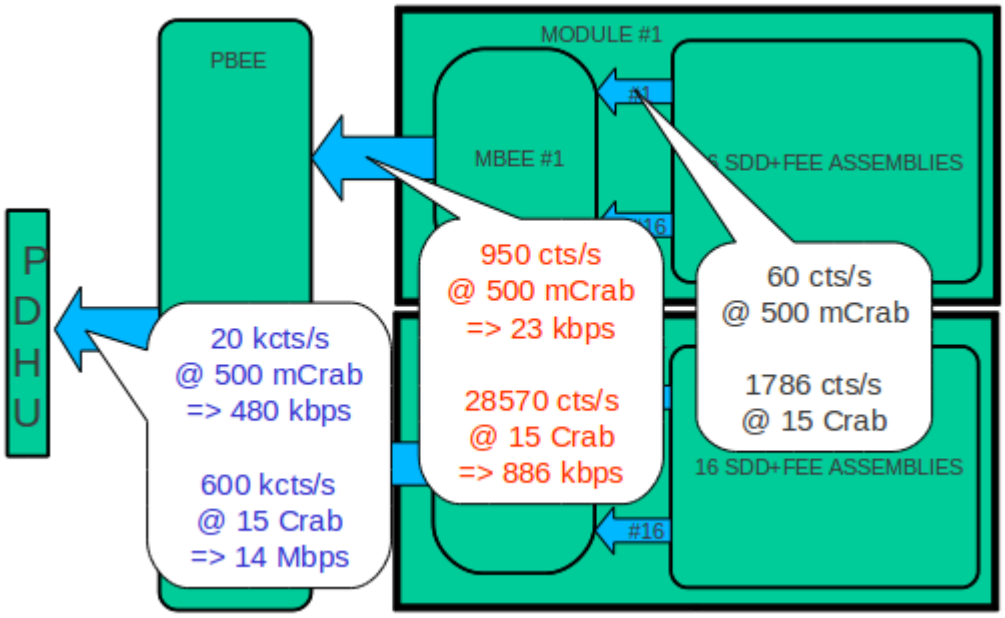

Figure 3-30: LAD Data Flow

3.3.8.2 Electrical Design and Components

The SDD detectors require a high voltage power supply (HV, nominal -1300 V, for the drift field) and a medium voltage power supply (MV, nominal -100 V, for the last portion of the voltage divider and the pull-up cathodes). The front end and back-end electronics require a low voltage power supply (LV, nominal 3.3 V and 5 V). As a baseline it is assumed that 50 V power supply will reach each Panel Back Electronics Board (PBEE) where it will be DC/DC converted and/or distributed to the MBEE and to the detector afterwards.

The interface between MBEE and FEE for the configuration of the ASICs and the transfer of trigger and energy signals to the MBEE will be a custom interface with LVDS connectors. Because of the high number of instances of this specific interface, data will be transferred serially in order to reduce the cable harness. It is anticipated that the final implementation of the ASIC solution will be as a daisy chain. The number of lines has an impact on the selection of the FPGA which is foreseen to perform the MBEE tasks due to the number of available I/Os for the different model families and packages. The current baseline device is the radiation-hard Actel RTAX 2000S with a clock frequency of 40 MHz. Depending on the

final design of the ASIC, a larger device with more I/Os and also a higher power consumption might become necessary.

The interface between MBEE and PBEE is a simple P2P high-speed serial interface. As shown above, typical rates are about 1 Mb/s. A number of off-the-shelf interfaces are available. The current baseline is to use a SpaceWire interface for the data and TC/configuration transmission. Additional lines are foreseen for the PPS and HK data.
The PBEE also features an FPGA. To achieve the reformatting of the event packets into the spectra at very high speeds and also the fast data transmission to the HD, a Xilinx Virtex-IV FPGA is foreseen, running at 100 MHz. A backup solution is to operate a larger Actel FPGA or more than one. The functional design of the PBEE is based on an existing prototype of the HTRS data processing unit for the International X-ray Observatory IXO. It was able to demonstrate that event rates as high as 2.000.000 cts/s can be reformatted from event packets into spectra in realtime with a Virtex-IV FPGA.

A SpaceWire connection is foreseen for the interface between PBEE and DH. It will be used to transmit science data, commands, configurations and HK data. The pulse-per-second is again transmitted in a separate LVDS signal.

3.3.9 On-board software

The on-board software's main functions are instrument control & monitoring and science data processing & formatting. Software will allow the instrument to have the functionality that it requires (more complex than the standard repetitive processing of the ASICs and FPGAs) and the ability to be updated and work around problems automatically and after input from the ground. Instrument control will be possible through the software via telecommands from the ground (e.g., power on & off, set-up of ASICs and FPGAs, loading parameters for processing/on-board calibration, investigations) and autonomously on-board (e.g., mode switching, diagnostic data collection).

The software will implement some standard ECSS telecommand packets for housekeeping, memory maintenance, monitoring etc. and some standard ECSS telemetry packets for command acceptance, housekeeping, event reporting, memory management, function management, time management, science data, diagnostics etc.

The software will collect and format the acquired science event data. At the lowest level it will be able to monitor and setup the registers of each of the electronic elements of the event processing hierarchy. The data from the 6 panels will arrive at the processor board and be handled where possible by dedicated electronics under control by the software. The resulting data stream will have the remaining processing done (e.g., energy reconstruction) be binned as necessary, reformatted ready for compression (possibly with the help of an FPGA) and packetised. The software will interact with the Spacecraft solid state recorder, sending the data over SpaceWire for eventual transmission to ground.

The software will be able to send a wave of setup information to the hierarchy of processing elements and receive and process the housekeeping data coming back, simplifying this for a lower rate transmission to the ground.

The software would optimally run on a single space qualified processor, the Leon, and be written in C using the RTEMS operating system. RTEMS, being the real-time executive, will schedule the software tasks, each at different priorities and communicating with each other as necessary and any errors will be trapped and handled. A software-controlled hardware watchdog will be used to reboot in case of a hang.

The software will be written in separate parts. "Basic" software, stored in a very reliable PROM(s), the "Golden boot ROM", would have enough functionality to receive, store and execute new software. "Operational" software, stored in EEPROM, would have the functionality of the "Basic" software and also the full science capabilities. This way new software can be loaded to the instrument without losing the basic functionality even if that software is incorrectly produced, loaded or written to the wrong location. If there is any problem with the software interface to the spacecraft, a reboot or power off/on of the instrument will reset the software into the well-tested "Basic" mode which does not produce science data, getting the instrument back to a well-defined initial mode.

Error messages will be limited so that they are not repeated unnecessarily as this could cause unnecessary traffic to the Spacecraft.

As the software has to operate in a remote space environment, it will be written to be robust against errors, to report as much information as possible on any problems encountered and progress made (to help investigations) and perform any operations required by EDAC/scrubbing.

The interfaces between the software and the rest of the instrument/satellite would be as clean as possible with the processor and software taking over the processing of the events and diagnostic data at the point they are joined into a single stream from the panels, and interacting with the rest of the satellite through SpaceWire.

3.3.9.1 Software functionality

Apart from the normal engineering functionality of the software as mentioned earlier like housekeeping, limit checking and memory maintenance (including loading new code) the functionality includes:

- Setup and monitoring of detectors
- Pedestal measurement
    - Force triggers
    - Collect data
    - Calculate values
- Electrical calibration
    - Gain & off-set
- Manage the data compression and packetisation
- Manage the data prioritisation and storage including re-transmission
- Time management
    - Set the time on the MBEEs as they are powered
    - Check the MBEE synchronisation every second
    - Resynchronisation if necessary.

3.3.9.2 On-board software

The telemetry rate will be chosen based on the buffering ability of the instrument and the efficiency of the ground station (fraction of ground-passes lost). Because the science output is so high and the telemetry so low we need to not only bin data when the rates get high but also to prioritise the data in case of a missed ground-pass or a 'pre-prioritisation' event. Science data will be stored in a number of partitions of differing priority with the highest priority data being telemetered down in the middle (optimal part) of the ground-pass. Telemetry lost in a down-link (e.g., because of bad weather or an antenna problem) would have to be requested by telecommand for re-transmission and so the instrument's software would need to keep data after transmission for some time until it is safe to overwrite (delete).

Note: an evaluation of a TM-management system similar to that proposed for EUCLID is currently underway in order to deal more simply with the problem of re-transmission of failed downlinks.

3.3.9.2.1 Software data storage

The following data storage requirements are foreseen:

- 450 KByte required for detector definition
  - This includes 128 bit per ASIC: fine threshold, enable channels; ideally this would be able to be telecommanded to the instrument
- 2.7 MByte for calibration data
  - This is 1 pedestal and RMS for each channel and gain per channel; ideally this would be able to be telecommanded to the instrument
- 64 GByte for science storage (ready to be telemetered)
  - i.e. enough for more than 1 orbit (as ground-passes can be lost) and enough for a 15 Crab source for a short time (300 minutes, full event info).

3.3.9.2.2 Inter-instrument messaging

The LAD and WFM will be able to send messages to each other (directly or via the spacecraft) to coordinate such things as telemetry share. If one instrument is making an observation which requires little telemetry bandwidth, that bandwidth could be given to the other instrument for some time. This is especially important during calibration, faults or other engineering investigations.

3.3.9.2.3 Implications for operations

With the ability to prioritise on-board and a quick-turnaround of data on the ground, optimal use of telemetry could be made by using a quick-look facility after minimal processing of the data and re-prioritising the data still on board. The more desirable data could then be telemetered first and the less desirable telemetered last or deleted. This would depend on the on-board storage ability but in any case would need to be done within a few hours. Calibration could be done on a longer timescale. Calibration data would be telemetered, analysed on the ground and new updated calibration parameters telecommanded after a few days.

3.3.9.2.4 Software development

3.3.9.2.4.1 Processes and procedures

We shall follow a structured software engineering approach. Software engineering processes are fully in-line with "best practices" in the industry and compatible with ECSS software standards. This would begin with establishing system and software requirements and continue with architectural design, code development, integration and testing, deliveries, and continued support. Software development will follow ECSS-E-ST-40C, tailored appropriately.

3.3.9.2.4.2 Software product assurance

The Product Assurance team will have oversight of all Software activities and they and the software engineers have much experience over a number of projects of issue tracking and reporting using both individual project systems and systems. Software development will be performed in-line with the applicable ECSS standards. Version control software (e.g., cvs, svn or git) will be used to control software and documentation with proper messages and tags to track the state of the code through issue resolution, testing and delivery.

The approach followed is consistent with the ECSS-Q-80C standard, tailored appropriately. The software engineer, in conjunction with the PA team, shall establish a testing strategy which covers all stages from unit testing to acceptance testing.

3.3.9.2.4.3 Software development environment

Development tools running on Linux will be utilised with an emphasis on well tested software with a long lifetime, large user base, (e.g., GNU), development and testing tools which allow good version control, visibility and repeatability (e.g., make and shell scripts rather than graphical user input) and tools and simulators that can be accessed remotely to enable efficient development and long-term testing. There will be little reliance on proprietary/closed-source software and equipment which could be at risk of a single company dropping support.

3.3.10 Ground support equipment

The following Ground Support Equipment (GSE) is foreseen for the LOFT-LAD programme.

3.3.10.1 EGSE

- General electronics systems support equipment (power, conditioning, etc.)
- EGSE to command and monitor the operational parameters of the electronics systems
- Local EGSE: Providers of subsystems will provide subsystem simulators for interface testing at various levels of integration within the LAD (e.g. ASIC to module, module to panel)
- Software development system - sufficient for the development of algorithms and scripts (in advance of more representative hardware being made available from the prime)

- Spacecraft simulator (note: it is expected that this - consortium manufactured S/C simulator - will be replaced at a later date by the S/C prime)
- Data analysis tools.

3.3.10.2 MGSE

- Detector manufacture tools: sufficient for the assembly/dis-assembly and alignment of individual detectors/modules. Given the large number of units, automated systems will be developed where convenient.
- Alignment GSE for all levels of LOFT-LAD alignment, including:
  - Individual modules
  - Modules within panels
  - Inter-alignment of separate panels
- Transportation equipment (e.g. dolly's)
- Purge GSE + sufficiently clean gas supply (LOFT-LAD cleanliness)
- Shipping containers.

3.3.10.3 OGSE

- Optical performance (alignment verification) GSE
- Detector calibration GSE.

3.3.10.4 Facilities

3.3.10.4.1 Calibration

The following calibration facilities have been identified for the LOFT-LAD programme.

- Marshall (USA) - has a suitable source and is sufficiently large (7 m diameter) for a single panel
- Panther (Germany) – too small for the complete LOFT (4m).

Additional work will be performed during the assessment phase in order to identify alternative (additional) facilities.

3.3.10.4.2 Assembly, integration and verification

Current assumptions are that industry will provide the panels (including deployment mechanism, harness, etc.) and that the LOFT-LAD consortium will provide the modules (with mechanical interfaces) and all LAD electronic units as far as, and including, the LAD PDHU.

In terms of AIV, it is expected that the panels will be delivered from the prime contractor/ESA to Consortium where integration, alignment and calibration will be performed. This work will progress during the assessment phase of work.

3.3.11 Instrument mode description

3.3.11.1Science, Non-Science

3.3.11.1.1 Science modes

- One “full resolution” mode (baseline)
- Two user-defined modes (user-defined energy and time) with backup modes for when the count-rate goes above user-defined limits for user-defined times. A simple algorithm in the software would change the mode to a more highly binned mode if the count-rate exceeds a pre-defined rate for a pre-defined time. Then when the count-rate reduces below a (slightly lower) pre-defined rate for a (possible different) pre-defined time, the normal user-defined mode would resume.
- Two always-on modes: reduced time and reduced energy to give a consistent data set throughout the mission.
- "Reduced energy" mode (always enabled in science mode) would send fewer bits of energy data but more bits of time data.
- "Reduced time" mode (always enabled in science mode) would send fewer bits of time data but more bits of energy data.
- Ratemeters always on.
- Housekeeping always on.

3.3.11.1.2 Engineering modes

- "OnTheFlyConfigure" mode in which it is possible to do configure while observing so triggers can be altered "on the fly". This would effectively allow simulator mode as well in which trigger levels could be lowered to produce more events.
- "Diagnostic and Calibration" mode would send all information about events including absolute time-tags, raw charge data (as detected on anode before reconstruction), channel address. This mode will be activated for diagnostic and testing purposes as well as for module-by-module calibration.
- "Pedestal" mode would be aimed at measuring channel-by-channel the mean value and rms noise of the electronics signal chains. If requested by TC, the data analysis will be carried out on-board, otherwise, the raw will be sent on-ground. As a result, the pedestal measurement will permit to estimate the rms value of the common mode of each read-out ASIC.
- "Electrical Calibration" mode will be composed of two sub-modes: the gain measurement and the threshold scan. The first sub-mode is aimed at measuring the gain of the acquisition chains stimulating each channel with a stream of pulses with different amplitudes. The second sub-mode will be the repetition of the first with different threshold values. If requested by TC, the data analysis will be carried out on-board, otherwise, the raw will be sent on-ground. Note. This is the subject of on-going analysis: the possibility of running electrical calibrations of individual modules while the others are in observation mode.

3.3.11.2 Non-operating modes

A preliminary list of LAD non-operating modes is the following:

- OFF - Used during launch, failure recovery or power shortage
- SAFE - Used after anomaly detection and failure recovery.

LAD can be set up with independent modes for each module. The LAD Instrument will appear as a mosaic of 126 independent pieces, one for each module, able to guarantee the maximum flexibility in the scientific configuration. The software will adopt a unique observation mode to be configured by a dedicated telecommand, "LAD Scientific Set-up" with the data field composed of 3 enumerated parameters for each module (3 x 126 total parameters) reporting the set-up for the Nominal Orbital phase, the Earth Occultation Orbital phase and the SAA.

3.3.11.3 Orbital phases

The various orbital phases will have a default mode: “normal observing” during the nominal orbit phase; an observing mode or non-observing mode during SAGA.

- Nominal orbit phase, including when the SC is sunlit (constrained in Field of Regards) and in the shade of the Earth (unconstrained in Field of Regard, allowing for short-term observations during eclipse)
- "SAGA" mode would be for a different setup during the higher radiation of the South Atlantic Geomagnetic Anomaly (SAGA) when rates could be much higher from the background noise. This mode could be triggered by the Spacecraft as it would have knowledge of its position with a LAD software backup implemented by counting triggers above an upper limit.
- Earth occultation - when the source is occulted by the Earth, LAD will switch to this mode which may simply produce just ratemeters and housekeeping or switch to the proper mode (see below) to perform periodic electrical calibrations.

3.4 Mechanical interfaces and requirements

3.4.1 Location requirements

The main requirement for the LAD is the deployment of a minimum of 10 m^2 co-aligned effective area in orbit and its operation at temperature lower than a certain value, depending on orbit or radiation dose. Any configuration of the panel surface alternative to the baseline 6-panel design can be considered. As for the electronic boxes, the MBEE boxes should be close to their relevant Module for: clean LV, MV and HV regulation and uniformly distributed power dissipation.

As a baseline, the PBEE boxes are mechanically interfaced to each relevant Detector Panel. The main motivation for this choice is the possibility to test and calibrate the Detector Panel independently of its assembly on the optical bench. Alternative options are being considered as well (Sect. 3.6.1), as they may turn out to be more favourable on the thermal balance and cabling through the deployment hinges.

3.4.2 Alignment requirements

LAD is a pointed, narrow field, non-imaging experiment. As such, the basic requirement is the presence of the source in the field of view during the observation. The LAD field of view is determined by the collimator aperture 60 arcmin FWHM, to be traded). Since the main goal of the LAD is to measure the time-variability of the celestial sources with an unprecedentedly high statistical accuracy, a spurious modulation of the detected flux induced by the satellite attitude instability convolved with a steep response of the collimator should be avoided. The uncertainty is determined by the internal LAD collimator response and misalignment, and by the spacecraft attitude accuracy and stability. In this section we discuss the sources of uncertainty internal to the LAD instrument. A detailed discussion of the complex issue of alignment tolerances is reported in the MSSL Technical Note [RD 5], while the requirement on the "response stability" is discussed in[AD 2]. Here we summarise the overall error budget break-down.

3.4.2.1 LAD alignment error budget

The overall alignment error budget can be broken down in the following components:

- **MCP channel axis to surface:** The orthogonality between the capillary axes and the MCP surface is ~1 arcmin as the error between the expected direction of one channel axis and its real direction.
- **MCP to Module:** The angular error on the FoV central direction is about 0.43 arcmin.
- **Module to Panel:** Using an isostatic mounting strategy, it is possible to position the Module in the Panel structure with uncertainty of 0.59 arcmin.
- **Panel thermo-elastic deformations (temperature gradient):** Figure 3-31 (from [RD 5]) shows a sensitivity analysis of the panel structure to thermo-elastic deformations, as a function of the temperature gradients. For a LAD Detector Panel CFRP structure and a temperature gradient corresponding to the 10°C on the detectors, the deformation is <0.39 arc min.
- **Panel to optical bench:** The panel to optical bench alignment relies on the hinge line and the hinge interfaces. Under normal conditions (see RD05), the latched hinge angular spread is evaluated as 0.34 arc min.
- **Optical bench internal tolerance:** Evaluated as 0.5 arc min.

The total error budget is summarized in Table 3-7. This budget, convolved with the LAD collimator angular response, determines the requirements for the pointing. After the LAD integration, the alignment of the individual panels with respect to an optical reference on the spacecraft will be measured.

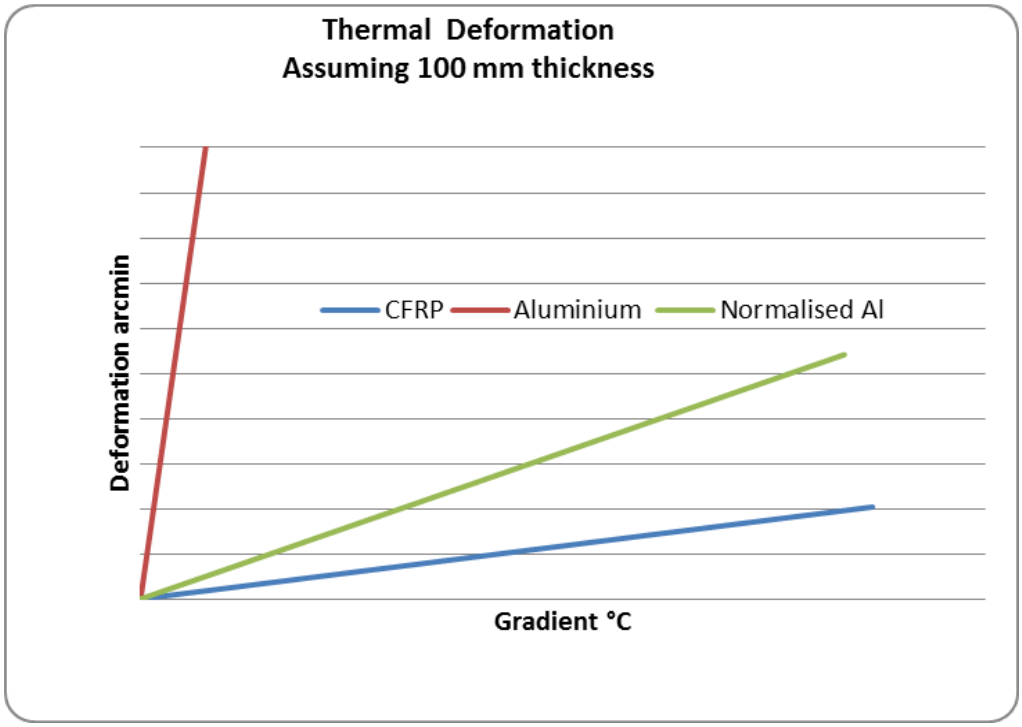

Figure 3-31: Panel angular deformation due to gradient over thickness

Item	error (arcmin)
Consortium responsible	
a. MCP internal	1.0
b. MCP-Module	0.43
Consortium subtotal (worst case)	1.43
Consortium subtotal (RSS)	1.09
Industry responsible	
c. Module-Panel	*0.59*
d. Thermo-elastic Panel deformation (10deg)	*0.39*
e. Panel-Optical Bench	*0.34*
Panel 1-g	*1.30*
f. Optical Bench	*0.50*
Industry subtotal (worst case)	*3.12*
Industry subtotal (RSS)	*1.60*
TOTAL (worst case)	4.55
TOTAL (RSS)	1.93

Table 3-7: The LAD internal alignment error budget breakdown. Items in italics are assessments by the consortium which now fall under industry responsibility, so should be considered as provisional

3.4.3 Pointing requirements and performance goals

The main pointing requirement for LOFT is derived from the LAD, according to the following:

- The target source should stay as close as possible to the centre of the collimator FOV (to maximize the effective area).
- During the observation the target source should not exit the 'flat-top' part of the collimator response (to avoid spurious modulation of the detected source flux to the AOCS feedback combined with the collimator response).

In the ideal case, with the satellite pointing infinitely accurate and stable, the LAD measurement would be unaffected by any internal misalignment (whatever it is, it would

be fixed). In reality, the satellite pointing will be somewhat inaccurate and unstable. The alignment tolerances in the previous section produce a natural 'rounded' (approximately Gaussian) top to the angular response, with a width ~4 to 5 arcmin, which makes the observation less sensitive to the pointing instability. Beyond this region, the collimator response is approximately triangular.

The result is that the requirement for effective area and temporal stability of the effective area (to avoid spurious time variation in the signal) is a combination of the shape of the effective area v. angle curve, and the accuracy and drifts of the pointing system. This has been analysed in [AD 2], where the requirement is now expressed in terms of pointing jitter. The AOCS is required to provide a 3-axes attitude control for pointing and slew using star trackers, Sun sensors, magnetometer, magnetic-torques, reaction wheels and gyroscopes. To comply with a short ground coverage period for up-link (about 8÷11 minutes per orbit), the AOCS shall be designed with a high level of autonomy. The AOCS is required to be programmable from ground to observe up to two separate targets per orbit (one exposure per target).

3.4.4 Interface control drawings

Interface Control Drawings are not yet available. Below we summarize the envelope dimensions of all components, as they are preliminarily estimated at this stage.

Panel
Width: 966 mm
Length: 3598 mm
Height: 100 mm

Module
Length: 512 mm
Width: 320 mm
Height: 40 mm

Panel Back End Electronics (PBEE)
Width: 220 mm
Length: 220 mm
Height: 100 mm

Module Back End Electronics (MBEE)
Width: 220 mm
Length: 220 mm
Height: 50 mm

LAD Data Handling Unit (DHU)
Width: TBC mm
Length: TBC mm
Height: TBC mm.

3.4.5 Instrument mass

The LAD mass budget has been updated with respect to the proposal, following a more accurate evaluation of the detector panel and module mechanics and components. Following discussions in the LOFT Science Study Team, the deployment mechanisms, including the tower, as well as the optical bench are no longer included in the LOFT payload and consequently in the LAD mass budget. The following table provides the LAD mass budget.

Margin	20%		
LAD mass budget	Basic	Margin	Nominal
LAD	654.34142	130.8683	785.2097
Number of DHU/PSU	2		
	12	2.4	14.4
Number of Modules	126		
Number of PBEE	6		
LAD Module	4.9074716	0.981494	5.888966
PBEE	2	0.4	2.4

Table 3-8: LAD BASELINE Mass Budget (all numbers in kg). Compared to the proposal LAD mass budget, this one does not include the support tower, the optical bench and part of the deployment mechanism (estimated as 145 kg CBE overall in the proposal). Also excluded are the hinges, panel structure and panel harness, now assumed to be industry-provided

Note: this mass budget has been modified by ESA study team during the AO-period to account for a risk that the increased collimator thickness has not been adequately reflected in the LAD Module mass budget – this will be confirmed with the payload consortium.

An important possible change to the mass budget of the LAD instrument would occur if the collimator technology choice was switched from the baseline glass-collimator, to the possible alternative Tantalum collimator technology from NRL. Should this switch occur, the LAD mass budget shall be as in the following table. This possible (probable?) change should be anticipated in the system design of LOFT.

Margin	20%		
LAD mass budget (Tantalum)	Basic	Margin	Nominal
LAD	812.96114	162.5922	975.5534
Number of DHU/PSU	2		
	12	2.4	14.4
Number of Modules	126		
Number of PBEE	6		
LAD Module	6.1663582	1.233272	7.39963
PBEE	2	0.4	2.4

Table 3-9: LAD Alternative Mass Budget (all numbers in kg) should the collimator technology switch to Tantalum

3.5 Thermal interfaces and requirements

The summary table of temperature requirements for the LAD instrument is given below – all values are TBC.

Component	NonOp Min [C]	NonOp Max [C]	OpMin [C]	OpMax [C]	StartUp [C]
SDD/FEE	-60	+60 (TBC)	-50	As given by operating temperature below	TBD
MBEE	-60	+40	-60	+40	TBD
PBEE	-60	+40	-60	+40	TBD
DHU	-60	+40	-60	+40	TBD

Table 3-10: Summary of LAD unit temperature requirements

3.5.1 Operating Temperature

The spectroscopy performance of the LAD is challenged by the radiation damage induced by the protons trapped in the SAA. [RD 4] shows the sensitivity of such an effect on the satellite orbit, and provides a definition of the SDD maximum temperatures required to achieve the desired energy resolution. Any orbit at lower inclination and/or smaller altitude will loosen the temperature constraints.

The following figures present the LAD-SDD energy resolution worsening at increasing temperature, for different orbits (different radiation doses) at the beginning of the Nominal Operations Phase (3 months into the mission) and at the end of the Nominal Operations Phase (4 years and 3 months into the mission); the 200eV and 295eV (single anode event) thresholds are shown. The corresponding tables present the required temperatures at 200eV and 295eV for the various candidate orbits.

Note: an update of [RD 4] will provide the same information as is presented in this document for the LAD SDD temperature requirements.

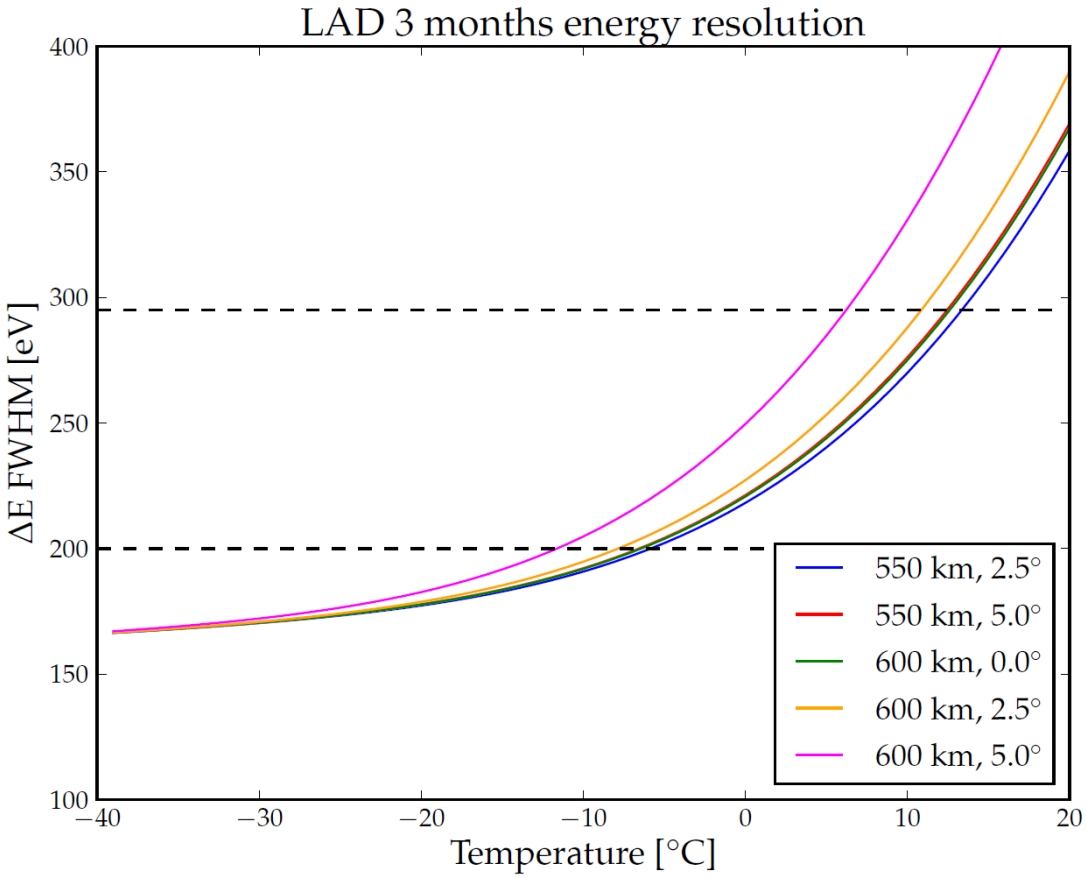

Figure 3-32: LAD-SDD energy resolution worsening at increasing temperature, for different orbits (different radiation doses) at the beginning of the Nominal Operations Phase (3 months into the mission); the 200eV and 295eV (single anode event) thresholds are shown

Orbit Altitude [km]	Orbit Inclination [°]	Maximum SDD Temperature

		[°C] within Nominal FoR
550	2.5	-6
550	5.0	-7
600	0	-7
600	2.5	-8
600	5.0	-12

Table 3-11: LAD SDD temperature requirements to fulfil the energy resolution requirement of 200eV FWHM @ 6keV (single anode events) at the beginning of the Nominal Operations Phase, for the candidate range of orbits

Orbit Altitude [km]	Orbit Inclination [°]	Maximum SDD Temperature [°C] within Degraded FoR
550	2.5	+13
550	5.0	+12
600	0	+12
600	2.5	+11
600	5.0	+6

Table 3-12: LAD SDD temperature requirements to fulfil the energy resolution requirement of 295eV FWHM @ 6keV (single anode events) at the beginning of the Nominal Operations Phase, for the candidate range of orbits

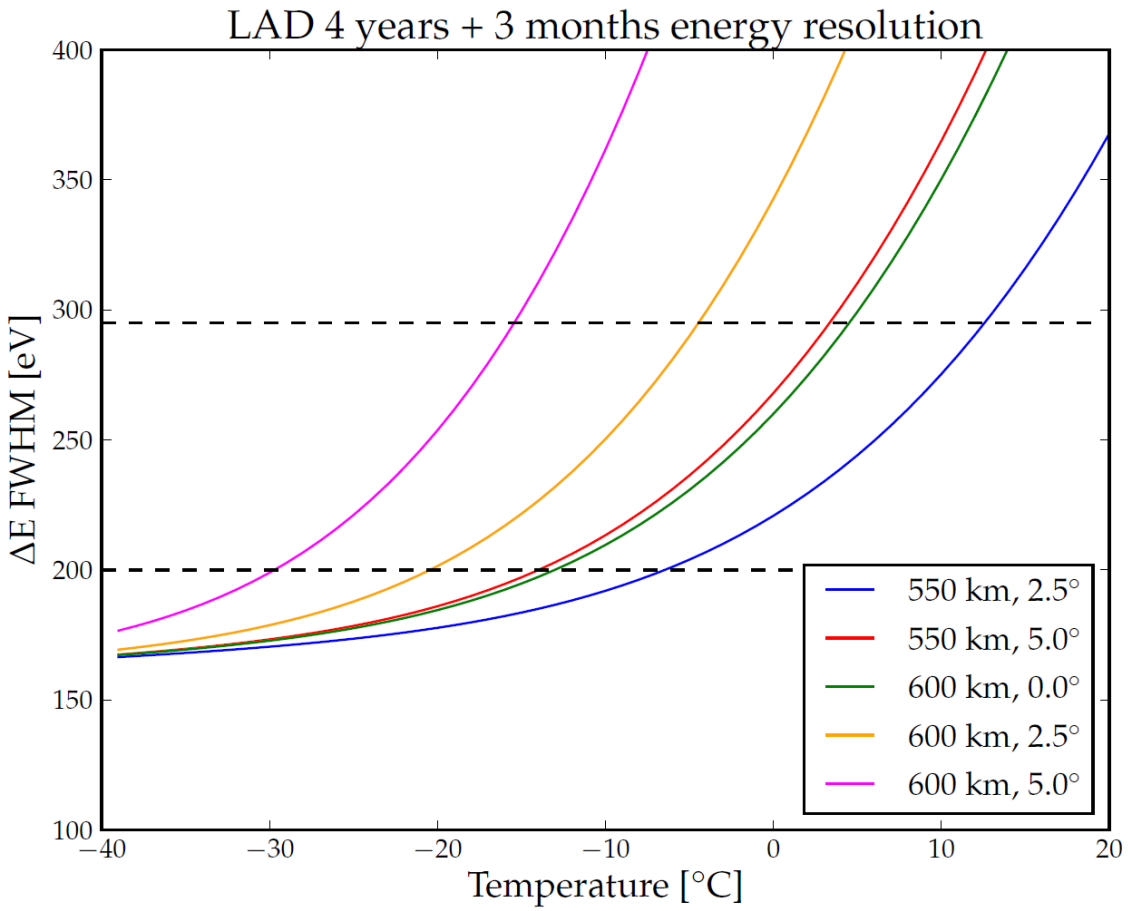

Figure 3-33: LAD-SDD energy resolution worsening at increasing temperature, for different orbits (different radiation doses) at the end of the Nominal Operations Phase (4 years and 3 months into the mission); the 200eV and 295eV (single anode event) thresholds are shown

Orbit Altitude [km]	Orbit Inclination [°]	Maximum SDD Temperature [°C] within Nominal FoR
550	2.5	-7
550	5.0	-14
600	0	-13
600	2.5	-21
600	5.0	-30

Table 3-13: LAD SDD temperature requirements to fulfil the energy resolution requirement of 200eV FWHM @ 6keV (single anode events) at the end of the Nominal Operations Phase, for the candidate range of orbits

Orbit Altitude [km]	Orbit Inclination [°]	Maximum SDD Temperature [°C] with Degraded FoR
550	2.5	+12
550	5.0	+3
600	0	+4
600	2.5	-5
600	5.0	-16

Table 3-14: LAD SDD temperature requirements to fulfil the energy resolution requirement of 295eV FWHM @ 6keV (single anode events) at the end of the Nominal Operations Phase, for the candidate range of orbits

3.5.2 Temporal and spatial temperature stability (operating)

The requirements of the temperature stability per orbit and gradient are being analysed by the team. Preliminary values are:

- **Temperature stability per orbit: <5°C**
- **Temperature gradient: <5°C, over each LAD panel.**

3.5.3 Dissipations

The thermal dissipation of each of the components in the LAD is given in the relevant power budget table (Table 3-16). The "local CBE dissipation" depends on the details of the configuration, mainly whether the DC/DC conversion occurs in the PBEE for all the voltages (LV, MV, HV) or some of them are converted in the MBEEs. Also, options are open to have the PBEE on the panel or on the optical bench. In the following table the average dissipation on the panel is given under different assumptions.

Configuration		**Local CBE dissipation on the module**	**Surface CBE dissipation on Panel(*)**
PBEE on the optical bench	All DC/DC converters in the PBEE	LV: 2.3 W MV+HV: 0.9 W MBEE: 2.2 W	31.4 W/m^2 on Panel
	HV DC/DC converter in the PBEE and LV, MV DC/DCs on the Module	LV: 3.264W MV: 0.016W HV: 0.896 W MBEE: 2.2 W	37.3 W/m^2 on Panel

PBEE on the Panel	Any configuration	LV: 3.264 W MV: 0.016 W HV: 0.896 W MBEE: 2.2 W PBEE: 3.0 W	38.1 W/m^2 on Panel

(*) Assumed Panel size: 96.6 cm x 359.8 cm x = 3.48 m^2

Table 3-15: the average power dissipation on the detector panel, under different assumptions on the configuration

3.5.4 Thermal control requirements

The baseline thermal control for the LAD is passive. Platform-provided survival heaters may be required to prevent subsystem temperatures exceeding allowed limits (see next sections), especially during non-operating conditions. The baseline assumption is that heaters will be included.

3.5.5 Thermal limits in the space environment

The temperature of the LOFT SDDs during space operations is driven by the requirements on the energy resolution. In fact, decreasing the SDDs temperature is the most effective way to reduce the bulk leakage current, being the most important component to the overall energy resolution, including the increase in leakage current produced by the radiation damage. To keep the LAD energy resolution FWHM better than the required 260 eV on any event, the temperature should not exceed -32° C (in the worst-case orbit – this requirement is significantly relaxed in lower altitude/inclination orbits). From an operational point of view, no issues are expected in operating the SDDs down to -50 °C.

The non-operative temperature range is not affected by the above considerations on the scientific requirements. The assessment of the LAD non-operative temperature range will derive from a detailed mechanical and assembly design. The most sensitive elements will likely be the interface points and the allowed ranges for the selected glues. Accordingly a preliminary allocation of standard NonOp temperature limits is made, TBC, +40°/-60°.

3.5.6 Thermal limits in laboratory environment

The considerations on the effect of the radiation damage on the bulk leakage current do not apply in laboratory environment, where the scientific requirement is fulfilled at a higher operative temperature, given the low intrinsic leakage current of the SDDs. The operative range in laboratory is the same as in space, with the difference that a better performance is achieved at the same temperature, due to the lack of radiation damage. Operation at room temperature is also possible, with reduced performance. The 'on-ground' operational temperature range is -60° C to +40° C.

3.5.7 Temperature sensors

The response of the detectors is dependent on their temperature of operation. A monitoring of the operating temperature by using local temperature sensors is required. The data from the temperature sensors will be used to make on-board calibration of the

LAD data (mainly ASIC gain and off-set, using look-up tables) and will be downloaded to ground as house-keepings to allow for the best data interpretation.

An assessment of the number, location and sensitivity of the temperature sensors will be the result of the thermal analysis of the payload and a sensitivity analysis on the detectors, to be carried out during the assessment phase.

Note: these sensors are internal to the LAD instrument, and are separate to the temperature sensors associated with the platform-provided survival heaters.

3.5.8 Heaters

As the LAD is expected to use passive cooling to meet the required operating temperature of <-32°C (worst-case), platform-provided heaters may be required to prevent too low temperatures during non-operating phases (instrument switched-off) and/or to mitigate cooling in specific attitudes.

3.6 Electrical interfaces and requirements

3.6.1 Instrument power distribution block diagram

The PSU requirements for LOFT and preliminary solutions/parameters are described in the M3 proposal to ESA. The basic requirements are as follows:

- HV PSU: Source at -1300 V to bias top end SDD resistive divider for drift of charge carriers.
- MV PSU: Sink at -100 V to bias SDD resistive divider for drift of charge carriers to anodes.
- LV PSU: 3.3 V and 5 V to supply ASICs, MBEE and PBEE.

Other aspects mentioned in the proposal are: PBEE located on panel, near the hinge. HV, MV and LV generation is done here. Voltages are then distributed to the MBEEs. MBEE contains post-regulation and filtering.

Unit of failure: a key question is what size of unit can be considered as an acceptable unit to switch off in the event of a local failure. Here it is assumed that a module is the acceptable unit. This affects the cable mass and distribution. Additional work is being performed in terms of failure scenarios during the assessment phase.

PBEE location: in the proposal, it is assumed that the PBEE is on the panel. A trade-off study has been made of the PBEE location [RD 12], Factors involved in the trade-off include the following:

- Thermal: If the PBEE (or some of its functions) is moved to the optical bench, then power dissipation on the panel is lower and more spatially uniform, decreasing thermal distortions

- Harnessing: If the PBEE is on the panel, the harness mass is reduced. Also, the number of conductors crossing the hinge is reduced, decreasing the mechanical resistance to hinge-opening.

Figure 3-34 illustrates one scheme which scores highly in the trade-off. Its 'pros' include:

- Small number of cables crossing the OB-panel hinge
- No long HV cables
- Redundancy/modularity: An individual HV supply per module.

One disadvantages of this scheme, compared with others, is that the individual HV supplies have higher mass than a single shared supply, operating inefficiency is also a consideration. Figure 3-35 shows the topology of a single HVPSU.

Figure 3-34: One scheme in [RD 12] which scores highly in the trade-off

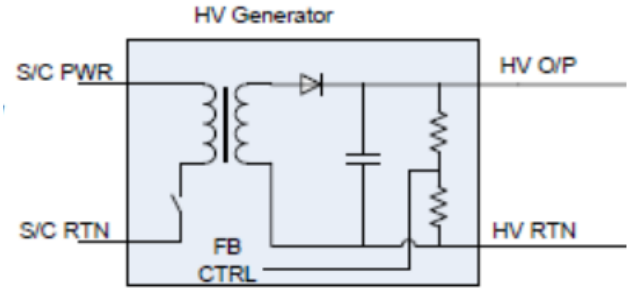

Figure 3-35: Topology of a single HVU

3.6.2 Power budget

The following power budget (Table 3-16) has been updated with respect to the proposal to account for the 70% efficiency in DC/DC conversion (in the proposal 80% was assumed), a 0.2 W higher budget allocated to each MBEE (~25 W CBE increase) and a small variation (order of 10 W CBE) due to a different choice in the anode pitch (970 µm instead of the 854 µm in the proposal).

		CBE [W]	CBE / 0.7 (DC-DC efficiency) [W]	DMM @ 20% [W]	CBE + Margin [W]	NUMBER OF ITEMS
LAD		**713.4**	**1019.1**	**203.8**	**1223.0**	**1**
1 x	DHU	15.00	21.429	4.286	25.714	1
6 x	PBEE	3.000	4.286	0.857	5.143	6
6 x	PANEL	113.4	162.0	32.4	194.3	6
21 x	MBEE	2.200	3.143	0.629	3.772	126
21 x	MODULE	3.200	4.571	0.914	5.486	126
16 x	SDD	0.200	0.286	0.057	0.343	2016
	HV	0.056	0.080	0.016	0.096	
	MV	0.001	0.001	0.000	0.002	
	LV	0.143	0.204	0.041	0.245	

Table 3-16: LAD Power budget

3.6.3 Instrument mode duration

LAD data collection observations will have durations dependant on the scientific goal, from a few minutes (in very exceptional cases) to ~1 week. The ~minute-long observations will be required to observe sources that are in an exceptional state and that are not in the accessible sky region given by the solar panel constraints (that is, a unique observation that would otherwise be lost). If the AOCS will allow such procedure, this will be implemented during the satellite 'night-time', when the solar constraints do not apply. From a power budget point of view, this is the only noteworthy case, as the satellite will need to recover the sun aspect angle at the end of the Sun obscuration. Standard observations will have typical duration from a few to a few tens of ks and they will have constant power requirements.

3.6.4 Telecommands

The software will follow closely ECSS-E-70-41A "Telemetry and telecommand Packet Utilization" to maintain standards and compatibility with ESA systems. The following telecommands are envisaged (ECSS service numbers in square brackets):

- Housekeeping control [3] (rate and possibly content)
- Memory management [6] (load, dump, checksum of absolute address)
- Time management [9] (request time from instrument software, resynchronise time)
- Test service [17]
- Science.

3.6.4.1 Telecommand Requirements

The payload (particularly the LAD instrument) requires a significant amount of calibration data to be uploaded periodically from the ground. An initial specification of the required TC data-rate to accommodate this requirement is 4kbps (during contact periods, not average). TBC

3.6.5 Telemetry

- Service 1: Telecommand Verification Service
- Service 3: Housekeeping and Diagnostic Data Reporting Service
- Service 5: Event Reporting Service
- Service 6: Memory Management Service
- Service 17: Test Service.

3.6.5.1 Telemetry requirements

The LAD scientific telemetry budget is estimated assuming default event-by-event data transmission, 24-bit per event. We conservatively assume a source with intensity 500 mCrab in the field of view at any time (this flux threshold includes >95% of the known X-ray sources with flux above 1 mCrab, Ebisawa et al 2003 A&A 411 L59). The expected count rate under the assumption is ~117 000 cts/s, in addition to the expected ~3000 cts $s^{-1}$from the background.

Taking into account the typical net source exposure in LEO (4000 s) and the full-orbit background counts, a total of ~11.5 Gbit are created over one orbit, corresponding to 1.9 Mbps orbit-average. This will be compressed to ~960 kbps through a lossless algorithm in the DHU. Preliminary simulations have been carried out using simulated LAD data streams and standard compression algorithms (gzip, bzip2, 7Z(PMMd), ZPAQ, PAQ8l), providing compression factors up to ~2.1. Therefore, adopting lossless algorithms for space applications (e.g., Rice compression) we assume that a 2 compression factor is affordable. The required computational resources are being evaluated as well. A 64 GB mass memory on the DHU will allow the temporary storage of excess telemetry.

Some of the key science targets (~10 persistent sources and some bright X-ray transients) will have average LAD count rate above 1.2×10^5 cts s-1. In these cases we will employ a flexible set of data modes, as was done with the Event Data System (EDS) on RossiXTE. These modes allow the time and energy binning to be optimized for the science goals within the available telemetry budget. The observing plan will be optimized by alternating bright and weak sources to allow for a gradual download of the excess telemetry, a strategy already successfully adopted by the RossiXTE/PCA. The strategy envisaged in the previous paragraphs is based on the assumption that telemetry down-link with a maximum net science data rate of 6.68 Gbit/orbit is available. Adopting any of the other options or technical solutions which will improve the down-link would provide the following advantages for the LAD operations and science return:

- Full event info transmission also for sources of intensity higher than the current 500 mCrab baseline limit (proportional to the down-link rate increase)
- Unlimited and unconstrained observation of sources with intensity higher than 500 mCrab (lower or cancel any constraints on the sources observation scheduling based on their intensity)
- Reduced complexity on: operations, data handling, mass memory, on-board software and ground software.

3.6.5.2 Telemetry description

3.6.5.2.1 Housekeeping telemetry

The LAD Housekeeping (HKs) consists of Analogue HKs (e.g., voltages, currents and temperatures) and Digital HKs (e.g., rate of events and dead-time counters).Table 3-13 reports the Analogue HKs definition as well as the bandwidth requested for the on-ground download.

Due to the very large number of Analogue HK parameters, we divide them into 4 groups, each related to a different quarter of the LAD module (4 SDDs and 56 ASICs each), and to acquire and transmit only one group of HKs at a time. Following this approach, we introduce an under-sampling by a factor 4 on each Analogue HK acquisition. In case of detected anomalies, it will be possible to fix the monitored quarter of LAD module obtaining a spatially coherent stream of HKs.

Analogue HK name	# parameters	sampling time (s) in *fixed mode*	# bits per sample	# groups	generation rate (kbps)
ASICs bias current/voltage	28.224 (2 per ASIC)	16	12	4	10.58
Temperatures	4.032 (1 per SDD side)	16	12	4	0.76
HV bias current/voltage	2.016 (2 per SDD)	16	12	4	0.76
MV bias current/voltage	2.016 (2 per SDD)	16	12	4	0.76
DH & Power distr.	200	16	12	1	0.15
				GRAND TOTAL (kbps)	**13.01**

Table 3-17: description of analogue housekeeping and telemetry requirement

Digital HK name	# parameters	integration time (s)	# bits per sample	generation rate (kbps)
Pipeline ratemeters	1260 (10 per MBEE)	16	24	1.89
Rejected event deadtime	4032 (1 per SDD side)	16	24	6.05
Good event deadtime	4.032 (1 per SDD side)	16	24	6.05
DH & Power distribution	500	16	16	0.50
			GRAND TOTAL (kbps)	**14.49**

Table 3-18: description of digital house-keeping and telemetry requirement

3.6.5.2.2 Science telemetry

The individual event-packet is composed of an event ID (3 bits), a differential time (12 bits) and the event energy (9 bits) for a total of 24 bits.

EVENT ID	DIFFERENTIAL TIME	ENERGY
Enumerated (3 bits)	**Integer (12 bits)**	**Unsigned integer (9 bits)**

Table 3-19: event packet definition: 24 bit word

Event ID: used to distinguish the 1-channel and 2-channel events, the dummy events and the Absolute Time events (ABT).

Differential Time: 2 μs resolution time-tag referred to previous event and to ABT event. The background rate (1 event every 0.3 ms for full LAD, or every 2 ms for individual DP) typically guarantees the reference to the Differential Time.

Energy: on-board reconstructed energy with ~60 eV energy bin below 30 keV and ~2 keV in 30-80 keV (expanded range).

The 1-channel events are characterized by a cluster composed of only one channel while the 2-channel events have energy summed over the two triggered anodes. The Dummy Event is a special event generated to provide the reference absolute time in case a real event is not detected within the full scale of the Differential Time counter. The Absolute time event (ABT) is generated every 100 ms and consists of a 48 bit resolution time-tag.

The Module Address (126 items), required for applying the relevant response matrix, is transmitted by the MBEE through the PBEE up to the DHU and encoded in the Sub-Type of the telemetry packet.

During the default LAD observation mode, a set of scientific rate-meters will be collected in parallel respect to event-by-event acquisition. The scientific rate-meters will be accumulated separately for each panel on 4 energy bands and on an integration time of 16 ms. Each rate-meter will be coded with 12 bits.

3.6.5.3 LAD telemetry budget

Table 3-20 reports the overall LAD telemetry budget, including event-by-event, science rate-meters and housekeeping. Compression ratios of 1.4-2 are more likely but further simulations need to be completed. However, additional ground stations alleviate this.

Source	Generation Rate (kbps)	Compressed TM rate (kbps)*
LAD TM	**1964.0**	**1004**
Event-by-event	1920.0	960.0
Scientific ratemeters	16.5	16.5
Analog Housekeeping	13.0	13.0
Digital Housekeeping	14.5	14.5

(*) Loss-less compression factor 2 only for event-by-event telemetry

Table 3-20: Overall LAD telemetry budget

3.6.6 Electrical interfaces

It is assumed that the primary S/C power (50 V, TBC) interfaces directly to the instrument PSU and DHU, where it is further distributed to the instrument sub-systems. With respect to data flow between the instrument and the spacecraft, it is assumed a maximum data flow from the DHU to the S/C OBDH corresponding to the maximum orbit downlink capability. Mass memory for excess telemetry storage is assumed to reside in the PL DHU.

3.7 Electromagnetic compatibility and ESD

3.7.1 Magnetic

The requirement of the SDDs with respect to magnetic fields (e.g., those from magneto-torquers) is that the deviation imposed to the drifting charge is significantly less than the pitch of the charge collecting unit (the anode) or the detector position resolution, whatever is smaller. In the LAD, the only constraint derives from the anode pitch, corresponding to 970μm. Indeed, in the event of charge displacement from one anode to the neighbouring one, the effect would be unimportant for the LAD measurement, which uses the detector segmentation only for reducing the pile-up and dead-time effects. However, the magnetic field causes a deviation of the order of 20% the anode pitch is $B\perp<300$ Gauss, where $B\perp$ is the component of the external magnetic field orthogonal to the LAD detection plane, as derived by the following computation.

The magnetic field produces a displacement of the electron charge cloud in the SDDs due to the Lorentz force (Hall effect). For an electron in a semiconductor under a drift field (Lutz, 1999), the angle between the electrostatic and magnetic force is given by $\tan(\theta n) = \mu nH\ B$, where μnH is the Hall mobility (1670 cm^2 / Vs at room temperature K) and B is the magnetic field. The unit of the magnetic field is 1 T = 10^4 G = 10^{-4} Vs / cm^2. Taking into account the maximum displacement of 0.2 mm over the full length (3.5 cm), we obtain $B < \tan(\theta n) / \mu nH = 1.45 \times 10^{-5}$ Vs / cm^2 = 300 G. At -30° C the Hall mobility increases of a factor ≈ 1.6, thus the maximum acceptable magnetic field is 190 G for the LAD. These are the requirements on the magnetic field component orthogonal to the plane defined by the LAD panels.

For comparison, the Earth magnetic field ranges between 0.1 and 0.5 G, while for typical magnetic torque actuators, at a distance of 1 m (the field scales as r^{-3}), the magnetic field is between 4×10^{-3} G and 0.8 G, when the magnetic device is active.

3.7.2 Electrical

The SDD detectors are operated with the negative high voltage (nominal -1300 V) on the surface, to sustain the drift field. The negative high voltage may have some plasma susceptibility to the open space. In the LAD, the detectors are completely covered by the lead-glass collimator and thermal screen. Plasma effects are not expected to take place. However, the issue is still under evaluation by the team. Should plasma effects be possible, a recovery action would be to put the LAD collimators to a (relatively) small positive potential (~10-20 V) to act as an electrostatic grid.

3.7.3 ESD

The electrical systems (including: ASICs and SDDs) are highly sensitive to electrostatic discharges (ESD), thus handling personnel must be trained accordingly and must use proper equipment in order to avoid ESD.

3.8 Optical requirements

3.8.1 Stray-light requirements

Diffuse X-ray background will be shielded by the collimator and by side/back shielding. UV/V/IR radiation will be prevented from reaching the detector sensitive area, from any direction. This will be achieved by Aluminium coating on the collimator and by the thermal/optical blanket. The level of UV/V/IR light rejection is under assessment; baseline is 10^{-6}, as it worked for Chandra. (It is worth noticing that a large fraction of the LOFT SDD surface is covered by Al electrodes, shielding from light. The Chandra requirement can then be seen as a conservative one for LOFT.)

3.8.2 Baffling requirements

Not needed (as long as it is not intended as the collimator).

3.9 Charged particle rejection requirements

The Silicon drift detectors operating in the LAD are 450 μm thick. The minimum ionizing particles release ~150 keV (MIP), on average. We made Monte Carlo (GEANT) simulations to estimate the spectrum of the energy depositions in the detectors. Based on these simulations, the upper amplitude discrimination threshold set at 80 keV and the event pattern identification will reject >99% of the particle-induced events. Such a threshold and cluster analysis can be implemented already at FEE or MBEE level. Active anti-coincidence for eliminating the residual particle-induced background is not strongly required by the scientific requirements (as the particle-induced background is not a main source of background) and it is hardly affordable on such a large-area experiment.

3.10 Micro-meteorites and debris

An analysis has been performed in order to evaluate the effects of micro-meteoroids and orbital debris (MMODs) for LOFT. Average flux rates (Figure 3-36; estimated using the ORDEM2000 software) have been calculated assuming a 600km, ~5° inclination orbit (it is worthy of note is that 550km altitude has little additional effect).

Initial findings suggest that the LAD external surface will collect many MMOD impacts due to its large area, the majority of which will hit the optical-thermal filter - with little effect. The model predicts that relatively few (~10) particles will reach the SDDs over 5 years. The team is performing specific tests to quantify the potential damage to the detectors of these 'few' hits.

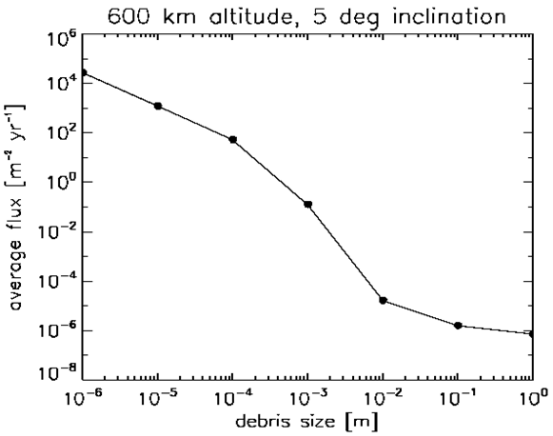

Figure 3-36: Average flux Vs debris size

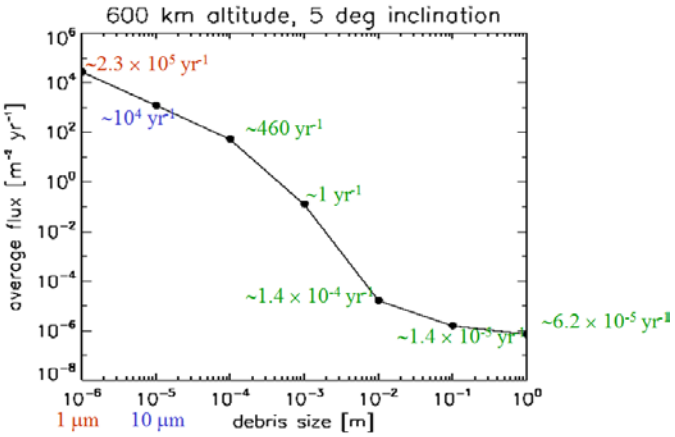

Figure 3-37 Expected rates assuming 18 m^2 area

Flexi-PCBs could be used to bridge the gap between the panels and optical bench (in order to assist the re-location of some of the electronics onto the optical bench). The flexi-PCB should use Kapton (with a protective Aluminium layer) in order to protect the flexi-PCB from: mico-meteorites, debris and AO (180 km and 650 km).

3.11 Transportation, handling, cleanliness and purging requirements

3.11.1 Transportation requirements

The LOFT SDDs are slightly sensitive to humidity only when fed with the HV power supply and they need low humidity or gaseous nitrogen purging during operation, not during transportation. The micro-capillary plates are also hygroscopic but need to be kept under controlled atmosphere only for long-term storage. Storage with a desiccant is dangerous because the collimators will actually pull moisture out of the desiccant (e.g., http://www.burle.com/dettechbrief_6.htm). For the transportation we put requirements on the temperature, that has to be kept within the non-operative range (-60°C / +40° C TBC), and the humidity, below 30% (TBC). During the LOFT transportation we require to enclose the panels in dedicated sealed boxes, in dry atmosphere.

When transporting the LOFT instrumentation, care has to be taken not to expose it to strong shocks and vibrations and high thermal gradients. In any case, shock gauges have to be mounted on the container case in order to verify the shock history during transportation.

3.11.2 Handling requirements

There are no specific handling requirements, which exceed the usual care to be taken while handling space-borne X-ray detectors within an experimental environment. The ASICs and SDDs are sensitive to the damage produced by electrostatic discharges (ESD), thus

handling personnel has to be trained accordingly and must use proper equipment in order to avoid ESD.

3.11.3 Cleanliness requirements

The LOFT instrumentation requires a cleanliness level corresponding to a class 100,000 or better, similarly to other space-borne experiments. The LAD collimators are sensitive to the cleanliness of the environment, thus the AIV activity involving the collimators have to be carried in class 10,000 (TBC) or better using degreased tools made of Ultra High vacuum compatible material (e.g., http://www.burle.com/dettechbrief_6.htm).

3.11.4 Purging requirements

The LOFT collimators and SDDs are hygroscopic. The latter only marginally, and only when in operation (no issue when the HV power supply is off). Consequently the instrumentation has to be operated in dry atmosphere (e.g., nitrogen purging).

The effect of humidity on the SDDs is an increase in the (surface) leakage current. This affects the performance but not the functionality (i.e. functional tests are possible anyway). Technical developments have been implemented in the new detector productions which largely reduce the effect of humidity on the SDDs in operation.

3.12 Ground and flight operations requirements

The LOFT-LAD operations requirements are summarised in this section. They will be updated as additional information is provided by the prime (ESA).

3.12.1 Ground and pre-flight operation

Ground and pre-flight operations will include:

- Software will be developed to ensure easy access to instrument performance interfaces, i.e. via ground test interfaces
- On-going verification of instrument
- On-going calibration of the instrument
- Support Integration of the instrument onto the spacecraft
- Support the prime in terms of performance verification (LOFT-LAD + S/C).

3.12.2 Launch and ascent phase

During the launch and ascent phase, the consortium will provide technical support and advice to the prime as required. There is no requirement to power the LAD or WFM during launch or ascent, so no critical items are foreseen.

3.12.3 Instrument commissioning phase

Instrument Commissioning Phase activities will include:

- Verify nominal performance following launch

- Perform post-launch calibration of the instrument
- Evaluate and test performance constraints (offset pointing etc.).

3.12.4 Flight operations

Flight operations activities will include:

- Planning of instrument operations
- Support of the MOC in the commanding of the instrument
- Coordinate the creation of the scientific products, their archiving and distribution to the scientific community
- Monitor instrument health and respond to changes.

3.13 Deliverable models and GSE

The LOFT-LAD model philosophy has been developed based on the assessment of project risk; which has in turn been developed through a detailed review of LOFT-LAD technologies and related programme constraints. A TRL assessment has been performed in order to identify those technologies requiring additional development. The LOFT LAD development programme is composed of the following models:

- BB (development)
- STM
- EM
- QM
- FM
- FS.

While it is recognised that the prime contractor/ESA might prefer a reduced model philosophy, the LOFT-LAD consortium believes that given the large number of equipment (>28,000 ASICS) a more detailed programme is required at instrument level, and at relatively low cost. Additional information is provided (below) for each model.

3.13.1 Bread board model

The LOFT-LAD breadboard model will be used for the early verification/validation of equipment. It will provide sufficient information (proof of concept/model correlation) to enable the progression of the project to the next, more representative model(s): Engineering model (EM) and Structure Thermal Model (STM).

It is planned that where possible the breadboard model will be manufactured from standard off the shelf components. However, in some instances this might not be possible (minimum order quantities and specialist fabrication constraints). Current planning shows that the LOFT-LAD breadboard model will include:

- Detector:
  - Collimator
  - SDD

- Electronics:
  - ASIC (proof of concept including performance)
  - Power converter operating efficiency: performance and resource requirements (many PSUs; hence a small change from the baseline can have a pronounced effect on resources).
- Software:
  - Most critical components (instrument control) including:
    - data compression
    - data time stamping
    - data synchronisation
- Structure :
  - Fabrication techniques (early validation of concepts)
  - Correlation of models (thermal and stability).

Validation programme: There is no formal test programme associated with the breadboard equipment.

Deliverable status: The LOFT-LAD breadboard is a non-deliverable piece of equipment.

3.13.2 Structural thermal model

The LOFT-LAD STM will be used for the verification/validation of structure/thermal related equipment. It is not realistic to manufacture the complete LOFT-LAD instrument (neither is it required at this stage) and as such only a small subset of equipment will be manufactured, i.e. sufficient for model correlation.

The STM will be manufactured from standard off the shelf components wherever possible (heaters will be used to simulate the operation of electronics units (thermal dissipation). However, in some cases, a more representative equipment may be required, i.e. specialist surface finishes in order to properly replicate thermal behaviour.

Validation programme: STM equipment will be subjected to a test programme as defined in Table 3-16.
Deliverable status: The LOFT-LAD STM is a deliverable piece of equipment and will be delivered to the prime contractor (ESA).

3.13.3 Engineering model

The engineering model will be the first ‘all-up’ verification of the LOFT-LAD design (all systems – although not a complete instrument). The following (non-exhaustive) elements are foreseen as part of the EM programme:

- 1 X Detector panel (DP) structure
- 2 X EM Modules and dummies (~500 ASICS).

Validation programme: EM equipment will be subjected to the test programmes defined in Table 3-16.

Deliverable status: The LOFT-LAD EM is a deliverable piece of equipment and will be delivered to the Prime contractor/ESA.

3.13.4 (E)Qualification model

The LOFT-LAD (E)QM will be used for the qualification of the LOFT-LAD design. It is not realistic to manufacture the entire LOFT-LAD instrument and as such only a small subset of equipment will be manufactured, i.e. sufficient for model correlation and proof of testing. Current planning is that the (E)QM will include the following pieces of equipment:

- Representative part of a Detector panel (DP) (supplied by Industry)
- Real Modules
- PSUs and BEE (back-end electronics) to support the modules.

Validation programme: (E)QM equipment will be subjected to a qualification level test programme (Table 3-16).
Deliverable status: The LOFT-LAD EQM is a non-deliverable piece of equipment.
Additional consideration: The EQM elements (e.g., modules) could be considered for re-use as a flight spare.

3.13.5 Flight model

The LOFT-LAD FM is the final deliverable instrument.

Validation programme: FM equipment will be subjected to acceptance level test programmes (Table 3-16).
Deliverable status: The LOFT-LAD FM is a deliverable piece of equipment and will be delivered to the Prime contractor/ESA.

3.13.6 Flight spare model

It is conceivable that EQM equipment could be refurbished and reused as the flight spare. However, if this is not acceptable (Prime/ESA) then a set of spares will be maintained; in addition to the following pre-assembled/calibrated items (i.e. sufficient for the timely replacement of large failed equipment (< 1 month TBC):

- 1 x detector panel
- 21 X PSU (one DM compliment)
- 21 X HVU (one DM compliment).

3.13.7 Equipment needs

Equipment requirements for the various models of the LOFT-LAD programme are summarised in the following table.

						STM - Deliverable			EM - Deliverable			EQM - non-deliverable			FM - deliverable			FS - deliverable as required			Total count
Level-1	Level-2	Level-3	Level-4	Level-5	Production yield	Count #	Corrective yield #	Total part count	Count #	Corrective yield #	Total part count	Count #	yield correction #	Total part count	Count #	Corrective yield #	Total part count	Count #	Corrective yield #	Total part count	
LOFT-LAD					99.7%	-	-	-	-	-	-	-	-	-	1	0	1	-	-	-	1
	(6) Detector Panel				99.7%	1	1	2	1	1	2	1	0	1	6	0	6	-	-	-	9
		(21) Detector module			99.7%	2	0	2	2	0	2	5	0	5	126	0	126	4	0	4	137
			(16) Detectors				-	-		-	-		-	-					-	-	
				SDD	75.0%	32	8	40	32	8	40	80	20	100	2,016	504	2,520	64	16	80	2,740
				FEE	90.0%	32	3	35	32	3	35	80	8	88	2,016	202	2,218	64	6	70	2,411
				MCPs	75.0%	128	32	160	128	32	160	320	80	400	8,064	2,016	10,080	256	64	320	10,960
				ASIC produ	90.0%	448	45	493	448	45	493	1,120	112	1,232	28,224	2,822	31,046	896	90	986	33,757
			MBEE		95.4%	2	0	2	2	0	2	5	0	5	126	6	132	1	0	1	140
			HV		99.7%	2	0	2	2	0	2	5	0	5	126	0	126	1	0	1	134
		PBEE			99.7%	2	0	2	2	0	2	5	0	5	126	0	126	1	0	1	134

Table 3-21: LAD equipment needs by model

3.13.8 Verification strategy

The LOFT-LAD verification strategy is summarised in Table 3-22.

Test	Model				
	STM	EM	QM	FM	FS
Physical properties	**A,T**	-	**A,T**	**A,T**	-
Functional & performance	-	**T**	**T**	**T**	-
Humidity	(not applicable)				
Leak	(applicable only on sealed / pressurised items)				
Pressure	(applicable only on sealed / pressurised items)				
Acceleration	-	-	-	**A**	-
Sinusoidal vibration	$\mathbf{T_Q}$	-	$\mathbf{T_Q}$	$\mathbf{T_A}$	-
Random vibration	$\mathbf{T_Q}$	-	$\mathbf{T_Q}$	$\mathbf{T_A}$	-
Acoustic	(spacecraft level)				
Shock	-	-	**T**	-	-
Corona & arcing					
Thermal vacuum	**T**	-	$\mathbf{T_Q}$	$\mathbf{T_A}$	-
Thermal cycling	**T**	-	$\mathbf{T_Q}$	$\mathbf{T_A}$	-
EMC/ESD	-	**T**	**T**	**T**	-
Life	(tested at equipment level only, where required)				

Table 3-22: LAD Instrument verification strategy; **A** = Analysis; **T** = Test; $\mathbf{T_Q}$ = Test at qualification level; $\mathbf{T_A}$ = Test at acceptance level

3.13.9 Ground Support Equipment

The Ground Support Equipment (GSE) foreseen for the LOFT-LAD programme is described in Section 3.3.10. Based on the overall schedule of the programme, parts of the GSE can be made available to ESA for model testing.

4 THE WFM INSTRUMENT

4.1 Introduction

In this part, the baseline design of the WFM is described and the corresponding resources, in terms of mass, envelope size, power and data rate are quantified. Such estimates play an important role in the context of the definition of the LOFT mission as they strongly influence the spacecraft requirements and corresponding resources. A summary of the baseline WFM instrument' characteristics is given in Table 4-1.

Instrument Characteristic	WFM
Detector type	Si Drift
Mass [kg]	79(1)
Peak Power [W]	109.3
Detector Operating T [°C]	<-20
Total Detector Effective Area (5 camera pairs)	1820 cm^2
Energy range [keV]	2-50 (50-80 keV, extended)(*)
Energy resolution [FWHM]	<500 eV @ 6 keV
Mask pixel size	250 μm x 16 mm
Field of View	180° x 90° FWZR plus 90° x 90° towards night hemisphere
Angular Resolution	<5 arcmin
Typ/Max data rate [kbps]	50/90(2)
	(1) including digital electronics
	(2) after compression
	(*) Extended range means that these data have lower priority

Table 4-1: Summary of WFM characteristics

4.2 WFM instrument description

4.2.1 Overview

The baseline WFM is a coded aperture imaging experiment designed on the heritage of the SuperAGILE experiment (Feroci et al. 2007 NIM A581 728), successfully operating in orbit since 2007 (e.g., Feroci et al. 2010 A&A 510 A9). With the ~100 μm position resolution provided by its Silicon microstrip detector, SuperAGILE demonstrated the feasibility of a compact, large-area, light, and low-power high resolution X-ray imager, with steradian-wide field of view. The LOFT WFM applies the same concept, with improvements provided by the higher performance (low energy threshold and energy resolution) Silicon Drift Detectors (SDDs) in place of the Si microstrips.

The working principle of the WFM is the classical sky encoding by coded masks (Fenimore & Cannon 1978 Appl. Opt 17 337) and is widely used in space borne instruments (e.g. INTEGRAL, RXTE/ASM, Swift/BAT). The mask shadow recorded by the position-sensitive detector can be de-convolved by using the proper procedures (e.g. IROS, Iterative Removal

Of Sources, Hammersley et al. 1992 NIM A 311 585) and recover the image of the sky, with an angular resolution given by the ratio between the mask element and the mask-detector distance. In order to avoid losing imaging sensitivity, the mask element should not be smaller than twice the detector resolution element. By using a mask with mask elements of 250 μm in the fine resolution direction and a mask-detector separation of ~200 mm we obtain an angular resolution <5 arc min. The coded mask imaging is the most effective technique to observe simultaneously steradian-wide sky regions with arcmin angular resolution.

As a first approach, each WFM camera can be considered a one-dimensional coded mask imager. This means that after the proper de-convolution is applied to the detector images, the image of a sky region including a single point-like source will appear as a single peak over a flat background. The position of the peak corresponds to the projection of the sky coordinates onto the WFM reference frame. The width of the peak is the point spread function, of the order of a few arc minutes in the LOFT WFM. If more than one source is present in the observed sky region, the image will show a corresponding number of individual peaks, whose amplitude will depend on the intensity of the source and on the exposed detector area at that specific sky location. By observing simultaneously the same sky region with two cameras oriented at 90° to each other (such a pair composing one WFM Unit), one can derive the precise 2D position of the sources, by intersecting the two orthogonal 1D projections. In Figure 4-1 we show an example of two such de-convolved 1D-images from a real observation of the Vela region taken with the SuperAGILE experiment (Feroci et al 2010 A&A 510 A9).

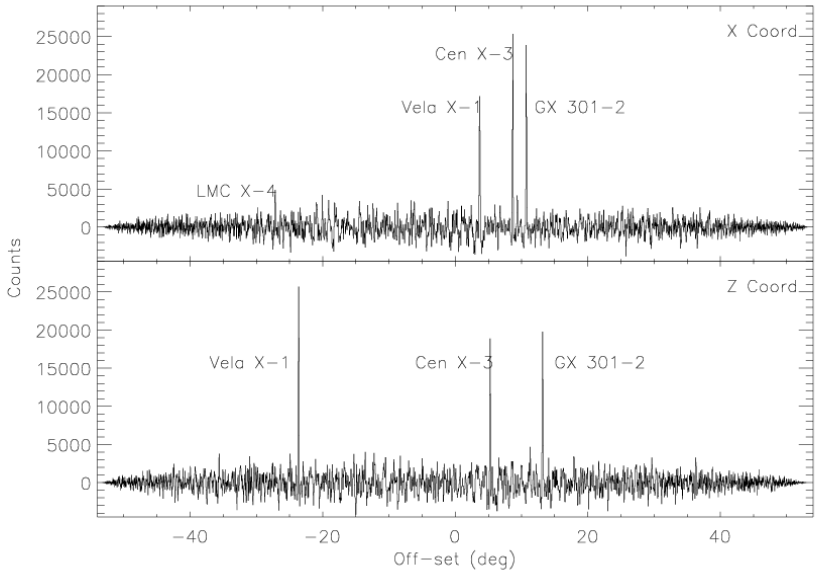

Figure 4-1: An example of 1D de-convolved mask images. The source sky positions are projected onto two 1D images

Indeed, the cameras of the LOFT WFM are not purely one-dimensional. As it is shown below, each detector has also a coarse position capability in the second dimension. While the fine position is of the order of ~30-50 μm, the second coordinate of each photon can be located with an accuracy of ~5 mm. When equipped with a proper (asymmetric) coded

mask, this capability becomes an asset for the WFM. In fact, assuming a pure 1D capability, each camera is individually able to locate a source in a strip that is few arcmin wide and several tens of degrees long (as wide as the field of view, unless other constraints such as earth occultation applies). Of course, the ambiguity is solved when the orthogonal camera is considered. However, by using the second coarse coordinate, the length of the error strip reduces to a few degrees, largely reducing the confusion limit for crowded fields. This is particularly useful for the spectral analysis of individual sources.

In the LOFT WFM we define:

- Camera: the assembly of a detector plane with its own collimator and mask, providing fine (arc-minutes) angular resolution in one coordinate and coarse (degrees) angular resolution in the orthogonal direction
- Unit: a set of 2 cameras oriented at 90°, covering the same field of view. The combined use of the 2 cameras in a unit enables a fine 2D angular resolution
- WFM Assembly: the total set of cameras composing the WFM, covering the entire field of view with fine angular resolution.

The baseline WFM design is based on the SDD detectors. A few but significant changes have been made by the LOFT consortium to the design relative to that described in the proposal:

a. The field of view of the instrument is now extended, covering a large fraction (about one half) of the sky accessible to the LAD at any time. To achieve this, the number of WFM units has been increased to 5 (compared to 2 in the proposal) for a total of 10 cameras. Each camera has a smaller collecting area with respect to the proposal baseline. This modification increases the overall resources required by the WFM by ~25%.
b. The SDD anode pitch has been decreased to 145 μm (as compared to ~300 μm in the proposal) to optimize the position resolution at low energies. This impacts the number of channels per SDD detector, now 896 (as compared to the 512 in the proposal) and consequently the power budget.
c. The open fraction of the coded mask has been baselined to 25% (as compared to the 50% in the proposal) to optimize the imaging sensitivity (e.g., in ‘t Zand et al. 1994, A&A 288, 665); see [RD 44].
d. Inclusion of a WFM sunshade. It has been realized that it will be very difficult to ensure the flatness of the mask to within the required precision (50 μm) if the Sun is allowed to illuminate the masks directly. Direct solar illumination will result in a very significant temperature increase, and temporarily large temperature gradients – causing the masks to flex. To avoid this we believe it is mandatory to include a sunshade protecting 4 of the five WFM units from being illuminated by the Sun during normal operations. The fifth WFM unit is mounted such that the Sun will never illuminate the masks.
e. A Beryllium window may be required to protect the detectors from soft protons, micro-meteorites and debris because a thermal blanket (7.6 μm Kapton) can only stop debris smaller than ~0.5 μm size. A Be window of 25 μm thickness can stop debris smaller than 20.1 μm size (~0.04 yr-1 per SDD expected) if it is placed

below the coded mask (0.5 mm distance from the thermal blanket) and 148 μm size (~2x10-3 yr-1 per SDD expected) if it is placed above the detector (20.5 cm distance from the thermal blanket); see [RD 36].

A few comments may be in place regarding the reduction of the mask open fraction from 50 to 25% (see [RD 44]). This change has three beneficial consequences:

- The sensitivity of the camera increases. Although the number of source photons are reduced the 'information content' of each photon increases enough to compensate for the photon loss.
- When telemetry is scarce it is of course advantageous to transmit few photons with a high information content rather than many photons with low content.
- In cases where a very strong source (e.g. ScoX-1) appears in the field its signal acts as an additional background for all other sources in the field. With a mask transmission of 25% there will (ideally) be 75% of the detector pixels which do not receive the Sco X-1 photons. De-convolution techniques have been developed which avoid source pixels illuminated by strong sources. In this way one can reconstruct an image from a substantial fraction of the detector surface which is only little affected by the presence of strong sources. Here one is making use of the 'holographic' nature of coded mask imaging – the whole field can be reconstructed from a fraction of the detector surface. With a 50% transparent mask the number of uncontaminated pixels decreases very significantly, particularly when the finite position resolution of the detector is taken into account.

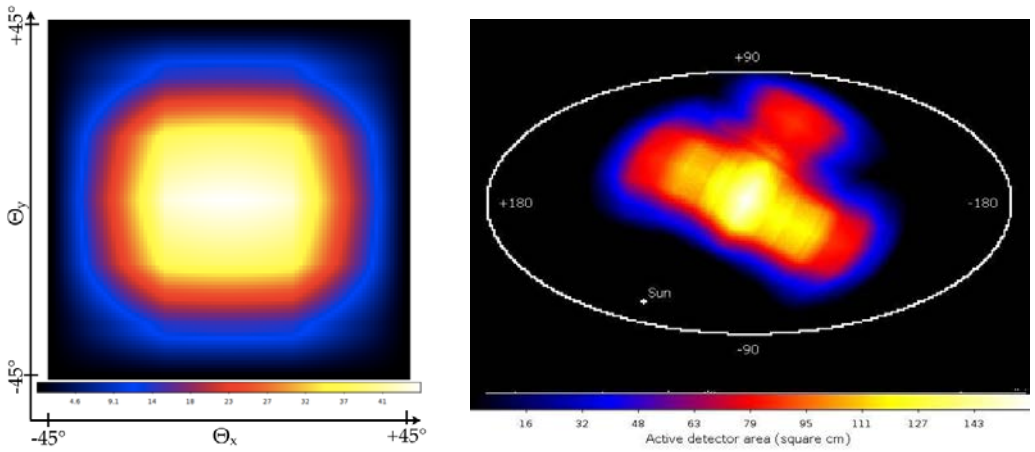

Figure 4-2: *Left panel:* map of the single camera sensitive area expressed in cm2 (see [RD 28]). The map takes into account the main geometrical effects (mask open fraction, vignetting, shadowing of the collimator walls, detector non-sensitive areas, cos(θ) effect). *Right panel:* map in Galactic coordinates of the active detector area for an observation on April 1st of the Galactic centre (see [RD 34]).

4.2.1.1 Imaging properties of the WFM SDD detectors

For the general working principle of the large-area SDD detector we refer to the relevant section of the LAD PDD/TN. In this section we mostly concentrate on the peculiarities of the WFM SDDs, where the optimization of the imaging properties has the highest priority.

When a photon is absorbed by the SDD, it generates an electron cloud that is focused on the middle plane of the detector, and then drifts towards the anodes at constant speed. During the drift time, the electron cloud size increases due to the diffusion.

The charge density of the cloud that arrives at the anodes will be described by a Gaussian function, with an area equal to the total charge (i.e the photon energy), a mean value representing the "anodic" coordinate of the impact point and a size sigma which depends on the "drift" coordinate of the absorption point. Furthermore, a baseline shift (due to the common mode noise (CMN)) could be superimposed on the signals.

The analysis of the charge distribution over the anodes has to be done on-board on each event and will result in the determination of the amplitude, and the position of the event along the anodic and drift directions. The processing will be done in the BEE (FPGA-based) of the WFM.

In order to study the SDD spatial resolution we developed a Monte Carlo simulator describing the charge drift and diffusion inside the SDD. This also allowed us to verify the consistence of the experimental results with the assumptions. Preliminary results obtained with the simulator were presented by Campana et al. (2011) Nucl. Instr. Meth. A, 633, 22. In this case, the experimental measurements were carried out at room temperature by using the a discrete-electronics FEE connected to ALICE-D4 SDD. The FEE/detector parameters used in these simulations are:

- JFET gate capacitance CGS=0.4 pF
- feedback capacitor CF= 50 fF
- Cstray = 750 fF
- anode pitch 294 µm
- 8 channel read-out
- CR-RC shaper
- HV = -1300 V
- Ileak (T=20° C) = 20 pA
- CMN = 125 e-.

In Figure 4-3 we show the comparison between the locations reconstructed using the method described below (left panels), and the results of the simulations assuming a perfectly Gaussian beam (right panels). The agreement is excellent, and we can conclude that the simulations give a consistent picture of the detector behaviour.

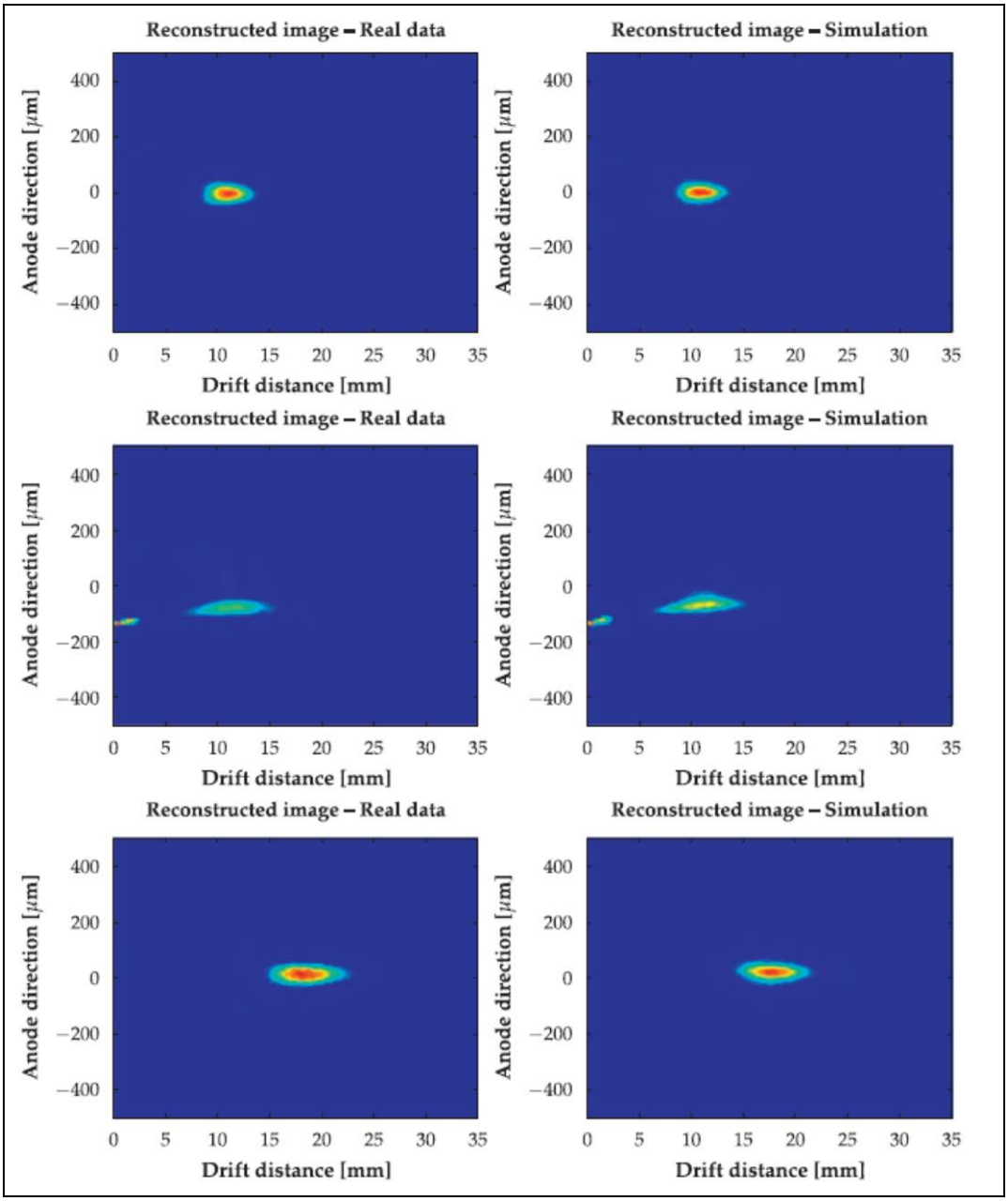

Figure 4-3: Upper left: Reconstructed detector image of a 4.6 keV, ~100 μm FWHM, at y0=0 and x0 = 10 mm. Upper right: Simulation of a gaussian beam with ~100 μm FWHM centered at y0=0 and x0 = 10 mm. Central left: Reconstructed detector image for a 30 min integration with a 4.6 keV monochromatic beam of ~100 μm FWHM centered in y0=-75 μm and x0 = 10 mm. Central right: Simulation of a gaussian beam with ~100 μm FWHM centered at y0= -75 μm and x0 = 10 mm. Lower left: Reconstructed detector image for a 30 min integration with a 4.6 keV monochromatic beam of ~100 μm FWHM centered in y0=10 μm and x0 = 18 mm. Lower right: Simulation of a gaussian beam with ~100 μm FWHM centered at y0= 10 μm and x0 = 18 mm. From Campana et al., NIM A 633 (2011)

In order to estimate the imaging and spectroscopic capabilities of the SDD that can be reached by using an ASIC based FEE (32 read-out channels, assuming the capabilities of the Italian test ASIC developed on the heritage of the StarX-32), several simulations were then performed using different anode pitches. It's worth noticing that SDD imaging

response considering such a integrated FEE is expected to be greatly improved, as demonstrated in the simulations described below.

The parameters used in these simulations are the following:

- MOS Gate capacitance C_G = 90 fF
- C_{feed} = 21 fF
- C_{stray} = 200 fF
- CR-RC shaper
- I_{leak} = 7176 pA cm^{-3} at 20° C (intrinsic)
- Anode pitches: 145 µm, 175 µm, 200 µm, 225 µm, 250 µm and 294 µm
- HV = -1300 V
- CMN = 25 e^- rms
- CSA Power: 0.722 mW/channel.

The reduced CMN value used for these simulations (~1/5 of the value used in the paper by Campana et al. 2011, Nucl. Instr. Meth. A, 633, 22) was measured in the laboratory with the 8-channels discrete electronics set-up after the power supply filtering was improved using low noise passive components (resistors and capacitors).

The following scheme provides a step-by-step description of the simulator:

1. A photon of energy E is generated in a position x_0 (along drift direction) and y_0 (along anode direction) in the SDD;
2. The photon is absorbed in the Silicon bulk and generates an electron cloud in x_0,y_0. The estimation of the total charge in the cloud takes into account the Silicon electron-hole pair generation energy (3.6 eV) and the Fano factor (0.115);
3. The cloud, which can be assumed to have an initial width of σ_0~0 µm, is propagated along the drift direction, reaching the read-out anodes with a width σ which is function of the diffusion coefficient D and of the drift time t. The width can be expressed through the formula:
$$\sigma = \sqrt{2Dt+\sigma_0^2} = \sqrt{2\frac{k_B T}{q}\mu\frac{x}{\mu E}+\sigma_0^2} = \sqrt{2\frac{k_B T}{qE}x+\sigma_0^2}$$
where k_b is the Boltzmann's constant, μ is the electron mobility, q is the electron charge, T is the absolute temperature and x is the drift length.
4. The electron cloud is then collected by a number n of anodes depending on the width of the cloud and on the photon conversion point y_0. Being Q_{tot} the total charge generated by the photon, the charge fraction which reaches each anode y_i can be expressed by the formula:
$$\psi(y_i) = \frac{Q_{tot}}{2}\left\{\mathrm{erf}\left(\frac{y_i+p/2-y_0}{\sigma\sqrt{2}}\right)-\mathrm{erf}\left(\frac{y_i-p/2-y_0}{\sigma\sqrt{2}}\right)\right\}$$
where p is the detector pitch and erf is the error function (cumulative of the Gaussian). At this stage, the simulator takes into account the ENC for each anode independently.

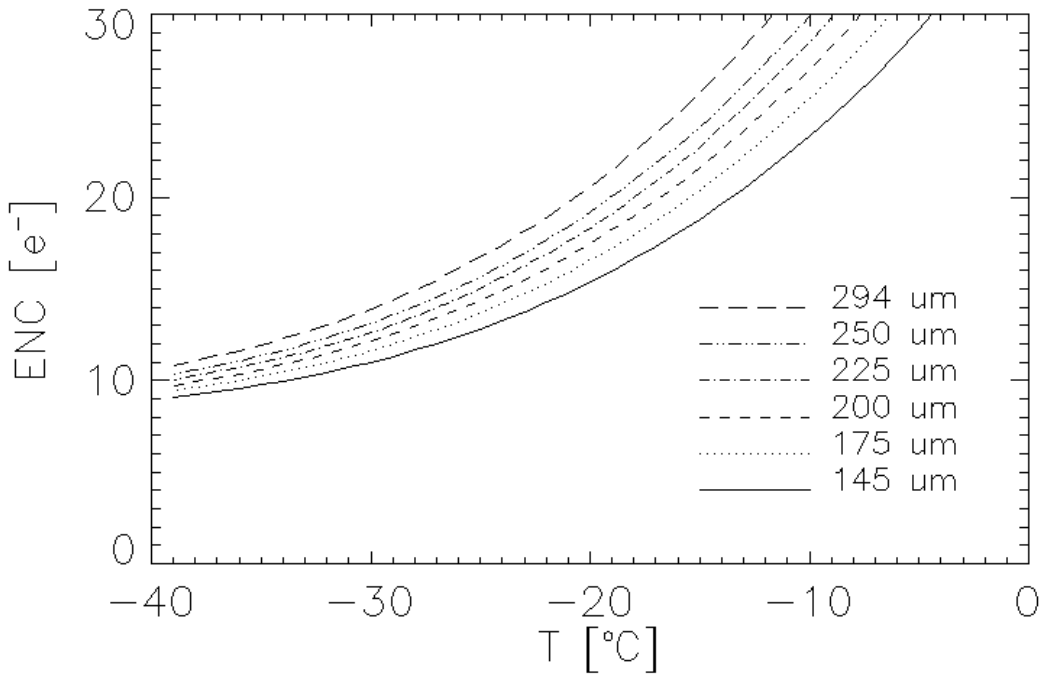

Figure 4-4: Channel ENC as a function of the detector temperature and of the channel pitch EOL (600 km orbit, 5.0° inclination, 4+1 years)

In Figure 4-4 the ENC as a function of the SDD pitch and of the temperature is plotted taking into account the FEE characteristics listed above, an intrinsic leakage current of 7176 pA cm^{-3} (20 °C, Beginning Of Life) plus the contribution due to the radiation damage of 104518 pA cm^{-3} (20 °C, 4+1 years, 600 km altitude, 5° inclination, see [RD 23]). In the following, we consider the requirement on the channel ENC of 12 e^- rms for an anode pitch of 145 µm.

A Common Mode Noise, with an rms value of 25 e^-, is then randomly added to the 32 ASIC channels. The charge distribution is eventually fitted using the formula in point 4 plus a constant value (which represents the CMN), the fitting parameters Q_{tot}, y_0 and σ allow to completely characterize the physical properties of the electron cloud (i.e. E, x_0, y_0).

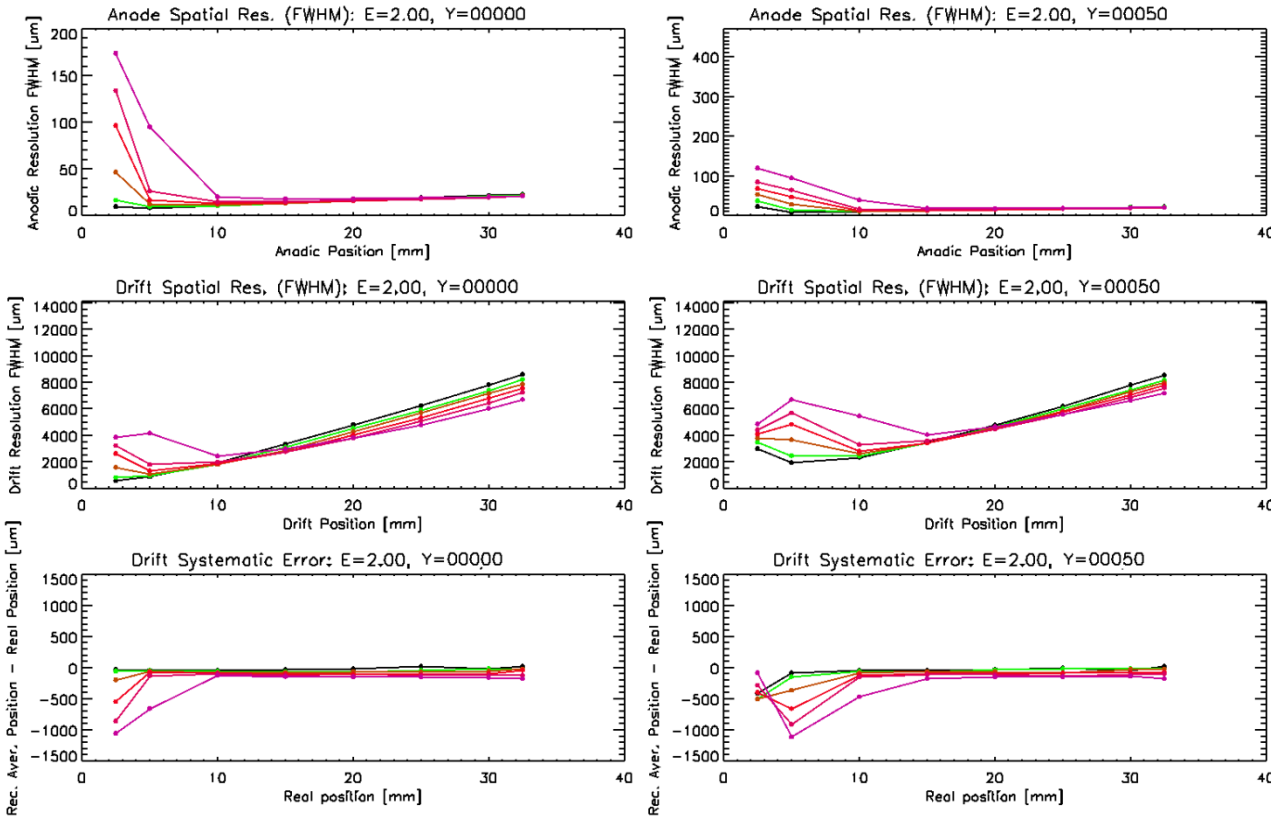

Figure 4-5: Anodic and drift spatial resolution for photons of 2.0 keV absorbed in y=0 µm (left panel) and y=50 µm (right panel) for different anode pitches. The single channel ENC is 12 e- rms for the 145 µm, while the ENC for the other pitches is estimated taking into account the leakage current and the FEE characteristics reported in the text

Figure 4-5 shows the anodic and drift spatial resolution (FWHM) for a 2 keV photon for different anode pitches, for several photon absorption points in drift direction and for two different positions in the anodic direction: in the center of the anode (y=0), and 50 µm away from the anode center. As it is clear from the plots, a pitch smaller than 175 µm is required to minimize the systematic effects on the position reconstruction introduced by the discretization of the charge cloud and thus to optimize the detector spatial resolution at low energies (~2 keV). Considering these results and the technological possibilities to build a SDD with a pitch smaller than 175 µm, we chose 145 µm as the optimal pitch for imaging performance of the WFM.

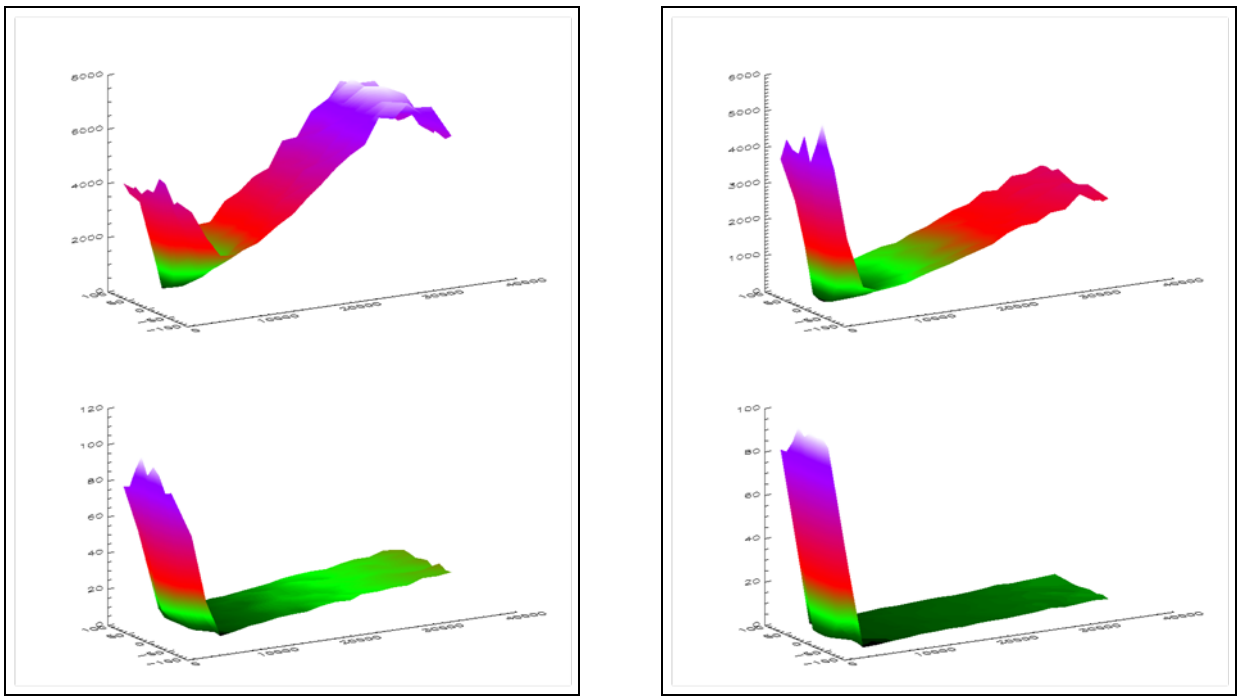

Figure 4-6: *Left panel:* Map of SDD spatial resolution at 2 keV along the drift direction (top) and the anodic direction (bottom) as a function of photon absorption point. *Right panel:* Map of SDD spatial resolution at 6 keV along the drift direction (top) and the anodic direction (bottom) as a function of photon absorption point

Of course, for energies larger than 2 keV, the Signal-to-Noise ratio in each bin of the integrated charge cloud increases, thus improving the spatial resolution. In the upper panels of Figure 4-6 we show the SDD spatial resolution along the drift direction for 2 keV photons (left) and 6 keV photons (right) as a function of the absorption point in both the anodic and drift directions. In the lower panel we show the anodic spatial resolution which is in general of the order of few tens of μm and becomes comparable with pitch/2 when the electron cloud is completely collected by one single anode.

4.2.1.2 Imaging properties of a WFM unit

The imaging properties of the WFM unit consisting of two orthogonal cameras has been described in general in the introduction above. We may add that the sensitivity of the WFM cameras is non-uniform, with the best sensitivity in the centre, gradually tapering off to zero sensitivity at 45° off axis (see Figure 4-2). The fall-off of the sensitivity is caused by three factors: a cosine fall off and a mask vignetting effect across the full field, and a partial shadowing of parts of the detector for off-axis angles beyond 16°. The fact that the WFM unit-images are constructed based on images from two cameras with strongly asymmetric position resolution increases somewhat the probability of source confusion in the analysis relative to a true two-dimensional system. This can be counteracted to some extent by angular offsets between the five WFM-units.

The imaging properties of a WFM camera are described in detail in the TN by Imma Donnarumma "End-to-end model of the LOFT WFM" ([RD 28]).

4.2.1.3 Imaging properties in the overlap region between two units

The proposed overall WFM configuration foresees four units arranged in an arc in the plane defined by the solar panels of the spacecraft plus one unit tilted by about 60° from this plane towards the anti-solar direction. Relative to the LAD pointing direction we have two WFM units in the arc tilted by ±15° and two units tilted by ±60°. This produces a large overlap region (nominally 60°x 90°) around the LAD pointing direction and three smaller overlap regions with the cameras at 60°. The original configuration with four units distributed along the arc would mean that the overlapping regions would be mapped with the same imaging artefacts from all of the contributing images. A significant reduction in the image artefacts will result if the direction of the fine position resolution in the four cameras were turned by just a few degrees – a 10° twist would reduce the source confusion region in the image from 5' x 300' to 5' x 30'. The WFM configuration may look uglier, but the images will look much better.

4.2.1.4 Imaging combining data from several observing sessions

The logic of improving the image quality can be extended to image mosaics created from several observations. One particular type of mosaics which will be much used is mosaics of specific source regions (e.g. the Galactic Centre) integrated over observing sessions separated by 6 months. Between such two observing sessions the spacecraft will typically turn by 180° as a result of the movement of the Earth relative to the Sun. For the WFM cameras this means that they are turned upside down. So the offset of the fine resolution line for a given camera relative to the Solar vector will change sign. It is therefore desirable that the camera offset angles are asymmetric relative to the Solar vector – then we will have four different orientations to use in the mosaics instead of only two. In fortunate cases we may even have 10 different orientations if the specific regions has been observed in all five WFM units in both the spring and the fall observing windows.

4.2.1.5 Spectral resolution of the WFM SDD detectors

Since the anode capacitance of the SDD is very small (~50 fF), the main source of noise for these detectors is represented by the leakage current of the volume corresponding to the drift channel. The results obtained in the lab at room temperature can be largely improved by lowering the operating temperature, achieving much smaller values of the leakage current.

The overall energy resolution of the LOFT/WFM detector is affected by various sources of noise and systematics. The reconstruction of the energy of an incoming photon depends on the following factors:

- Fano noise (~118 eV at 6 keV)
- Electronic noise
- Charge reconstruction (number of anodes, common-mode noise subtraction)
- ADC quantization noise.

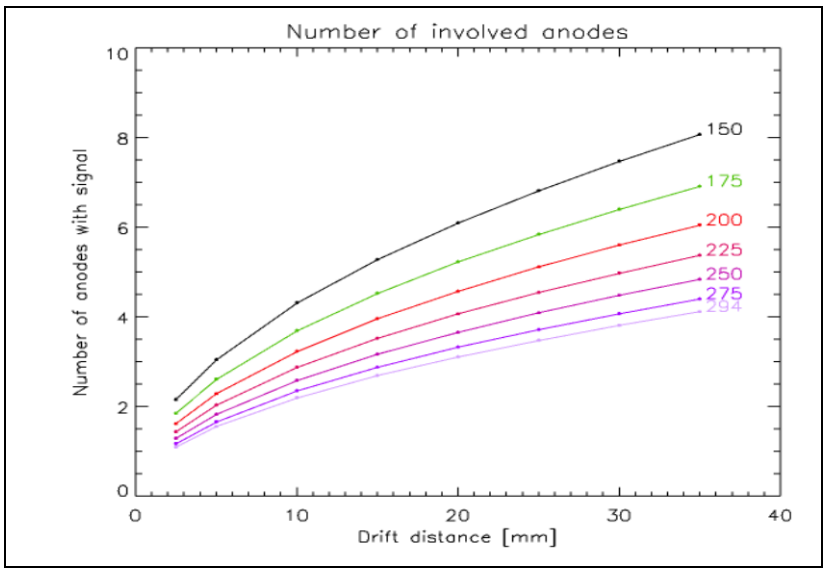

Figure 4-7: Number of anodes collecting the electron cloud as a function of the photon absorption point along the drift direction for anode pitches from 150 µm to 294 µm

As described above, in general the cloud will be sampled by one or more anodes and, moreover, the signal will be affected by a coherently varying baseline due to the common-mode noise. The energy resolution, therefore, decreases with the number of anodes over which the signal spreads, and increases with the number of channels used to evaluate the Common-Mode Noise. Figure 4-7 shows the number of anodes collecting the electron cloud as a function of the photon absorption point along the drift direction for anode pitches from 150 µm to 294 µm. The cloud width is estimated for with T= 253 K and E = 360 V cm^{-1}.

The estimation of the spectral resolution is carried out by dividing each channel in 10 (anode direction, 145 µm total size) × 20 (drift direction, 35 mm total size) bins, and then generating ~10^3 photons in each bin with the following energies: 2 keV, 3 keV, 4 keV, 5 keV, 6 keV, 8 keV, 10 keV, 12 keV, 16 keV, 20 keV, 25 keV, 30 keV.

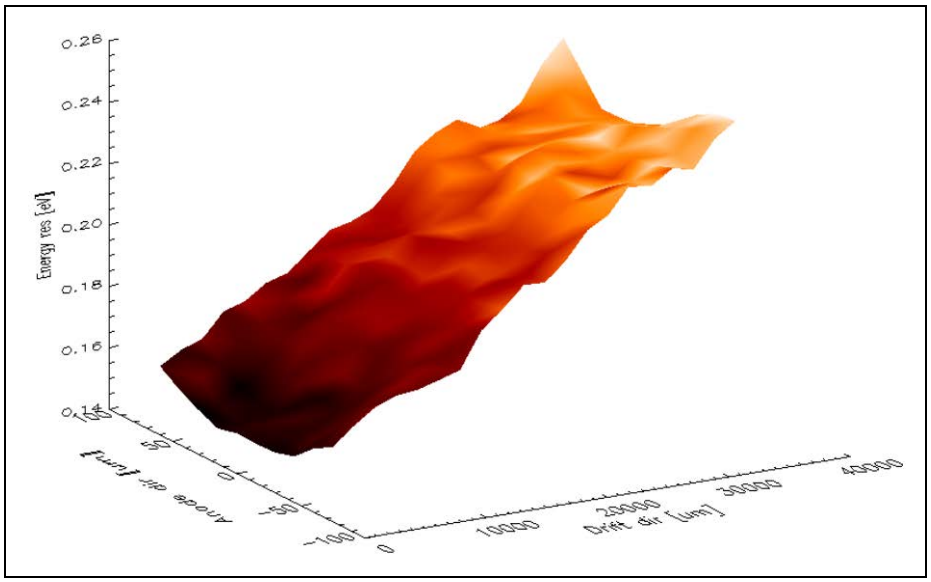

Figure 4-8: Spectral resolution (CMN+ENC+Fano) for a 2 keV photon as a function of the photon absorption point x_0, y_0

Figure 4-8 shows the spectral resolution (CMN+ENC+Fano) of a 2 keV photon as a function of the photon absorption point x_0, y_0, for a detector with 145 µm pitch. In Figure 4-9 we report also the spectral resolution as a function of the photon energy. Solid circles represent the resolution values averaged on the whole SDD channel while the shaded area shows the range of energy resolution for each photon energy (the resolution depends on the photon absorption point).

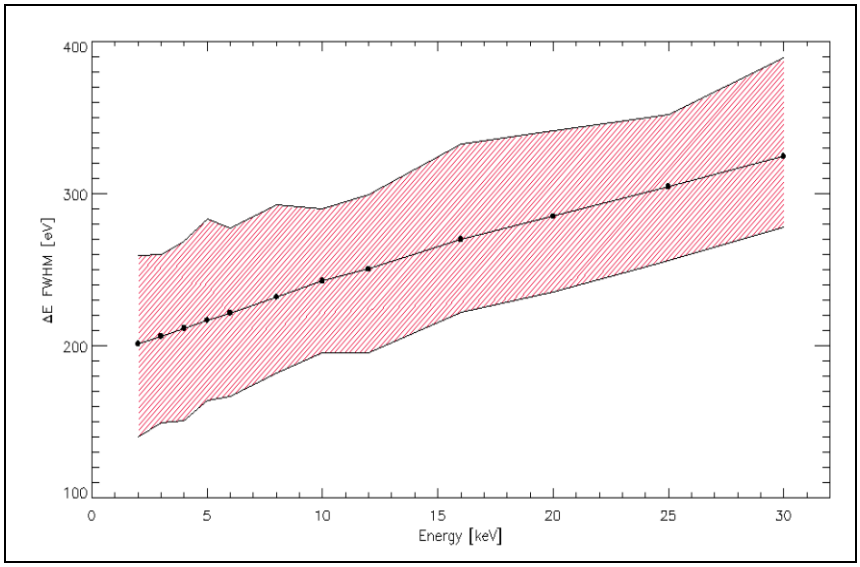

Figure 4-9: Spectral resolution as a function of the photon energy. Solid circles represent the resolution values averaged on the whole SDD channel while the shaded area shows the range of energy resolution for each photon energy

4.2.1.6 Lower energy threshold and detection efficiency

Taking into account the required ENC of 12 e^-, the expected single channel lower energy threshold is foreseen to be of the order of 390 eV, which corresponds to 9 times the channel noise rms and guarantees an absolutely negligible chance probability of spurious triggers. In Figure 4-10 we show the detection efficiency as a function of the photon impact point in both the drift and the anodic coordinates for 2 keV photons. The simulation was carried out considering:

- An electronic noise of 12 e-
- A common mode noise of 25 e-
- A pitch=145 um
- A single channel threshold of 390 eV.

As it is shown, the detection efficiency is greater than 99.5% for each position on the SDD drift channel (99.97% average value). This simulation thus confirms the capability of the SDD to detect 2 keV photons, even when they are absorbed at the very end of the drift channel, ant the charge cloud is split over the maximum of 8 anodes.

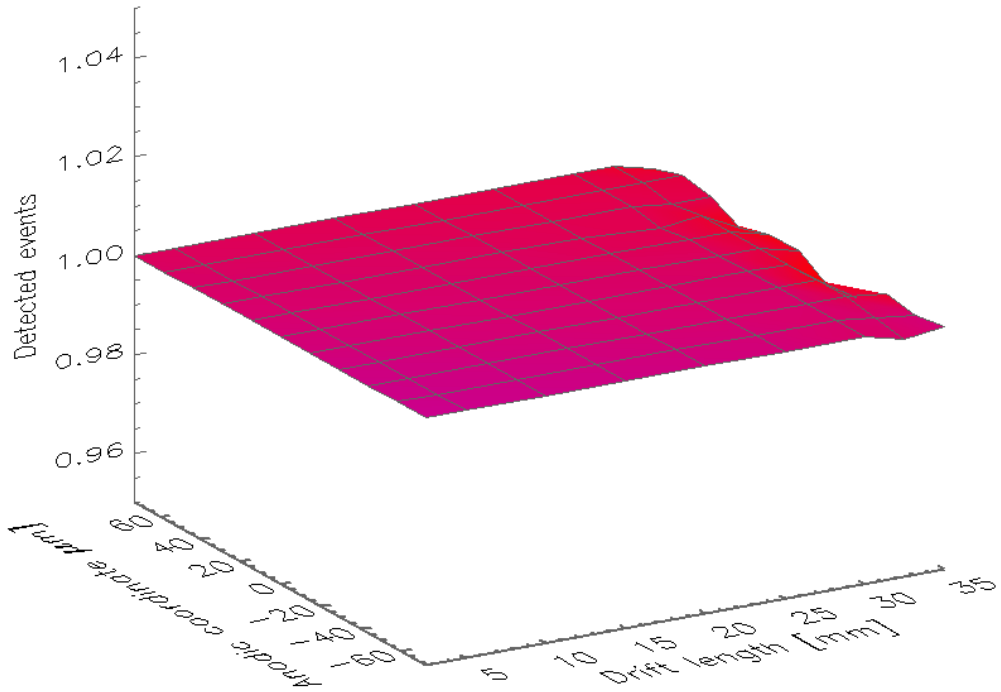

Figure 4-10: SDD detection efficiency to 2 keV photons as a function of the photon absorption point in both the drift (x) and anodic (y) direction. The single channel energy threshold used in this simulation is 390 eV

The expected dispersion on the threshold values in the ASIC was simulated by means of a post-layout Monte Carlo simulation for the ASIC prototype developed within the XDXL program. The simulations were carried out considering both the minimum and the maximum values of the discriminator threshold allowed by the ASIC design. In Figure 4-11 we show the threshold dispersion for Ethr=194 eV (minimum threshold) and Ethr=5.62 keV (maximum threshold). As it can be seen, the expected rms dispersion is of the order of few percents in both cases, and the effect on the detection efficiency of 2 keV photon can thus be considered negligible.

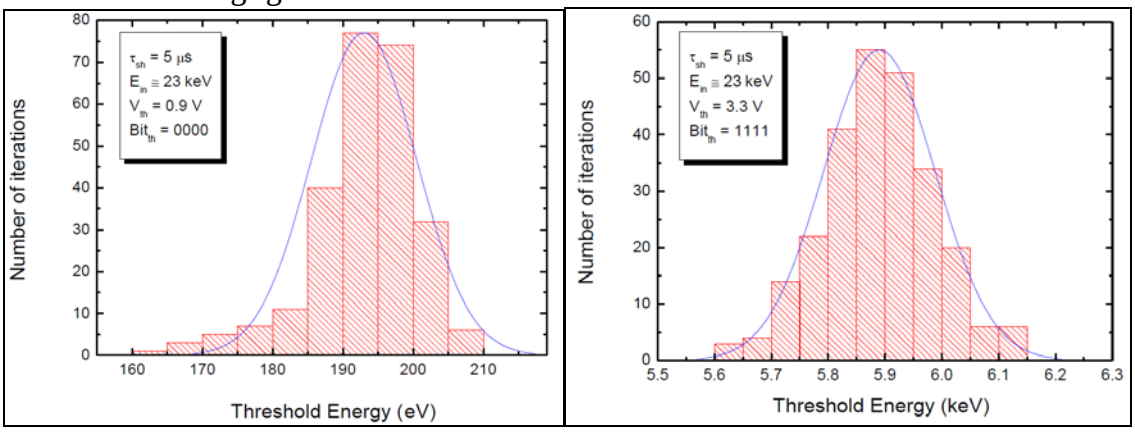

Figure 4-11: (Left Panel) MC Simulated dispersion of the lower energy threshold values for a Ethr of 194 eV. The distribution standard deviation is 7.5 eV (3.8%). (Right Panel) MC Simulated dispersion of the lower energy threshold values for a Ethr of 5.62 keV. The distribution standard deviation is 99 eV (1.8%)

4.2.1.7 In-flight calibration

There are four types of in-flight calibration to be considered:

1. Unit and camera pointing relative to the spacecraft coordinate system (the star trackers)
2. Camera internal alignment
3. Camera energy resolution and absolute energy scale
4. Camera, unit and system sensitivity.

The calibration of the precise pointing directions of the individual cameras can be done quickly and easily using the known positions of the observed X-ray sources. For this reason the requirements on the mounting precision and ground verification of the cameras can be quite relaxed. This information is easily obtained in flight – as long as the mountings are stable over time and insensitive to the temperature variations experienced in orbit.

The internal alignment is much more critical since it affects directly our ability to calculate on-board the positions of new sources. If the internal alignment shows time drifts or temperature dependencies it may require data taken for several months (or even years) to disentangle the variations. Poor or unstable internal alignment will lead to reduced sensitivity of the cameras.

The camera energy resolution and the absolute energy scale can be checked in-flight using fluorescent X-ray lines from the shielding materials in the mask, collimator and back shielding. Like the pointing calibration the energy calibration will be a standard element in the on-ground data analysis.

The sensitivity of a coded mask system is a complex issue which depends as much on the software used for source flux extraction and background reduction as on the mechanics of the flight hardware. The most stable of the brighter X-ray sources in the sky is the Crab Nebula and this has for many years served as the “standard candle” to which all experiments referred their flux calibrations. Unfortunately it is now clear that the Crab Nebula do indeed vary by maybe 10% over time, and for the moment there is really no generally accepted way to get around this uncertainty.

Compared to previous instruments the WFM will have one important advantage, namely the many overlapping fields of view. This means that there will be in every observation the possibility to compare the sensitivities of the cameras – in a unit and also between units.

(see [RD 32] for more details).

4.2.2 Instrument performance specifications

In Table 4-2 we list the instrument specifications of the current WFM design.

Parameter	One Camera	One Unit	Overall WFM
Energy Range	2-50 keV primary 50-80 keV	2-50 keV primary 50-80 keV	2-50 keV primary 50-80 keV extended

	extended	extended	
Active Detector Area	182 cm^2	364 cm^2	1820 cm^2
Peak Effective Area (on-axis, through mask)	>40 cm^2	>80 cm^2	>80 cm^2
Energy Resolution FWHM	< 300 eV EOL @ -30°C	< 300 eV EOL @ -30°C	< 300 eV EOL @ -30°C
Field of View at Zero Response	90° x 90°	90° x 90°	180°x90°+90°x90°
Angular Resolution	5' x 5°	5' x 5'	5' x 5'
Point Source Location Accuracy (10σ)	< 1'x30'	< 1'x1'	< 1'x1'
On-axis sensitivity at 5σ in 3 s (Gal. Center)	380 mCrab	270 mCrab	270 mCrab
On-axis sensitivity at 5σ in 58 ks (1 day Galactic Center pointing, see [RD 34])	3.0 mCrab	2.1 mCrab	2.1 mCrab

Table 4-2: WFM instrument performance specifications

4.2.3 Instrument configuration

The structure of one single camera follows the classical design of coded mask experiments. The coded mask is composed of a 150 µm thick Tungsten foil. The mask pattern consists of open/closed elements of dimensions 250 µm x 16 mm. The detector-mask distance is baselined at ~20 cm to achieve the required angular resolution (5 arc min or better). The size of the mask is ~1.7 times larger than the detector, in order to achieve a flat (i.e., fully coded) region in the centre of the FoV.

Each SDD detector has fine (~30-60 µm) position resolution in one direction and coarse (~5-8 mm) in the other direction. This is reflected into the asymmetrically coded mask, providing each camera an angular resolution of 5 arcmin x ~5°. The fine position resolution in the two coordinates is guaranteed by 2 orthogonal and co-aligned cameras forming each WFM unit.

All of the WFM field of view should be coded (partially or fully) by the mask. X-ray photons outside the field of view are shielded by the collimator which also acts as the mechanical structure holding the mask. The mechanical structure of the collimator can be very light (e.g., carbon fibre), covered by a thin (e.g., ~150µm) Tungsten sheet providing the required shielding for X-rays.

The overall configuration of the WFM consists of 5 units. Each unit is composed of 2 co-aligned cameras (see Figure 4-12). Four of the five units are arranged such that their viewing axes lies in the Y-Z plane of the SC reference frame, and the fifth unit is tilted out of this plane, away from the Sun, by 60°. Relative to the LAD pointing direction, which also lies in the Y-Z plane, the viewing directions of the four units are off-set by ±15° and ±60° relatively.

The units are individually rotated ***around their boresight axes*** (keeping the relative orientation of the two cameras in a unit). The turning angles for the four units covering the arch in the Y-Z plane of the SC reference frame are 14°, 10°, -6° and 2° counting from one end of the arch to the other (the direction along the arc, and the sense of rotation around the boresight [as long as it is consistent] is freely selectable). The fifth unit viewing into the anti-Solar hemisphere is not rotated. A sketch of the WFM configuration is given in Figure 4-12. A Sunshade protecting the WFM masks from direct Solar illumination is required for the WFM instrument.

The exact angles of rotation are not critical, but there are some imaging advantages to be considered, and certain combinations of relative rotation angles optimize the combination of images in different pointings, as discussed in [RD 40]. Therefore, the angles given here are just one example to illustrate the size of the angles to be considered. This is considered feasible with the individual mounting of camera units, but may be reconsidered if it becomes an obstacle for AIV activities. The main point to stress is that a strict alignment with no rotation is the least desirable from an imaging performance point of view.

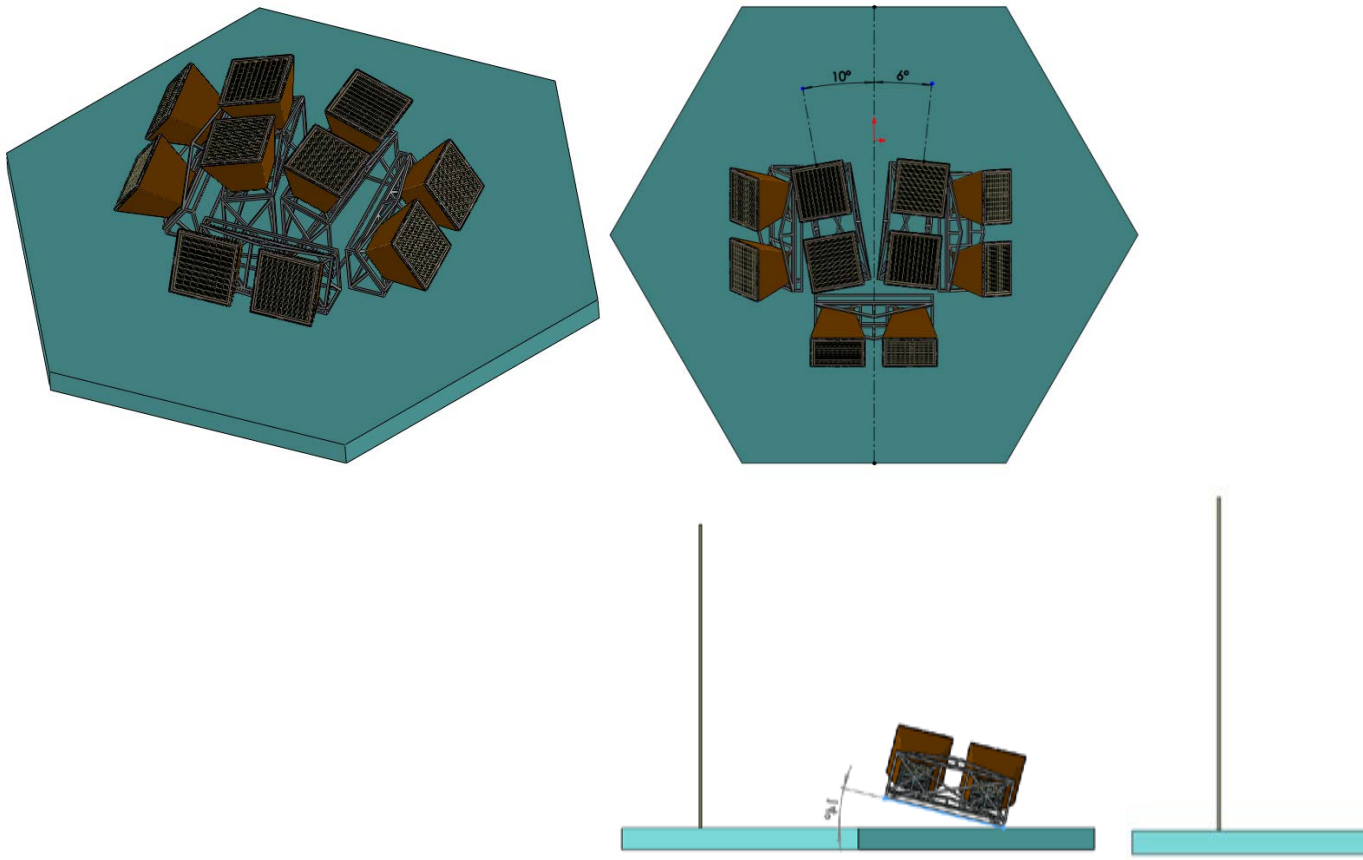

Figure 4-12: The Wide Field Monitor assembly (5 units, for a total of 10 cameras). The relative positions are shown for illustration purposes only

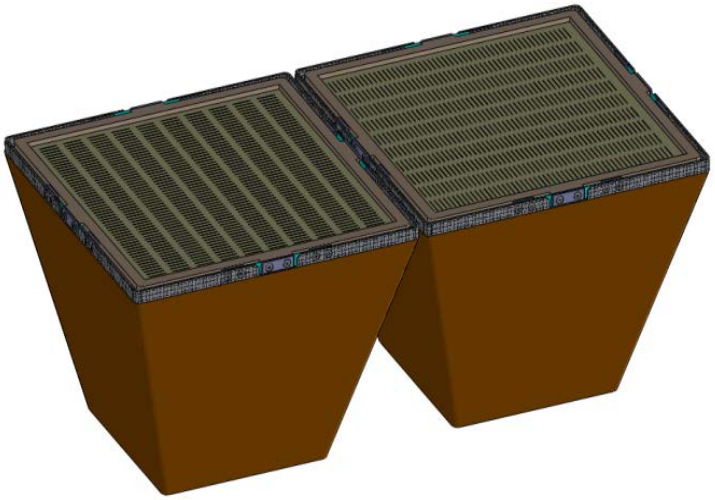

Figure 4-13: One WFM unit (2 cameras)

4.2.3.1 WFM instrument architecture

The WFM Assembly is composed of 5 Camera Units, 5 BEE Units (possibly in a single box) and 1 Data Handling Unit (2 units, in cold redundancy). Each Camera Unit is composed of 2 Cameras. The Back-End Electronics and Power Supply Unit (providing low, medium and high voltages power lines) for each Camera Unit are all collected into a single electronics box which is located in proximity (up to 1.5m) to the Camera Units. Each Camera is composed of 1 Detector Tray, 4 Silicon Drift Detectors, 4 Front-End Electronics, 1 Coded Mask, 1 Collimator. The Units and the Cameras in the WFM are organized to achieve a high level of redundancy. In Figure 4-14 we show the functional block diagram for the WFM.

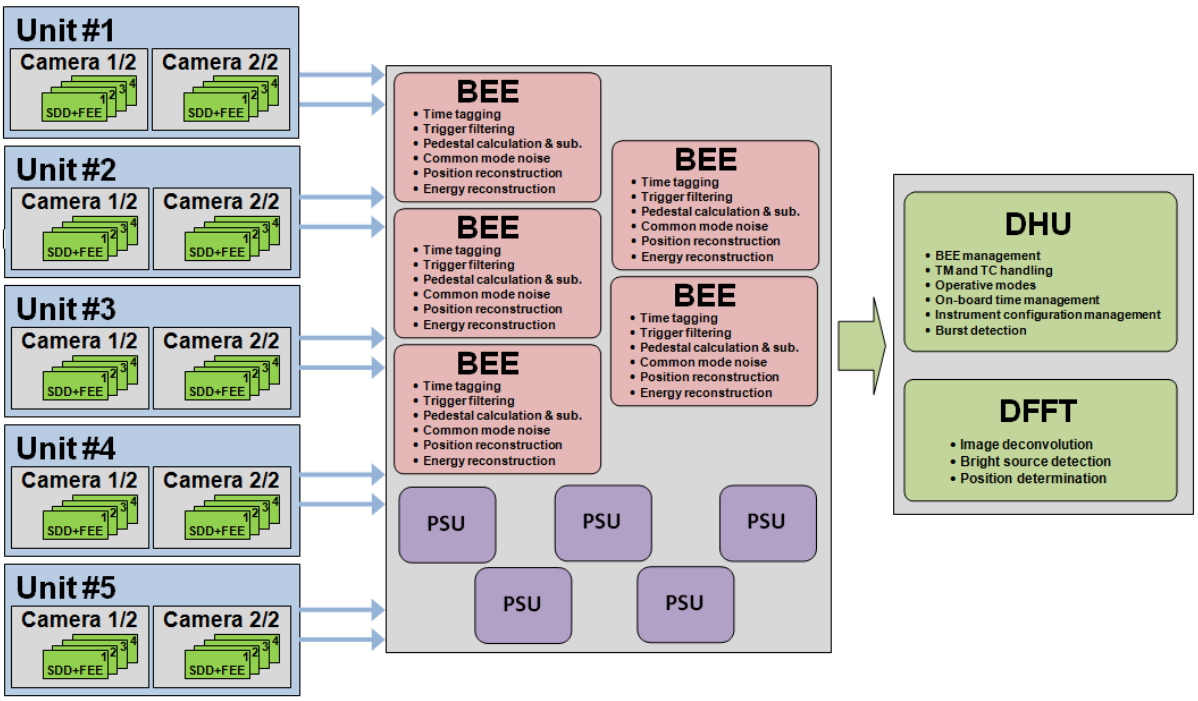

Figure 4-14: Functional block diagram of the WFM experiment. Note that the figure indicates independent power supplies for the five units

The baseline concept of the WFM electronics chain is similar to that of the LAD [RD 31].

The main functions of the WFM FEE are:

- Forward filtered biases to the SDD
- Provide power and configuration biases to the ASICs
- Read-out and A/D convert the SDD signals (ASIC)
- Interface the Back-End Electronics
- Mechanical support for the SDD.

The main functions of the BEE are:

- time tagging
- trigger filtering

- pedestal subtraction
- common mode noise subtraction
- determination of charge cloud center
- energy reconstruction.

The main functions of the WFM Data Handling are:

- interfacing the BEEs
- TC and configuration handling
- on board time management
- image integration.

4.2.3.2 Signal processing

The front-end electronics for the WFM is largely similar to that for the LAD detector, with the exception of the finer pitch of the detector. The read-out architecture is based on an ASIC whose main building blocks (both analogue and digital) are similar to the ASIC for the LAD. The finer pitch in the WFM detectors leads to a larger number of anodes per ASIC or a larger number of ASICs. In addition, the charge from one event is spread over more anodes and allows for a sub-anode position determination of the event. This is done by a fitting process of the charge distribution, which allows to determine the following parameters: the center, the width and the total charge in the distribution. With these, it is possible to conclude back to the original interaction location for a sub-anodic position resolution in one direction and a determination of the drift distance in the detector in the other direction.

Since the event multiplicity (number of anodes affected by each event) is typically larger (up to 8 anodes) in the WFM SDD than in the LAD (where the multiplicity is 1 or 2), it is foreseen to have the WFM ASIC handle more anodes (most likely 32 anodes, possibly 64) than the LAD ASIC (16). The other major difference is that the finer pitch of the detector requires a smaller pitch for the ASIC, mostly limited by the physical size of the ASIC die. Finally, in the LAD ASIC the low power consumption is a design driver, due to the large number of units, while the number of units in the WFM is much smaller, so that a small increase in the power/channel value is affordable. This will allow to use more power for the first stage of the pre-amp, improving the noise figure.
The main functions performed by the ASIC are:

- Trigger detection
- Full analogue event processing chain
- Providing the trigger map of all triggered anodes
- A/D conversion.

Data handling:

Similar to the LAD, in the event of a signal charge above a pre-defined threshold on at least one anode, the ASIC will store all anode charges in an analogue memory and send a trigger signal to the BEE and the BEE will request a trigger map from the ASIC. The

trigger map is analysed to validate the trigger event (not more than ~8-9 channels are triggered and all channels are next to each other). In case of a valid event, the BEE sends a command to start the A/D conversion inside the ASIC, providing an 11-bit output to the BEE for each anode. In case of an invalid event pattern, the BEE will send a reset command. Due to the small SDD pitch size, the charge generated by an X-ray photon event will typically affect many anodes, which may in turn be connected to physically different ASICs. In such cases (i.e. a trigger generated by anodes close to the ASIC edge), the neighbouring ASIC will also be forced directly into the analogue storage of the charges via a dedicated line between the ASICs.

The main processing functions of the BEE are:

- Time tagging
- Trigger validation and filtering
- Pedestal subtraction
- Common noise subtraction
- Location determination
- Energy reconstruction
- Event threshold application
- Differential time calculation
- Event reformatting
- Collecting housekeeping data.

The BEE is designed to process the events within a pipeline structure that handles the events from one side of a single detector (most likely 7 ASICs). This pipeline is initiated 16 times within the BEE FPGA (see section below) to allow processing of data from all 8 detectors (=16 detector halves) of two cameras. After the data transfer from the FEE to the BEE, the first step within each pipeline is the pedestal subtraction. A set of pedestal values (one for each anode) are stored within the BEE.

The next step in the processing pipeline is the common noise (CN) calculation and subtraction. The CN component is a noise component common to all channels connected to the same ASIC and consists of two components: the CN produced by the detector and the CN introduced by the ASIC. The CN is an unwanted signal that is added equally to each channel. Since, however, each channel has its own gain (CSA, shaper, ADC) the pedestal subtracted data needs to be normalized to a uniform gain before CN calculation. To reduce the CN, the average noise after pedestal subtraction is calculated on all anodes that were not in the vicinity of the charge cloud (+/- 2- 4 channels around the triggered anodes to avoid charge from the charge cloud which would be below the trigger threshold). The CN has to be calculated individually for each event.

The gain values for each anode are stored as look-up tables in the FPGA. As the temperature HK is also handled by the BEE, a real time temperature correction is possible. A linear correction E=E*(1-C*(T-T0)) is applied to the energy value of the event. The correction parameters are either uploaded from ground by tele-command, or can be measured automatically on board and stored as look up tables in the FPGA. Threshold

Rejection: In each pipeline there are two values stored for an upper and lower energy threshold. High energy events, which only triggered a few anodes and were therefore not rejected earlier, will show a total energy above this threshold and will be discarded. Events which fall below the lower energy threshold after the subtraction of the CN and the pedestal noise will be also discarded, due to the fact that most likely not the whole event was measured. Each discarded event will be counted in the housekeeping data, where the rates are monitored.

The reconstruction of the event location from the energy corrected charge distribution can be used to achieve a higher spatial resolution than the implemented anode pitch. In addition, the determination of the width of the charge cloud can be used to estimate the drift distance, and give a rough spatial resolution towards the middle of the detector (orthogonal to the anode direction). The most obvious method to determine the shape of the charge distribution is to fit the shape of the measured charge cloud with a Gaussian or more correctly an erf-function distribution, which determines the position of the peak and the width of the distribution, and which then can be used (together with the total charge signal) to reconstruct the drift distance. This is done by a fit of the single cluster channel values with the function "anode_ x = q * [erf((x+0.5-m)/s) - erf((x-0.5-m)/s)] " with x = anode position, q = total charge and the fitting parameters m=center of distribution, s= width of distribution. Because of the incapability to perform fitting operations inside an FPGA in hardware alone, an additional processor has to be included in the FPGA design, to perform and handle the fitting procedure. An additional concern is also the handling of non-convergence cases, where the fitting procedure has to be aborted after some specific time.

An alternative (simpler) approach is the usage of the weighted centroid method, where the centroid of the charge distribution is calculated by summing over the product of each anode and its position and then dividing by the total charge: centroid of charge distribution = sum (C_i * x_i)/sum(C_i). Assuming a Gaussian distribution, the width can then be calculated by using the following equation: width = ((1/sqrt(2*Pi)) * total charge / amplitude)*pitch.

The final solution depends on the capabilities of the finally selected FPGA. We are in the process to compare these possibilities for a variety of energies and positions, solving the question if a simplified method, such as the calculating the centre of the charge distribution method, would be sufficient to reconstruct the position of the event to the desired requirements. According to the final implementation, the energy is reconstructed either through the same fit that yields the impact position or by summing the signals in the channels over threshold.

In the final event packet that is passed on to the DHU, differential time is used instead of absolute time for the time tags in order to reduce the amount of data to transfer. To calculate the differential time, the events are first stored within a buffer, reordered if necessary and finally the time difference is calculated. If the differential time can use also negative integers for encoding, the reordering will not be needed. This is still under consideration. If the evaluated differential time is greater than the upper limit of the codeable range, a dummy event will be generated. Every 100 ms an Absolute Time Event

will be generated in order to stop errors from propagating through the differential time from event to event. The event packet passed on to the DH consists of 40 bits (X,Y, E, deltaT) per event.

Current calculations estimate a background count rate of 2200 counts/s and 910 counts/s (before mask per unit) for an observation of the Crab. This leads to a data stream of 31.1 kbits/s from the BEE to the DH for this typical observation.

One BEE will process signals for two cameras so in total there will be five BEE boards (hosting an RTAX 2000S FPGA and an ADC to convert the sensor data for housekeeping) within the same electronics box. The respective power supply boards will be hosted most likely in a dedicated power supply box. It is currently an option to have a dedicated onboard image reconstruction board in order to be able to determine the sky position of a bright source automatically on-board. This board will be part of the DHU and will host a LEON3 microprocessor inside a Virtex-IV or Virtex-5 FPGA. This board would be inactive until a bright transient source or burst is detected by the rate meters and then derive the position within seconds.

4.2.4 Instrument optical design

4.2.4.1 Collimator

The coded mask and the detector plane are the key elements of the WFM cameras. The image quality depends on the mechanical stability of the structure connecting these two elements. But it is also important to reduce the X-ray background coming from outside the field-of-view i.e. from outside the mask region. Therefore the mask support is covered with X-ray absorbing material (Tungsten) and also underneath the detector plane an X-ray shield is present.

In addition to X-rays the SDDs are sensitive to visible and UV light, which causes an increase in the leakage current. Shielding against the optical- and UV light is achieved by a light tight – but well ventilated - design of the detector tray and collimator structure.

4.2.4.2 Sunshade

A sunshade will be quite helpful to protect the two key elements of the cameras, the mask and detectors, from the fluctuations of the environment mainly by the solar radiation. The location of the sunshade in the Optical Bench should be such as it does not obstruct neither the field of view of the units nor the LAD. For illustrative purposes, we adopt a tentative height of 1390mm in Figure 4-15.

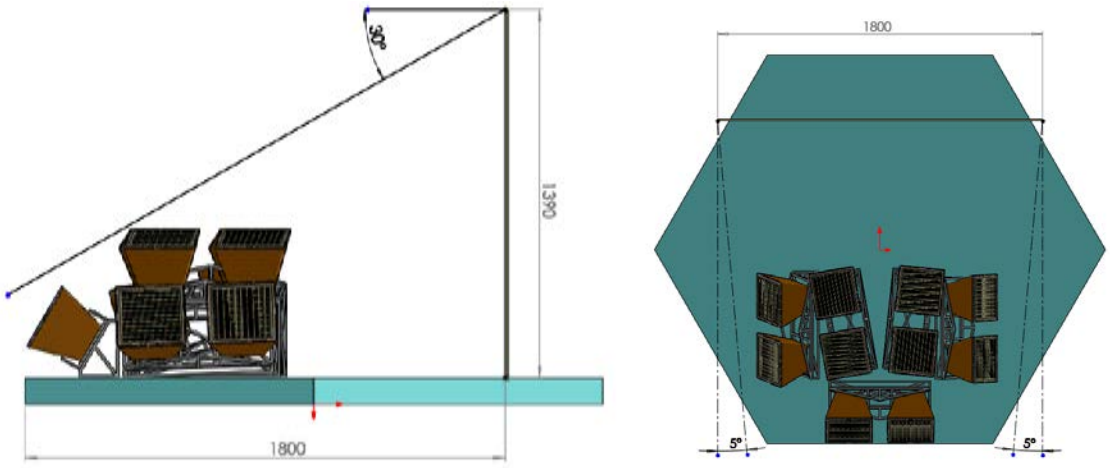

Figure 4-15: Sunshade placement on the optical bench

4.2.4.3 Filters

Two types of filters will be employed: a thermal foil in front of the mask and a thin Beryllium foil above the detector. The thermal foil is important in order to reduce as far as possible the temperature variations of the mask. A stable mask temperature is very important for maintaining the flatness of the mask. The Beryllium foil (25 μm) serves both as a light tight cover for the detectors and, together with the thermal foil and the mask, as protection against micrometeorites. The thermal foil will be made resistant against Atomic Oxygen by an overcoat of 0.16 μm layer of SiO2.

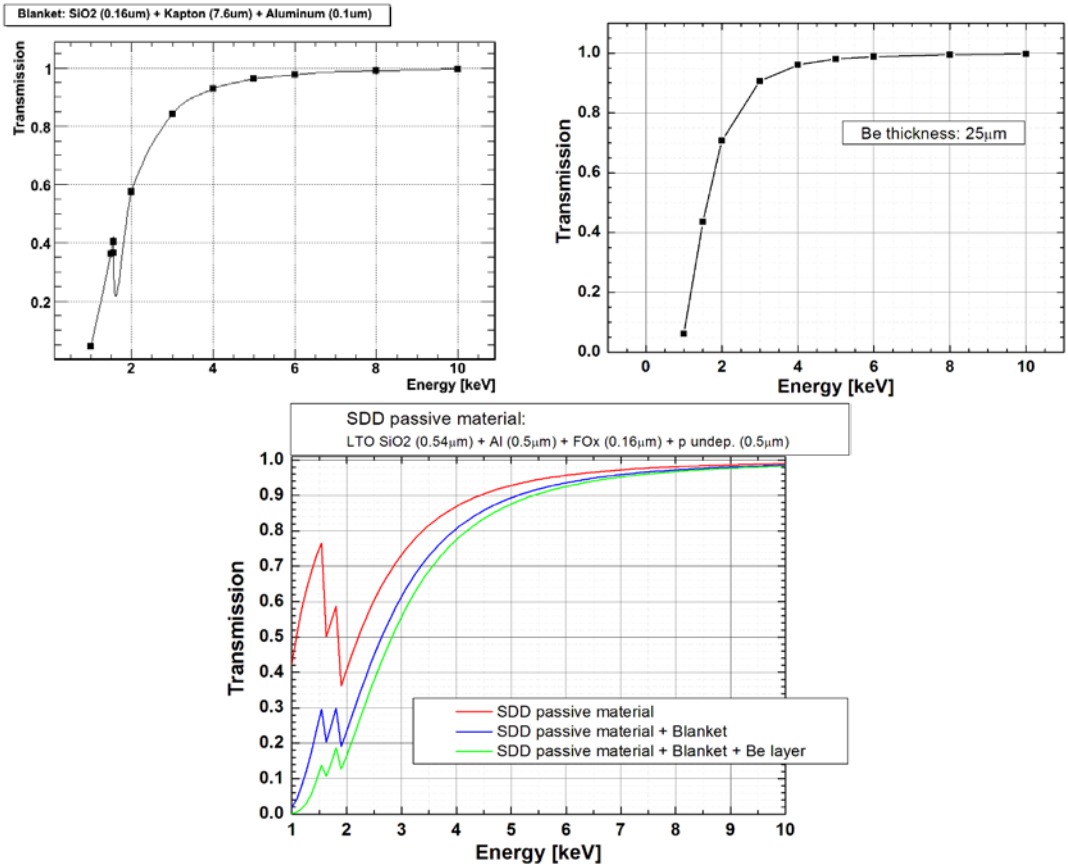

Figure 4-16: Soft X-ray transmission of commercially available thermo-optical filter (upper panel left), Beryllium window (upper panel right) and sum of the contribution of all layers in front of the detector plane (lower panel)

4.2.4.4 Be layer placement

The Be window is located about 8 mm above the detectors in order to prevent HV discharges. To hold the Be window, a CFRP frame of 1mm thickness, providing mechanical strength and stiffness, is used, see Figure 4-17. This structure is fixed to the collimator walls and does not obstruct the field of view of the detectors.

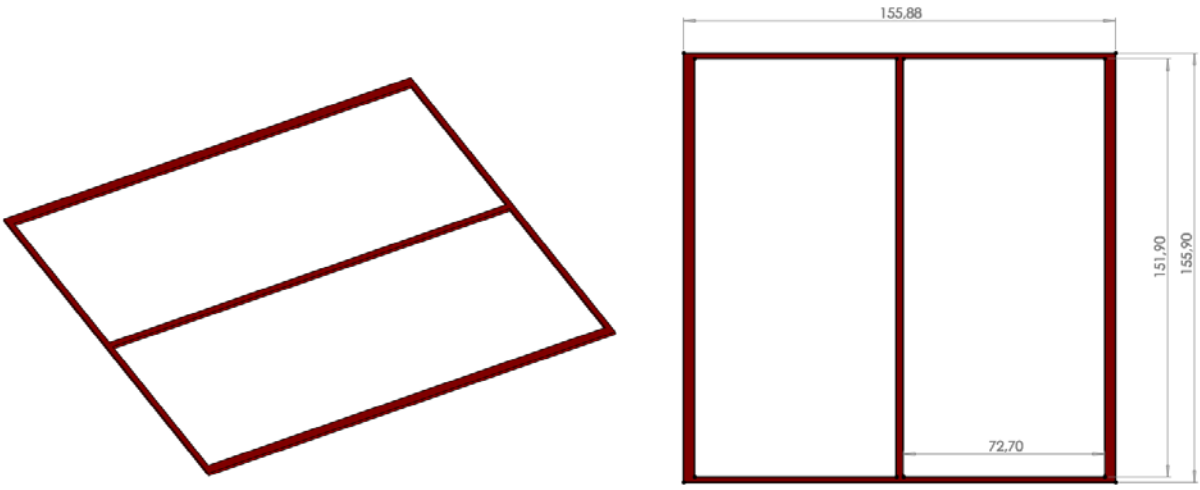

Figure 4-17: Be layer support structure

4.2.5 Instrument units' mechanical design

4.2.5.1 Overall instrument

The overview of the WFM instrument is shown in Figure 4-18. The system is composed of 10 cameras, each employing 4 SDD detectors. Each camera is fixed to the optical bench through an aluminium structure that will provide mechanical strength and stiffness.

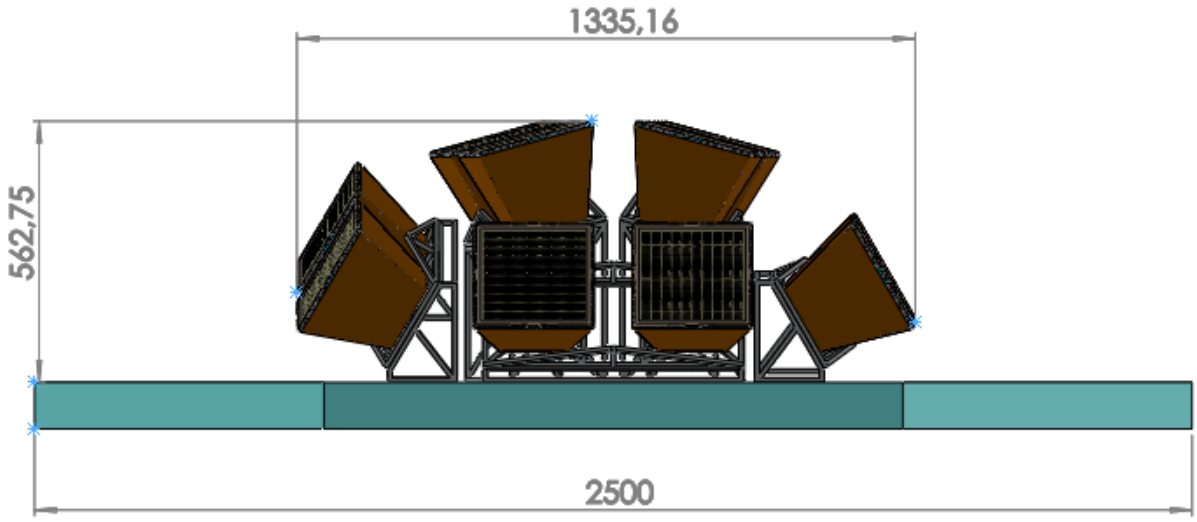

Figure 4-18: Side view of the WFM assembly

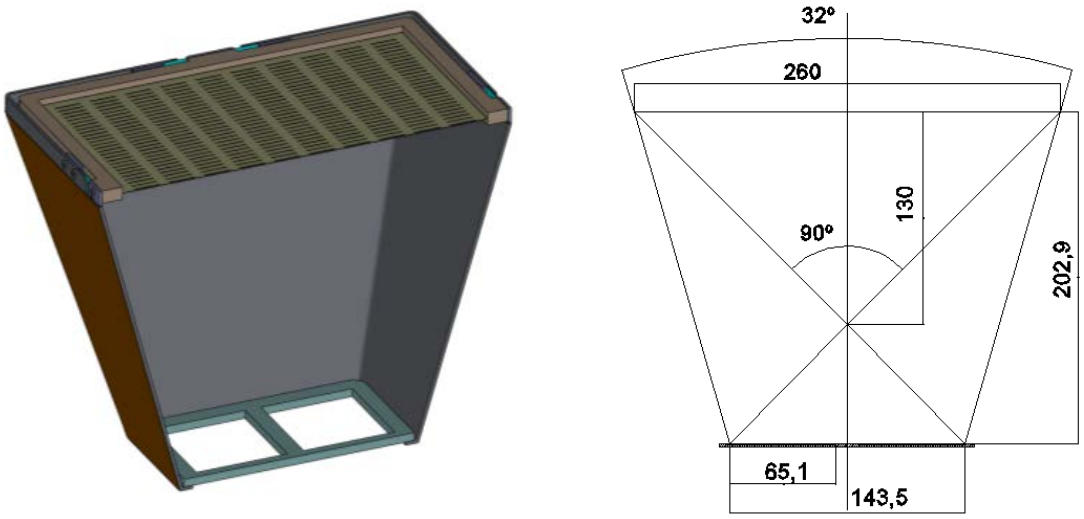

Figure 4-19: View of “half” of one camera and the “other-side” view of the WFM

4.2.5.2 Detector Plane

The detector plane of each camera is composed of a Detector Tray (the support structure), 4 SDD detectors and their front-end electronics (FEEs). Below we provide for each of the elements the current level of definition and the mass budget. The latter is then used as an input for the overall mass budget of the WFM.

4.2.5.3 Detector Tray

A detector tray made of Aluminium will allocate the 4 detectors and the corresponding FEEs. This kind of tray will enhance the conduction of heat losses to the structure and to the optical bench. The tray shall also be de-coupled of the CFRP to avoid thermal stresses. The detector tray for one SDD is shown in Figure 4-20, Figure 4-21.

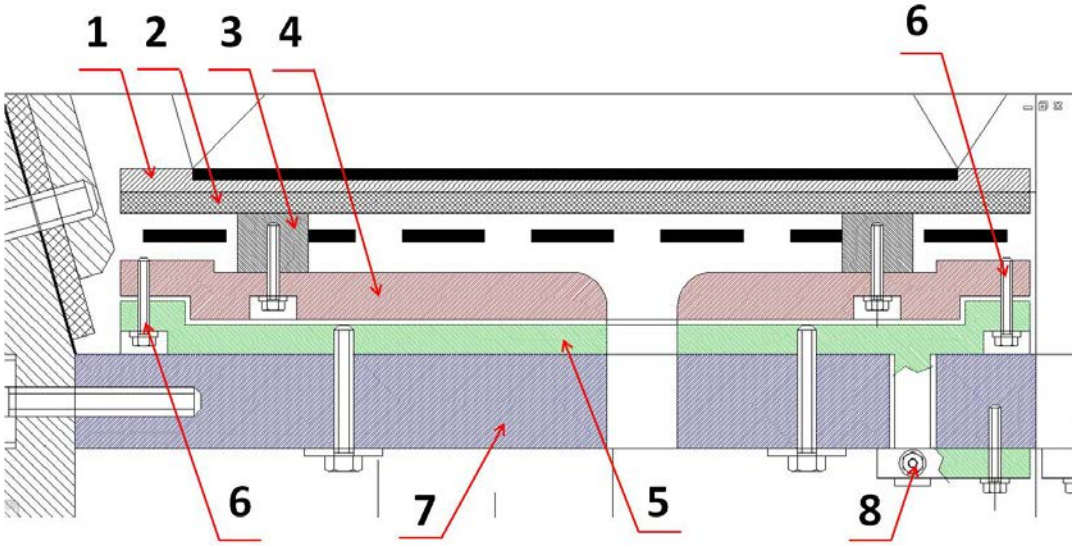

Figure 4-20: A preliminary design of the support structure of each SDD/FEE, with alignment mechanisms. (Frontal cross-section)

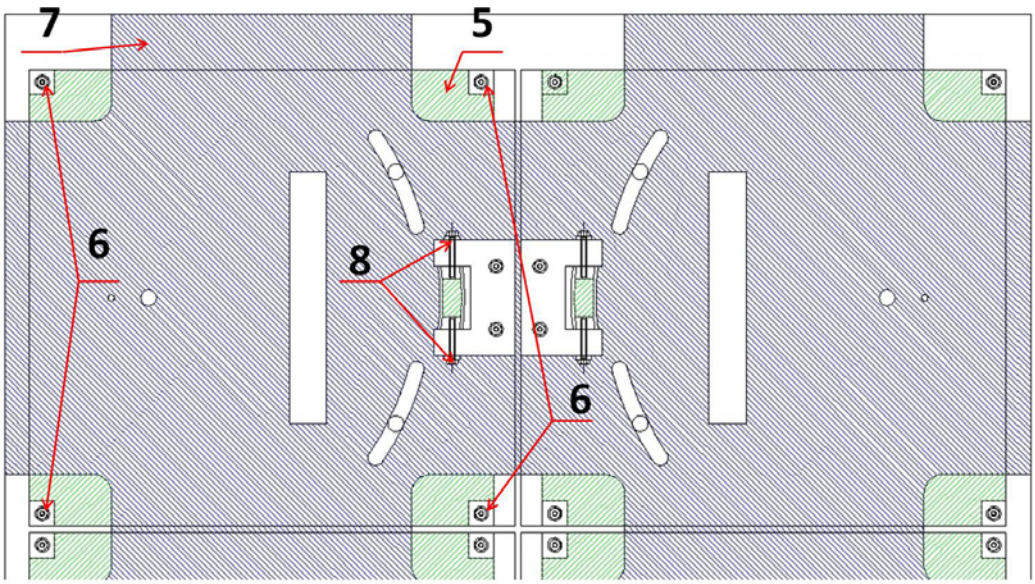

Figure 4-21: A preliminary design of the support structure of each SDD/FEE with alignment mechanisms. (Bottom view)

1) SDD
2) FEE
3) Fix pins (4 units)
4) Detector alignment plate
5) Detector base plate
6) Micrometer screws (4 units, tilt alignment)
7) Detector tray
8) Micrometer screws (2 units, twist alignment).

Each SDD/FEE will have an independent support structure in order to enable its independent alignment after assembling the camera. Four pins will be used for the FEE board fixation to the detector alignment plate (4) in order to increase the alignment capability of SDD/FEE. The alignment will be performed in tilt and twist directions.

The thermal dissipation will be performed through the fix pins and flexible thermal straps (SDD/FEE – alignment plate (4), alignment plate (4) – base plate (5)). Using the flexible thermal straps will not affect the alignment of the SDDs.

Material	**Thickness**	**CBE Mass**
Al	10 mm	717 g
Total one camera		717 g
Total one unit		1434 g
Total WFM		7170 g

Table 4-3: Mass budget for the detector tray

4.2.5.4 Detectors and Front-End Electronics assembly

4.2.5.4.1 The SDD detectors for the WFM

The Silicon Drift Detectors (SDDs) foreseen for the WFM have the same design and characteristics as those for the LAD, with the only difference in the smaller overall size of the Si tile (for the WFM: 77.4 mm x 72.5 mm, vs 120.8 mm x 72.5 for the LAD) and in the smaller anode pitch (145 μm for the WFM, vs 970 μm for the LAD). The individual SDD for the WFM have therefore the characteristics listed in Table 4-4.

Parameter	**Value**
Si thickness	450 μm
Si tile geometric size	77.4 mm x 72.5 mm
Si tile active area	65.1 mm x 70.0 mm = 45.57 cm^2
Anode pitch	145 μm
Number of read-out anodes per tile	448 x 2 rows = 896 total
Drift length	35 mm

Table 4-4: Characteristics of the SDD for the WFM

A total of 4 SDDs composes the detector plane of each individual WFM camera. The overall dimension of the SDD assembly is 145 mm x 154.8 mm. The total number of read-out channels per WFM camera is 3584 (=896x4). The active area of each WFM camera is squared, 142.5 mm x 142.5 mm. This allows to arrange two identical cameras at 90° (in order to achieve fine angular resolution in two coordinates) but still having the same field of view, to compose one WFM Unit.

The choice of the SDD size is driven by the requirement of a square active area for the overall camera and by the requirement of not increasing the drift length much longer than 35 mm. Instead, the choice of the anode pitch is the result of an optimization study of the detector performance, based on experimental tests and simulations.

Table 4-5: Mass budget for the detector units

One SDD			
Material	**Size**	**Thickness**	**CBE Mass**
Coating	72.5 mm x 77.4 mm	-	-
Silicon	72.5 mm x 77.4 mm	450μm	5.7 g
Aluminum TBC (Radiator)	72.5 mm x 77.4 mm	1 mm	14.6 g
4 x SDD			
Tungsten (Back shield)	164 mm x 164 mm	200μm	103.8 g
Total one camera			185 g
Total one unit			370 g
Total WFM			1850 g

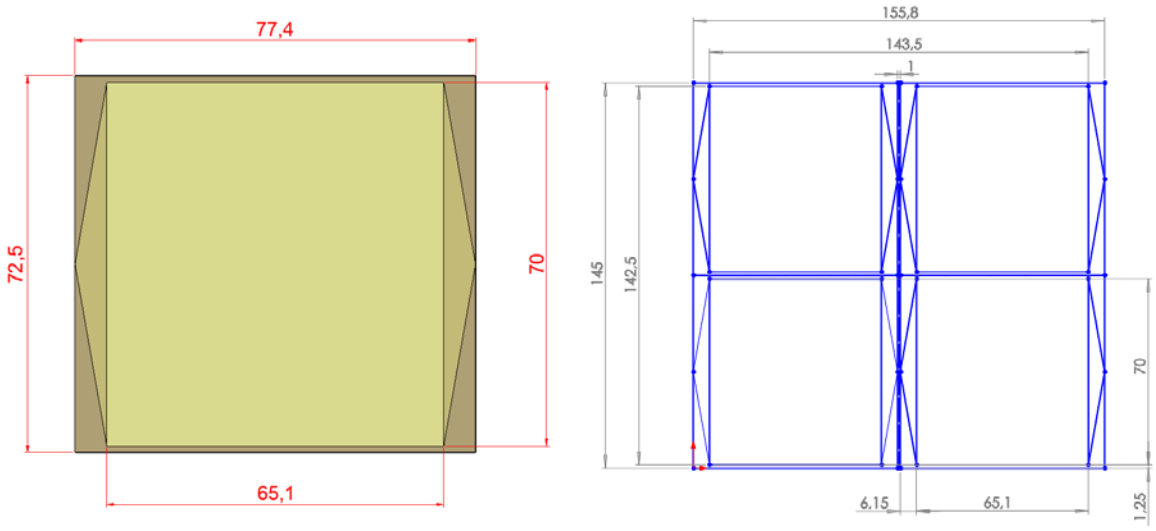

Figure 3-22: left: A single SDD detector for the WFM. The anode pitch is 145 µm, for a total of 896 channels (448 each side). Right: The 4 SDDs composing the detector plane of each WFM camera

4.2.5.4.2 Front-End Electronics

The FEE hybrid board for the WFM SDD will have similar architecture, functions and interfaces as the LAD FEE. Each SDD will be read-out by 14 ASICs of 32 channels each (to be confirmed: 64 channels per ASIC may also be an option), for a total number of 28 ASICs/SDD, 112 ASICs/Camera, 224 ASICs/Unit, 1120 ASICs for the whole WFM Assembly. From the mechanical point of view, the FEE board will be glued to the SDD, on the side of the read-out anodes. A proper FEE hybrid design will enable a standard 2D wire bonding connection from the SDD anode to the ASIC input. The HV bias to the detector will be provided on the same side, and then it is brought to the other side (the entrance side for X-rays) by a wrap-around cable (already used in ALICE along with the bias of the collection zone cathodes derived from the medium voltage (MV). The FEE board will host the connector to the BEE.

Preliminary sketches of the FEE board are shown in the following figures. The size of the FEE board is anticipated as 66.0 mm x 77.4 mm x 2.0 mm. The FEE board will be fixed to detector tray via 4 fix pins, which also will have the function of thermal interface. Given the number of components on the FEE, it might be necessary to decouple the thermal interface from the pins, using a dedicated thermal strap. A thermal plane integrated will be implemented in the FEE PCB. Dedicated thermal simulations will determine which shall be the best thermal strategy. To monitor the local temperature, a thermal sensor will be implemented on each SDD.

The WFM design is planned to be as similar as the LAD one, although some of the thermal aspects might drive to different implementation choices. In particular, the LAD FEE BB will be developed using the same ASICs as for the WFM, thus having a common electronics design between WFM and LAD on the BB development.

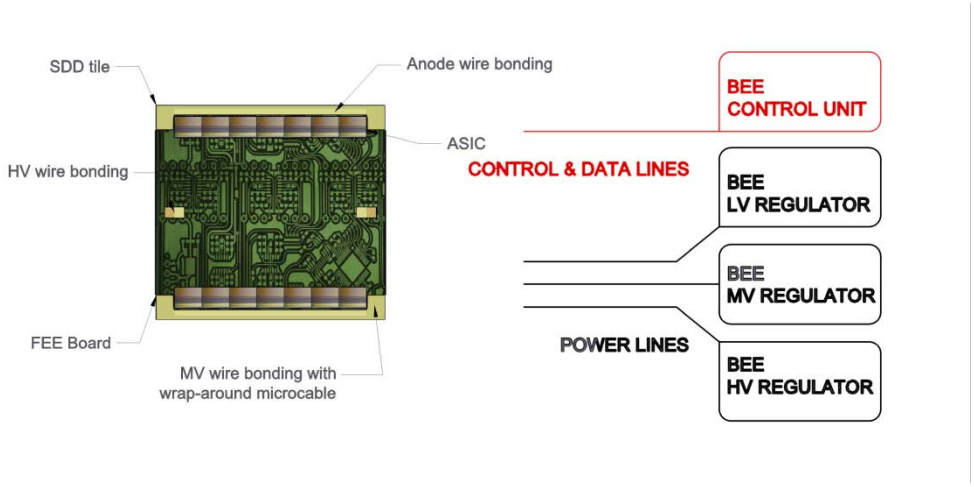

Figure 4-22: Preliminary sketch of the WFM FEE board and electrical interfaces

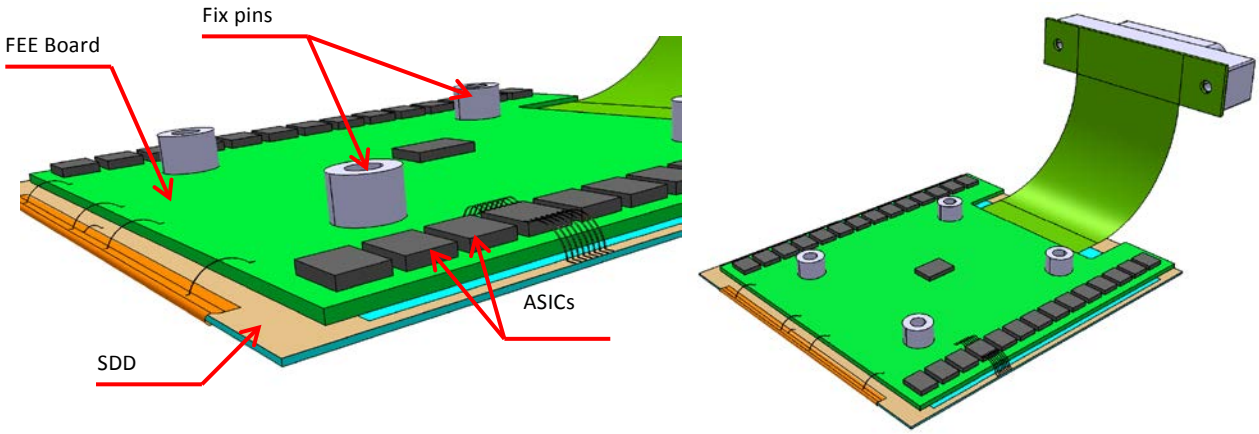

Figure 4-23: The assembly of the individual detector and FEE for the WFM ("bottom" view)

The estimated FEE mass for one camera is approximately 80 g. Total WFM is 800 g.

4.2.5.5 Back-End Electronics

In the current WFM architecture there is a Back-End Electronics (BEE) board for every Unit, each BEE handling two cameras. The five BEE boards, together with the five power supply (PS) boards, will be located in one central box to be placed at the optical bench with interfaces to the 10 individual cameras and to the data handling unit (DHU).This choice will increase the redundancy of the WFM design. While in earlier designs one BEE/PS handled a unit of two orthogonal cameras with the same viewing direction, in the current baseline the priority is given to preserving the total sky coverage and ensuring a good LAD direction coverage in case of failure of one BEE/PS. For this reason one BEE/PS now handles two orthogonal cameras of different viewing directions.

Table 4-6: BEE Electronics Box: (1 Al Box with 3 PCBs)

Material	Size	CBE Mass

Al	200x200x100 mm	1200 g
Total one unit		1200 g
Total WFM		6000 g

4.2.5.6 Collimator and mask support

The collimator that supports the coded mask is made of 2 mm thick of CFRP covered by a layer of 150µm thick Tungsten to shield X-rays. The collimator also prevents X-rays coming from outside the field of view to reach the detector (this is achieved by the Tungsten sheets, CFRP is mostly transparent to X-rays) and shield the detectors against optical and UV light (the interfaces between the collimator and the detection plane and the mask will need to be light-tight). From the mechanical perspective, the collimator acts as support structure for the coded mask.

The preliminary drawings of the collimator structure are shown in Figure 4-19. Venting of the air inside the collimator during launch will be assured through light tight venting channels in the collimator walls.

Table 4-8: Mass budget for the collimator

Material	**Thickness**	**CBE Mass**
CFRP	2 mm	633 g
Tungsten	150 µm	597 g
Total one camera		1230 g
Total one unit		2460 g
Total WFM		12300 g

4.2.5.6.1 Coded mask

Each one of the 10 WFM cameras has its own coded mask. The open fraction of the mask is currently baselined at 25% (i.e., 75% of the area in full elements and 25% in holes). The size of the individual elements is 250 µm x 16 mm. The overall size of the mask is 280 mm x 280 mm and the thickness is 150 µm, the coded area is 260 mm x 260 mm. In the coded area there are 14 columns of slits uniformly distributed and there is a separation space between slits of 2.77mm, as shown in the following figure.

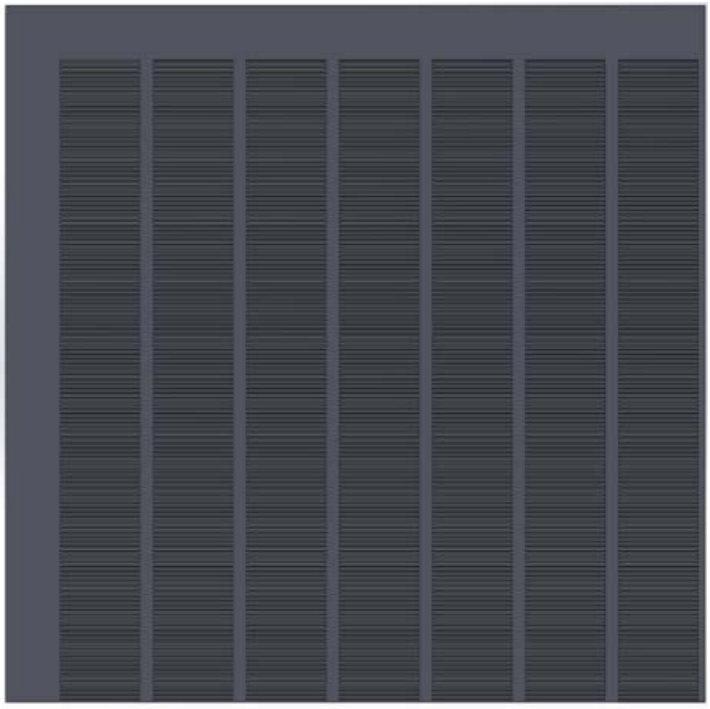

Figure 4-24: A quarter of the coded mask

The choice of W among the high atomic number materials is justified by the heritage of SuperAGILE (117 μm thick, 440 mm x 440 mm overall size, 242 μm minimum strip, e.g., Feroci et al. 2007, NIM A 581, 728) and by a preliminary comparative (mechanical) analysis of Tantalum. The coded mask is mounted in a pretension frame and this frame interfaces to the CFRP structure using flexure elements to reduce the thermal stresses. The pretension frame for the coded mask is shown in Figure 4-27.

There are strict requirements on the flatness and stability of the coded mask. The mask must be flat (or at least maintain its shape) to ±50 μm over its entire surface across the full operational temperature range. This requirement implies that we cannot tolerate large gradients in temperature and consequently that the Temperature excursions between the sunlit and the dark parts of the orbit must be less than 10 ˚C. This is the prime reason why a sun shield is a necessity for the WFM.

The mask code is presently based on the biquadratic residue set based on the prime number 16901. This set has perfect coding properties for an ideal detector. The WFM cameras are not perfect, but we suspect that the good coding properties are only marginally affected by the deviations from perfection. This assumption will be checked in the course of the development programme.

Table 4-7: Mass budget for the WFM masks

Material	**Size**	**Thickness**	**Mass**
Tungsten	280 mm x 280 mm	150 μm	226.44 g
Open fraction 25%			
Coded mask			178.4 g
Mask frame			1406 g
Ribs (4 per mask)			64 g

Total One Camera	1648.4 g
Total One Unit	3296.8 g

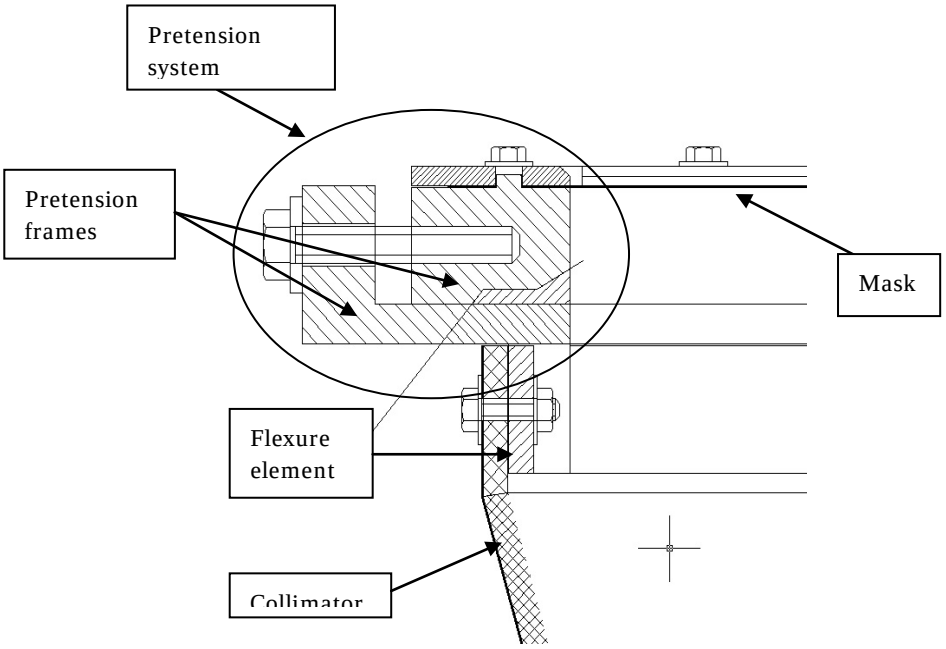

Figure 4-25: The interface between the coded mask and the pretension frame, and the interface between the flexure element and the collimator

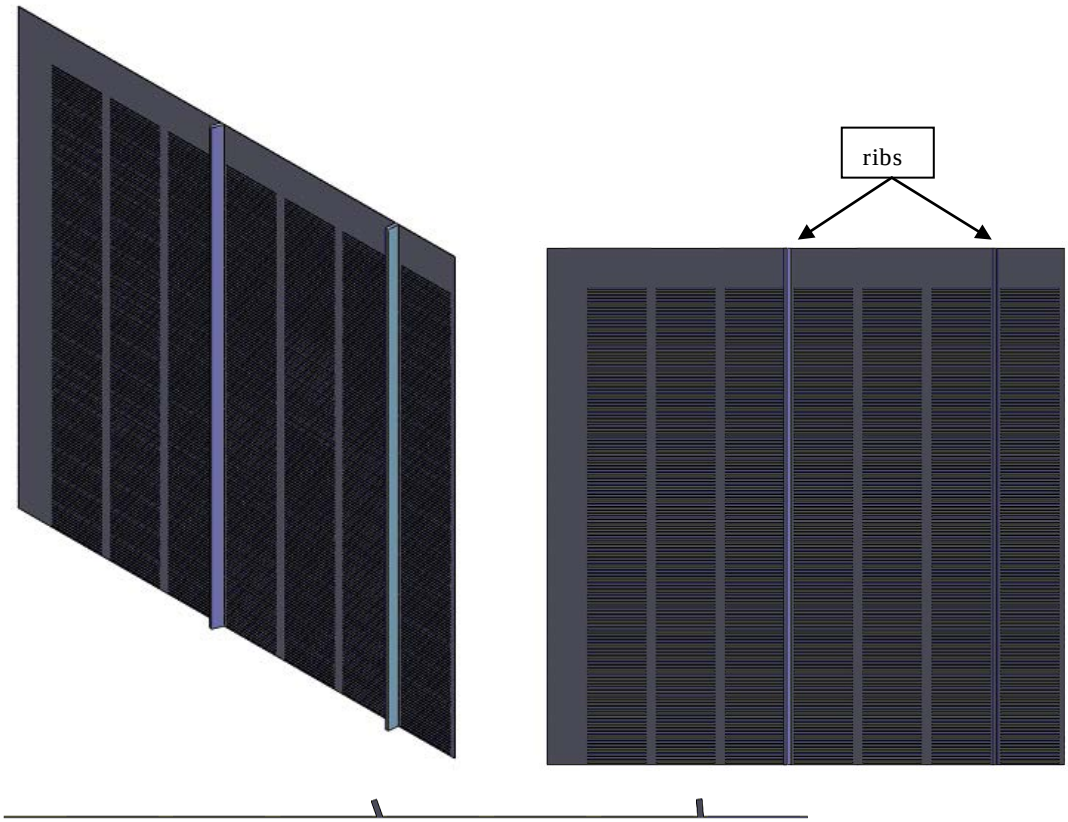

Figure 4-26: A quarter part of the mask with the ribs, there are a total of 4 ribs. Detail of ribs inclination

In order to minimize the vertical displacements of the mask during the operational mode the pretension mechanism is introduced. The mask will be pre-tensioned in all ranges of the temperatures to assure that buckling on the mask does not appear under different loads.

4.2.5.6.2 Coded Mask support structure (skeleton)

In order to overcome the loads produced during launch, a support structure for the mask has been designed. This support structure provides mechanical strength and stiffness to overcome an inertial load of 30g.

The support structure is made up of 4 ribs placed between the slits columns as shown in Figure 4-26. The rib size is 280 x 3 mm with a thickness of 1mm. In order to not cast shadows on the detectors active area, the ribs have a different inclination depending on their position. The ribs can be placed below the mask, above the mask or at both sides. Calculations indicate that 4 ribs located above the mask are enough to overcome an inertial load of 30g.

4.2.5.7 WFM Support Structure

An Aluminium structure of 10x10 mm cross section will anchor the WFM assembly to the optical bench. The support structure may possibly also serve as a thermal conductive path

to the optical bench. Each unit may be placed independently on the optical bench. The independent assembly will give flexibility in the distribution on the optical bench. However, if at SC-level it is desirable to co-locate the WFM camera units together (probable because of the need for a heatshield), then a common structure is probably more suitable for maintaining co-alignment.

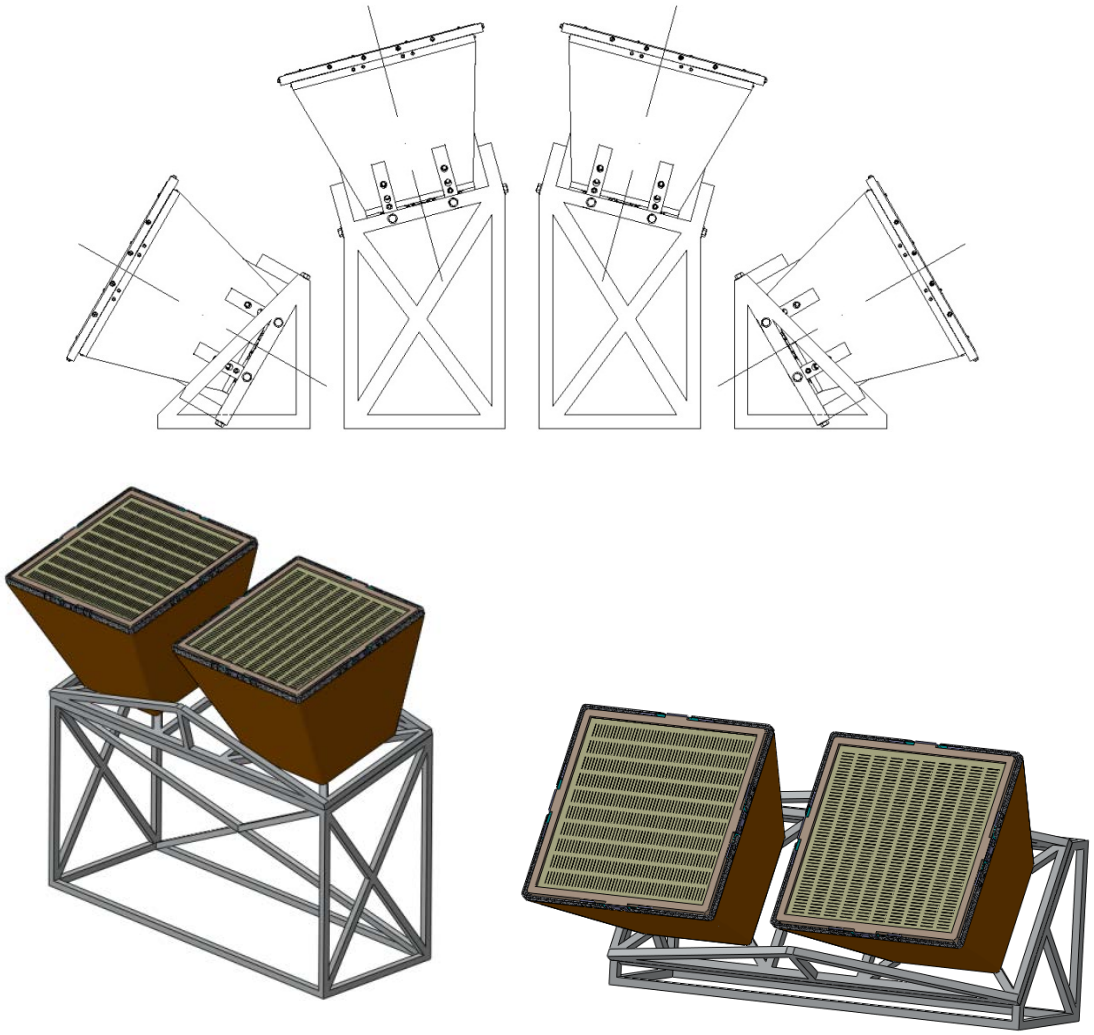

Figure 4-27: WFM support structure

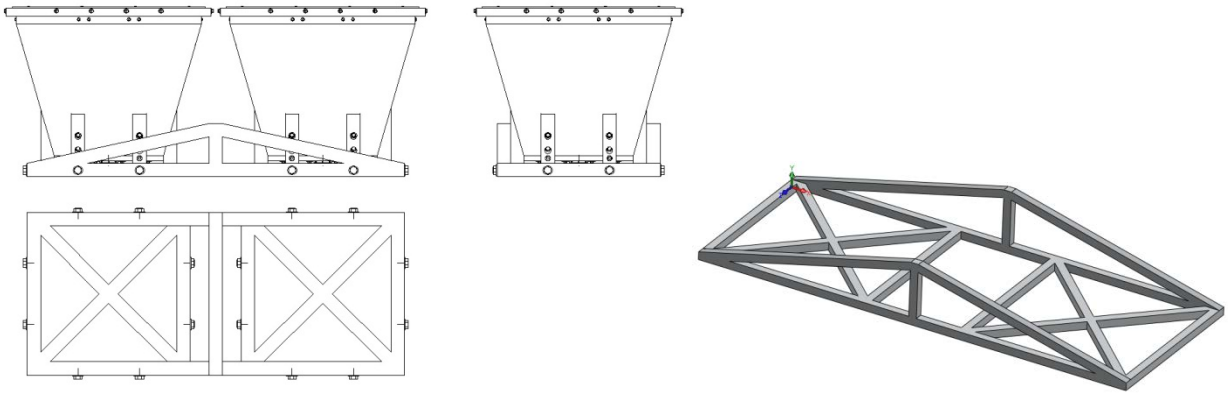

Figure 4-28: WFM unit support structure

Table 4-8: Support structure mass budget

Material	Thickness	Mass
Al	10 mm	13200 g
Bolts		320 g
Total		13520 g

4.2.5.8 Mechanisms

No mechanisms are foreseen for the WFM.

4.2.6 Instrument units thermal design

Thermal analysis has been carried out for a WFM unit, assuming the current design baseline for the mechanics and the power dissipation and reasonable assumptions for the thermal parameters (environment and interfaces). ESARAD/ESATAN software packages have been used.

The thermal model unit includes 80 nodes for both cameras+ 2 external nodes (deep sky and Optical Bench) + 2 nodes for the sunshade (if required) + 2 nodes for the radiator plate (if required). The camera nodes are now described:

- Mask: 18 nodes (9 outer nodes corresponding to the thermal blanket, 9 inner)
- Collimator: 8 nodes (4 outer corresponding to the tungsten external layer, 4 inner nodes corresponding to the CFRP internal layer)
- SDDs: 8 nodes (4 outer, 4 inner)
- FEE: 2 nodes (1 outer, 1 inner)
- Mounting structure: 4 nodes (non-geometrical thermal nodes).

The WFM unit is located parallel to the Optical Bench at a distance of 0.3m.

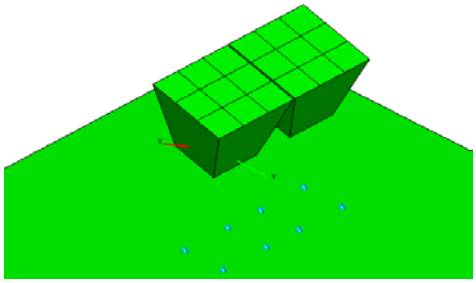

Figure 4-29: Geometric thermal mathematical model of a WFM unit

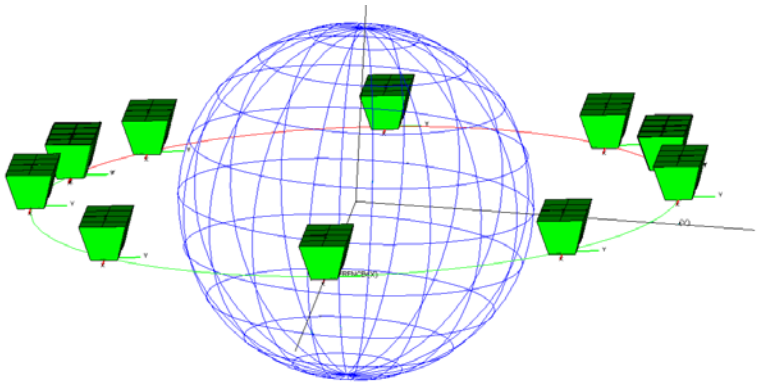

Figure 4-30: WFM unit in LOFT orbit for Sun aspect angle 90°

The working assumptions used to perform the thermal analysis are:

- LOFT orbit is LEO 600km with +5° inclination. The orbit duration is 97min. The satellite is 36min in eclipse per orbit
- 0.704W are dissipated from each SDD/FEE (CBE values)
- The collimator is externally MLI finished and internally black finished
- The coded mask is externally thermal blanket finished and internally Kapton finished (other finishings such as black painted and the same Tungsten material are under study)
- Detector trays are thermally coupled between them. The backside of the detector tray is white painted finished
- The mounting structure is thermally isolated from the Optical Bench
- The Optical Bench temperature is +20°C and is externally MLI finished.

The optical bench (thermal interface to the unit structure) is assumed to stay at constant temperature of +20°C. Here we summarize the preliminary results. They provide the following indications shown in the following table.

Table 4-9: Preliminary thermal analysis of the WFM

Case	**Mask temperature (°C)**	**Detectors temperature (°C)**
Sun aspect angle 60	+45 / -12.5 -64 /-69.2 (see Note 1)	-2.5 / -9 -12 / -18 (see Note 2)

Note 1: A sunshade is introduced in the thermal mode.

Note 2: An aluminum plate of 0.2 x 0.2m is introduced in the model, acting as a radiator, and is located at the same plane as the detector tray of the camera and looking to deep sky.

As it is shown, a large temperature excursion can be observed in the mask due to the environment radiation when the Sun aspect angle is 60°. This mask temperature variation is clearly mitigated if there is a sunshade (see note 1).

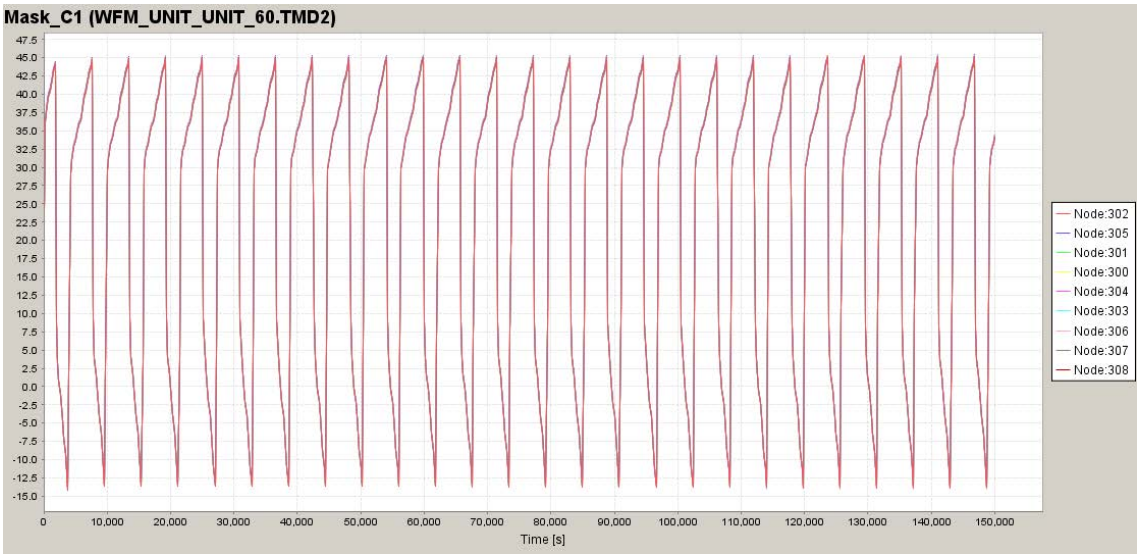

Figure 4-31: Temperature variations of the mask (Y axis) with time, during several orbits (X axis). Assumed Sun aspect angle is 60deg.

The detectors are too hot for Sun aspect angle 60, but the temperature requirements are almost fulfilled if an Aluminium plate is included in the model (see note 2). The detector temperature requirements will be respected for the critical case (Sun aspect angle 60), if the WFM unit is able to radiate the internal heat by means of extra elements such as radiators together with the utilisation of a sunshade. This conclusion was already reached after the CDF study. The sunshield will also help to have a more homogeneous temperature distribution in the detector plane, as well as to protect the WFM instrument.

In addition, the detectors temperatures for other Sun aspect angle cases are presented below, from a previous ESATAN model computed for the previous baseline of the WFM (4 units=8 cameras in arch configuration), with radiators of different sizes. It can be noticed that temperatures for Sun aspect angle such that the WFM is not pointing to the Sun (+0, -30, -50) are in agreement with the requirements.

Table 4-10: Summary of detectors temperature depending on the radiator area

90- Sun Aspect Angle [deg]	WFM Temperature [°C]	
	0.25 x 0.25m radiator area/unit	0.2 x 0.2m radiator area/unit
+40	[-5, -15]	**[+11, +3]**
+30	[-10, -19]	[+7, -1]

+0	[-40, -45]	[-25, -30]
-30	[-35, -42]	[-20, -25]
-50	[-33, -39]	[-15, -22]

Note 3: Several thermal ESATAN models of the previous WFM configuration, for a range of Sun aspect angles and for various working assumptions, have been computed. However, these are not presented here since the new WFM baseline (defined in the 3rd LOFT Consortium meeting in Tübingen, 11-12 April 2012, and in the Rome WFM meeting, 2-3 May 2012) is very different: single units of 2 cameras not touching each other and without the BEE back cover used as a radiator. Simulations for the new configuration are ongoing, and also the sunshade will be included in a systematic way, because we have concluded from previous models that it is required to guarantee as much as possible a stable temperature for the masks, and to improve the detector temperatures for all Sun aspect angles.

4.2.6.1 MLI and thermal screen

The selected thermal film covering the coded mask is Sheldahl 146455: 7.6μm of PI (Kapton) + 100nm VDA (vacuum deposited aluminium). The absorptivity is $\alpha = 0.35$ and the emissivity $\varepsilon = 0.40$. The continuous allowable temperature range for this film is -250°C to +290°C. The membrane shall have a layer of SIO2 (0.16μm) added to the Kapton side to protect against Atomic Oxygen with minimal effect on the absorbance and emittance of the material. The impact of the thermal screen on the X-ray transparency has been evaluated and included in the performance estimates for the detectors. The collimator external walls will be MLI blanket finished in order to provide an optimum isolation to the camera, and specially the detector plane. Studies for more X-ray transparent technical solutions are still on-going.

4.2.7 Electrical design

The SDD detectors require a high voltage power supply (HV, nominal -1300 V, for the drift field) and a medium voltage power supply (MV, nominal -100 V, for the last portion of the voltage divider and the pull-up cathodes). The front end and back-end electronics require a low voltage power supply (LV, nominal 3.3 V and 5 V). These voltages will be provided by a dedicated power supply board within the BEE.

The interface between BEE and FEE for the configuration of the ASICs and the transfer of trigger and energy signals to the MBEE will be the same custom interface with LVDS connectors as in the LAD. The current baseline device is the radiation-hard Actel RTAX 2000S with a clock frequency of 40 MHz.

The interface between BEE and DH will be a SpaceWire interface for the data and TC/configuration transmission. Additional lines are foreseen for the PPS and HK data. For the interface between PBEE and DH, again a SpaceWire connection is foreseen. It will be used to transmit science data, commands, configurations and HK data. The pulse-per-second is again transmitted in a separate LVDS signal.

The electrical architecture of the WFM experiment is shown in the block diagram in the following figure.

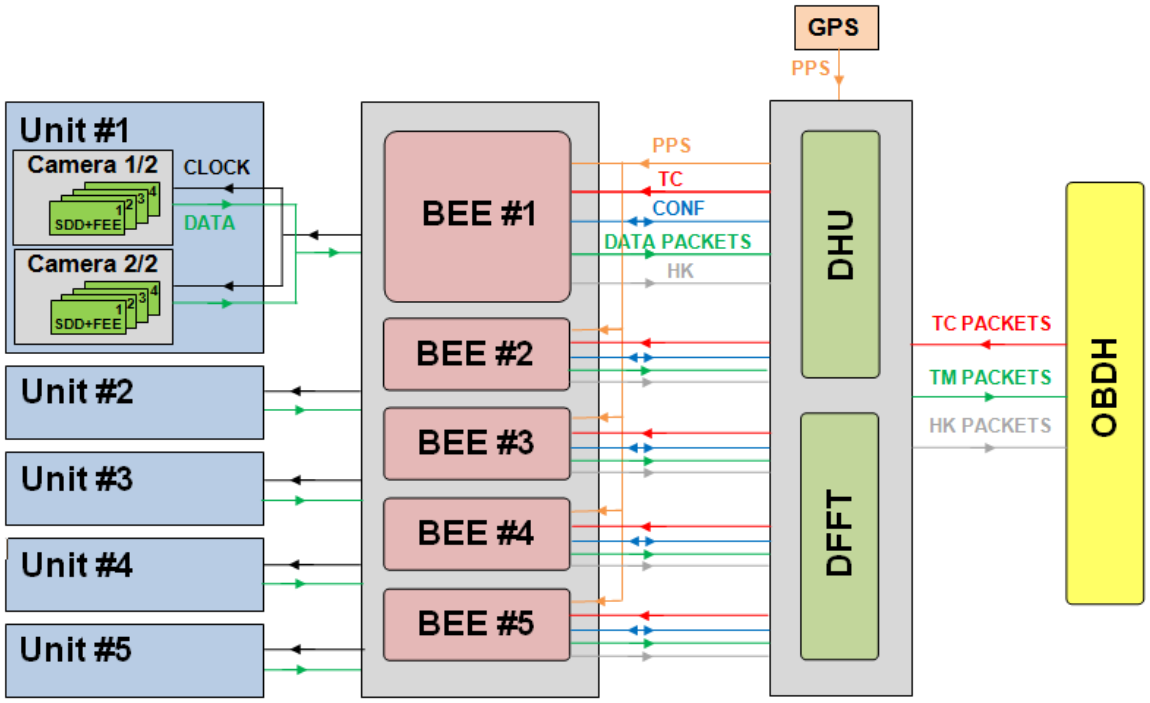

Figure 4-32: The electrical architecture of the WFM

Cold redundancy is foreseen for the DHU and the PSU. The relevant mass is accounted for in the overall mass budget.

4.2.8 On-board software

The WFM onboard software will in many respects be similar to the LAD software in the sense that its main functions are instrument control and monitoring, and science data processing and formatting of X-ray event data coming from somewhat similar front end electronics. The main difference is that the data rate is lower, while the tasks performed on the data are more complicated, as the WFM onboard software will perform some data analysis to identify transient sources (trigger algorithm).

The software will allow the instrument to have the functionality that it requires (more complex than the standard repetitive processing of the ASICs and FPGAs) and the ability to be updated and work around problems automatically and after input from the ground. Instrument control will be possible through the software via telecommands from the ground (e.g., power on & off, set-up of ASICs and FPGAs, loading parameters for processing/on-board calibration, investigations) and autonomously on-board (e.g., mode switching, diagnostic data collection).

The software will implement some standard ECSS telecommand packets for housekeeping, memory maintenance, monitoring etc. and some standard ECSS telemetry packets for command acceptance, housekeeping, event reporting, memory management, function management, time management, science data, diagnostics etc.

The software will collect and format the acquired science event data. At the lowest level it will be able to monitor and setup the registers of each of the electronic elements of the event processing hierarchy. The data from the 10 WFM cameras will arrive at the processor board (DHU) and be handled where possible by dedicated electronics under some control by the software. The science data from the detectors consists of position, energy and time information for individual X-ray events (X,Y,E,T). The resulting data stream will have the remaining processing done (e.g., energy reconstruction). In normal science operations the data will be stored in order to produce the 4 possible types of science TM products from the WFM:

- Photon-by-photon event data
- Camera images accumulated over time in several energy bands.
- Camera rate meters in several energy bands
- Energy spectra accumulated over time.

We note that the photon-by-photo data forms the basis for constructing the other data types. For each data type the onboard software will employ dedicated compression algorithms to reduce the required space to store the data in telemetry packets.

During normal operations the photon-by-photon event data will not be transmitted to ground. However the software will employ a trigger algorithm to identify transient X-ray sources (new sources or rapid changes in persistent sources). In case of a trigger, the photon-by-photon data for a period of before and after the trigger will be transmitted to ground. This requires the storing of a buffer of photon-by-photon data.

A separate part of the WFM software will contain logic for the onboard burst alert system. In its basic form, the burst alert system will monitor the detector count rates and search for statistically significant increases on several time scales and in several energy bands in order to maximize the sensitivity to different types of events. This system will ensure that interesting events will be recorded with detailed information for analysis on ground.

An enhanced version of the onboard trigger logic, which is capable of determining the position of the burst source is now the baseline for the WFM. It requires significant computing power to calculate a sky image and this is done by a dedicated board attached to the DHU. Once a source position is derived relative to the detector coordinate system, it must be transformed to sky coordinates. Therefore it is also essential that the onboard software has access to pointing information, and is able to verify the pointing using the location of known sources in the field of view of either the camera detecting the burst or one of the other camera units. The burst location will also be checked against an onboard catalog of known sources to avoid sending out burst alerts caused by well known sources.
In order to stay within telemetry allocation limits the onboard software will need to contain logic for estimating the telemetry usage and the bandwidth available. In addition, it will be possible for the WFM SW to receive information from the LAD regarding its telemetry usage. In the case, where LAD is observing a weak source and not using its nominal 90% of the total TM budget, it can be used by the WFM for increasing the number of energy bands and/or increasing the fraction of time spent in event-by-event mode.
The data will be stored in the WFM mass memory before transmission.

The software will interact with the Spacecraft OBDH, sending the data over SpaceWire for eventual transmission to ground.

The software will be able to send a wave of setup information to the hierarchy of processing elements and receive and process the housekeeping data coming back, simplifying this for a lower rate transmission to the ground.

The software would optimally run on a single space qualified processor, the Leon, and be written in C using the RTEMS operating system. RTEMS, being the real-time executive, will schedule the software tasks, each at different priorities and communicating with each other as necessary and any errors will be trapped and handled. A software-controlled hardware watchdog will be used to reboot in case of a hang.

The software will be written in separate parts. "Basic" software, stored in a very reliable PROM, the "Golden boot ROM", would have enough functionality to receive, store and execute new software. "Operational" software, stored in EEPROM, would have the functionality of the "Basic" software and also the full science capabilities. This way new software can be loaded to the instrument without losing the basic functionality even if that software is incorrectly produced, loaded or written to the wrong location. If there is any problem with the software interface to the spacecraft, a reboot or power off/on of the instrument will reset the software into the well-tested "Basic" mode which does not produce science data, getting the instrument back to a well defined initial mode. Error messages will be limited so that they are not repeated unnecessarily as this could cause unnecessary traffic to the Spacecraft.

As the software has to operate in a remote space environment, it will be written to be robust against errors, to report as much information as possible on any problems encountered and progress made (to help investigations) and perform any operations required by EDAC/scrubbing.

The interfaces between the software and the rest of the instrument/satellite would be as clean as possible with the processor and software taking over the processing of the events and diagnostic data at the point they are joined into a single stream from the cameras, and interacting with the rest of the satellite through SpaceWire.

4.2.9 Instrument mode description

The WFM instrument consists of five independent camera units, observing different (but partly overlapping) parts of the sky. Regarding modes, each unit operates independently of the others, one can be in BURST mode, while the other ones are in normal DATA TAKING mode.

From a power consumption point of view, the WFM instrument consists of one common Data Handling Unit (DHU), and five camera pairs. Each camera is connected to a Back End Electronics and a power supply, which handles two cameras.

Note that the 5 BEEs and PSs are located in a common box on the (or near) the optical bench with a maximum camera to BEE/PS cable length of <1.5 meters. For redundancy

reasons the 2 cameras connected to a particular BEE/PS is not necessarily part of a pair observing the same region on the sky.

Switching between instrument modes can be done via commands (from ground or from a timeline), or autonomously, as determined by the onboard software logic.
A non-exhaustive list of potential causes for autonomous mode switches follows:

- S/C or instrument anomalies (out of limits on power or temperature monitors ...)
- AOCS state (Slew, LAD on-target flag, ...)
- South Atlantic Anomaly entry/exit
- Earth occultation of LAD target (entry/exit)
- Burst trigger in one or more WFM camera units
- Data taking sub-mode change due to
    - Information about space craft systems (AOCs etc)
    - Burst trigger in one or more WFM camera units
    - Predicted shortage or surplus of available TM bandwidth.

Table 4-11: WFM subunit power status versus instrument mode. *) Independently for each camera block

WFM mode	DHU	BEE*)	HVC*)
OFF	Off	Off	Off
SAFE_IDLE	On	Off	Off
SAFE	On	Off	Off
ASIC_SET-UP	On	On	Off
OBS_SET-UP	On	On	On/Off
DATA_TAKING	On	On	On
CALIBRATION	On	On	On
OBS_IDLE	On	On	On/Off
DIAGNOSTIC	On	On/Off	On/Off

4.2.9.1 Operating modes

Below is given an outline of the WFM operating modes. These modes can be used for each camera individually.

- **DATA_TAKING**: Used during all normal, quiet time observations. All sub-modes are related to TM formatting of the event-by-event data from the detector. BEE mode and data traffic to the DHU is unchanged by DATA_TAKING sub-modes:
- **DATA_NORMAL_SUB:** data are recorded in event-by-event format, but binned in detector images, detector rate meter, and detector spectra for the TM (default sub-mode) Note that parameters can define PIF filtering and other refinements.
- **DATA_SLEW_SUB:** data are recorded in event-by-event format, but only binned in detector rate meter and detector spectra for the TM
- **DATA_AOCS_SUB:** data are recorded in event-by-event format, but only binned in detector rate meter and detector spectra for the TM, the detector image collection is suspended due to temporary loss of pointing
- **DATA_BURST_SUB:** data are temporarily recorded in event-by-event format for TM. Note that entering DATA_BURST_SUB mode is activated retro-actively to

allow pre-burst data to be included, when a trigger is called. This is based on buffered data. The burst mode is specifically design to save data on short time scale events (increases in source flux on time scale from a fraction of a second to ~100 s).

- **DATA_EVENT_SUB** data are recorded in event-by-event format for TM until commanded into DATA_NORMAL from TC, time-line, or autonomous memory management (preferred mode, if TM allows)
- **CALIBRATION** Used regularly for verification of the ASIC/FPGA parameter settings by injecting an electrical signal into the SDD detector and verifying the resulting signal
- **IDLE** Used during SAA interruptions of DATA_TAKING. No science TM is recorded. Entered and exited by TC, time-line, or autonomously by checking rates and rejection on upper threshold
- **DIAGNOSTIC** Used on request. Rarely in orbit, but extensively during ground testing to obtain the maximum information about the detected X-ray and background events. Records all details of the ASICs outputs and BEE processing (the level of detail may be set by parameters). Used for general trouble shooting and performance verification.
- **DIAGNOSTIC_ALL_SUB** all output is recorded
- **DIAGNOSTIC_ACCEPTED_SUB** only data on accepted events are recorded
- **DIAGNOSTIC_XXX_SUB** other settings to be defined, depending on the detailed event processing in the BEE.

The different data taking modes of the WFM only differs in the way the data from the detector pipeline FIFOs are handled by the Data Handling Unit. Normally all FIFO data (with time stamps) are stored in a circular buffer in the WFM mass memory capable of holding at least ~10^7 events (100 Crabs during 300 sec). Which data are extracted from this buffer and how they are packed depend on the current operating mode.

4.2.9.2 Non-operating modes

WFM non-operating modes, where no science telemetry is generated

- **OFF** Used during launch, failure recovery, power shortage or other periods, where collection of scientific data is not possible and it is required that the WFM be powered off
- **SAFE_IDLE** Used for updating the DHU software (may also be referred to as memory patching mode)
- **SAFE** Used after anomaly detection and failure recovery. This is the lowest mode of operating, where it for example is not possible to execute any “dangerous” commands, like switching on the high voltage of the detector.
- **ASIC_SET-UP** Used for setting up analysis parameters in ASICs and FPGAs
- **OBS_SET-UP** Used for setting up observation parameters and data formats.

4.2.9.3 Near Real Time Burst Alert Mode

The burst trigger logic is active during data taking mode and is based on detecting increases in the count rate of X-ray events in the WFM cameras, which are likely to originate from activity in cosmic X-ray sources and not from increases in the general background. When the onboard software detects a potential transient event it will (as

described above) save data for transmission through the normal TM in the “event-by-event” format in order for the ground software to be able to analyse the event in full detail.

In addition the onboard software will try to localize the position in the sky of the source responsible for the increase. In particular the objective is to localize gamma ray bursts (GRBs), which is a class of explosive astrophysical events of short duration. Scientifically it is highly desirable to observe these sources with other telescopes and instruments as soon as possible after (or even during) the event. Therefore LOFT will employ a VHF transmission capability to send a short message about the occurrence of such events with minimum delay to a network of VHF receiving stations on the ground for further distribution to interested observatories.

As a result of burst trigger the onboard software will enter a mode to determine the position of the source. The transformation from coded mask detector images into images of the sky is highly non-trivial and requires significant computer power to perform certain discrete fast Fourier transform (DFFT) operations on the detector images. Therefore the DHU controls a special board optimized for performing the FFT and determining the location of the source.

If the rate increased can be localized and thereby confirmed to be an outburst of a real X-ray source the position is initially defined relative to the camera coordinate system. The position is then, based on the pointing information, transformed into a position on the sky, which is compared with a catalog of known X-ray sources. If the position does not correspond to a known source and the calculations meet a certain set of quality/reliability criteria the software will send a short message with brief information about the event to the OBDH in order for it to be transmitted immediately to ground via the spacecraft VHF transmitter system. The message will contain information on burst time, burst location, duration, and a set of quality flags for the use of the ground based users. The total amount of data to be transmitted is on the order of 1 kbits. The “event-by-event” data that form the basis of the onboard localization will be stored for transmission through the normal telemetry channel during the next regular ground station pass.

4.3 Mechanical interfaces and requirements

4.3.1 Location requirements

The wide field of view of the WFM should be unobscured by other satellite structures. The current position of the WFM on top of the optical bench responds to this requirement. This location should also favour an operating temperature on the cold side (e.g., <-20°C) by using the irradiation to the open sky from the shadow side of the WFM assembly. Note: part of the partially coded FoV for central cameras could be obscured by the sunshade (10 degrees, TBD).

4.3.2 Alignment requirements

The field of view of the WFM should include the FoV of the LAD in its most sensitive region. ***The WFM does not require any specific fine alignment with the spacecraft or the LAD***. A pre-launch optical alignment with the Star Trackers as well as

in flight calibration with known sources will allow to establish the 3 axis orientation of the WFM relative to the ACS axis and the LAD FoV.

Internal alignment will concern the integration of the 4 SDDs on the detection plane and between the latter and the coded mask. The requirement on the internal alignment is that the detector and mask element should be parallel to better than 0.05 times the width of the slits in the mask measured over the full width of the mask (12.5 μm over 26 cm). Heritage on this type of mounting is available in the team after the experience of AGILE, AMS and ALICE, for which similar constraints have been satisfied.

4.3.3 Pointing requirements and performance goals

The pointing direction of the WFM must be known in all 3 axes to better than 1 arcmin in order to interpret the WFM imaging data correctly. This is a more strict requirement than that of the LAD, because the LAD does not care (too much, as the collimator has squared aperture) about rotations around its pointing axis.

Otherwise the pointing requirements of the WFM are no different from those of the LAD as regards the accuracy, knowledge and stability – with one important exception: the WFM will be taking data continuously, also when the LAD target is being occulted by the Earth. It is therefore important the onboard attitude system is able to switch between different star trackers as the occulting disk of the Earth blocks one or the other star tracker.

4.3.4 Interface control drawings

At this moment only the dimension envelope can be given. The WFM assembly on the optical bench resides inside a box of dimensions shown in Figure 4-18. ***The location of the Data Handling Unit and Power Supply is TBD, but dimensionally they can be housed within the WFM assembly box. The location of the individual WFM units is not tightly constraint, as long as their FoV is preserved.***

4.3.5 Instrument mass

The preliminary mass budget is given in the following table.

Table 4-12: WFM preliminary mass budget

Item	CBE [kg]	DMM @ 20% [kg]	CBE + DMM [kg]
Coded Mask	16.484	3.297	19.781
Collimator	12.300	2.460	14.760
Detector tray	7.170	1.434	8.604
SDDs	1.850	0.370	2.220
FEEs	0.800	0.160	0.960
BEE box including PSU+ Harness	6.000	1.200	7.200
Flexure	0.471	0.094	0.565
SubTotal	45.075	9.015	54.090
WFM structure	13.520	2.704	16.224
2 x(DHU+DFFT)	7.2	1.44	8.64

(assumed cold redundancy)			
Total	65.795	13.159	78.954

4.4 Thermal interfaces and requirements

Note: the information presented here is based on [RD 4], which presents analysis that needs to be updated based on a refined soft proton flux calculation (which takes into account the directionality of both the soft proton population and the FoV of the instrument), and also to calculate the required temperatures at the end of the Nominal Operations Phase rather than the end of the Extended Operations Phase. However, because the WFM FoV is much wider than the LAD FoV, the expected relaxation of the required temperatures is expected to be less pronounced than is the case for the LAD instrument.

The summary of the thermal I/F requirements of the WFM instrument are given in the following table.

Component	NonOp Min [C]	NonOp Max [C]	OpMin [C]	OpMax [C]	StartUp [C]
SDD/FEE	-60	+60 (TBC)	-50	As given by [RD 4]	TBD
BEE/PSU	-60	+40	-60	+40	TBD
DHU	-60	+40	-60	+40	TBD

Table 4-13: Summary of WFM unit temperature requirements

The spectroscopy and low-energy threshold performance of the WFM is challenged by the radiation damage induced by the protons encountered in the SAA. [RD 4] shows the sensitivity of this effect on the satellite orbit. The key elements are the SDD detectors and their FEE. For a circular orbit at 600 km, 5° inclination the analysis in [RD 4] shows that the ***required operating temperature must be below -23°C to fulfil the energy resolution requirement at the end of life*** (see Figure 4-33, Figure 4-34, Table 4-14). A better orbit (lower inclination and/or smaller altitude) may relax the temperature constraints. The requirements of the temperature stability per orbit and gradient are being analysed by the team. Preliminary values are:

- ***temperature stability per orbit: <5°C***
- ***temperature gradient: <5°C, over detection plane***
- ***operating temperature of SDD: -23°C/-28°C, depending on the orbit.***

The requirements are derived assuming as a front-end electronics an ASIC developed on the heritage of the StarX-32 design (see RD03), whose preamplifier is optimised for the available power per channel in LOFT. Each SDD+FEE should always operate at a temperature below the one listed in Table 4-14 (depending on the flux). A lower operating temperature will improve the WFM detector performance.

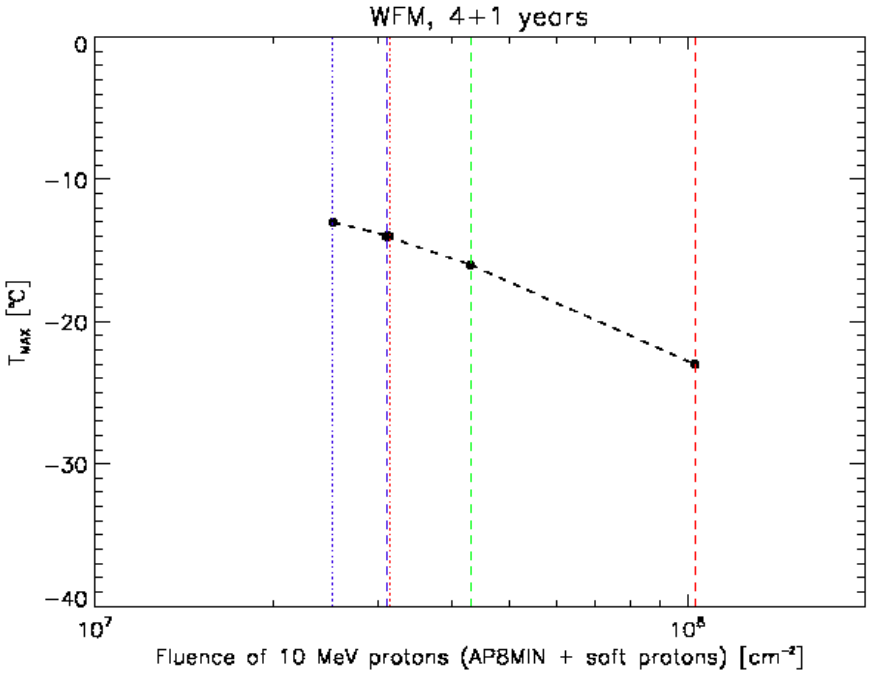

Figure 4-33: Maximum EoL temperature of the WFM SDDs in order to fulfil the requirement of ENC < 12 e- after five years, as a function of radiation dose. The vertical dashed lines correspond to various baseline orbits – see legend in figure below

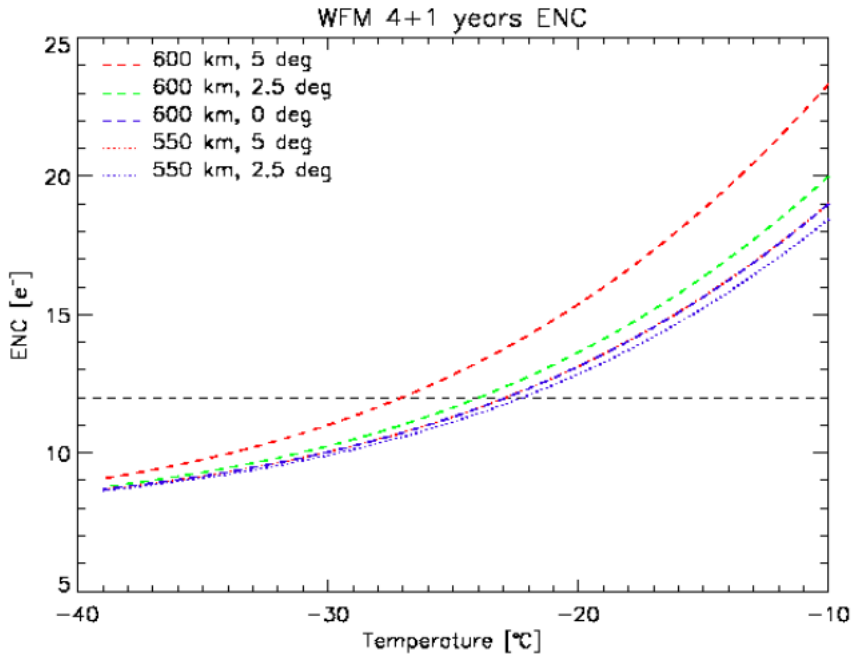

Figure 4-34: EoL LAD-SDD ENC worsening with increasing temperature, for different orbits (different radiation doses); the 200eV energy resolution (single anode events) is shown

Altitude [km]	Inclination [°]	$\Delta I_{AP8\text{-}MIN}$ at 20° C [pA]	$\delta I_{AP8\text{-}MIN}$ at 20° C [pA cm^{-3}]	T_{max} [° C]
550	2.5	<1	<93	-23
550	5.0	12	5168	-23
600	0.0	11	5008	-23
600	2.5	33	14386	-24
600	5.0	112	49018	-28

Table 4-14: WFM SDD EoL maximum temperature requirement as a function of various possible baseline orbits

A second critical item in the WFM in addition to the detectors is the masks. In order for the cameras to perform well the mechanical stability of the mask and the mask alignment is essential. The mask in particular gives rise to concern because the thermal models indicates dramatic temperature variations between sunlit and dark periods of the orbit for spacecraft attitudes which allow direct Solar illumination of the monolayer thermal cover protecting the masks. ***Our analyses have shown that for the mask we must require thermal stability to <10 °C on orbital timescales***. A sunshield preventing direct solar illumination of the mask surfaces of the WFM cameras is the simplest way to achieve this temperature stability. A sunshield will also simplify the thermal design of the WFM instrument in its entirety. The shield can be accommodated within the SOYUZ fairing constraints without requiring active deployment mechanisms.

The dissipation of each of the components in the WFM is given in the relevant power budget table (see Sect. 4.5.2). The local CBE dissipation, including a 70% efficiency of the DC/DC converters in the BEE, is:

- Power dissipated in each camera: 2.8 W
- Power dissipated in each BEE (serving 2 cameras): 2 W.

4.4.1 Thermal control requirements

The baseline thermal control for the WFM is passive. The location of the WFM units on the optical bench should offer the possibility to use the surfaces exposed to the open sky as well as extra elements (aluminium plate acting as a radiator) to control the operating temperature. This cold-plate could be connected to the camera's detector tray and located such a manner to see as much the deep sky as possible. This fact could help the unit to get rid of the internal heat generated by the SDD/FEE in a better way. Although a dedicated WFM radiator would be more desirable solution. Heaters may be required to prevent subsystem temperature to go below the allowed limits (see next sections), especially during non-operating conditions. These heaters may also work as "operational heaters" in order to maintain a stable temperature in the detector plane (see heaters section).

4.4.2 Thermal limits in space environment

The operating temperature of the WFM SDDs in space is substantially dictated by the requirements on the energy resolution. In fact, decreasing the SDDs temperature is the most effective way to reduce the bulk leakage current, being the most important component to the overall noise budget and thus the energy resolution, including the increase in leakage current produced by the radiation damage. Consequently, the operating

temperature range in space is defined in order to fulfil the requirements on the energy resolution.

In order to keep the WFM Equivalent Noise Charge ENC better than the required 12 e- at end-of-life, the temperature should not exceed the values listed in Table 4-15.

The non-operative temperature range is not affected by the above considerations on the scientific requirements. The assessment of the WFM non-operative temperature range will derive from a detailed mechanical and assembly design. The most sensitive elements will likely be the interface points and the allowed ranges for the selected glues. ***Preliminary value for the non-operative temperature range is -60°C to +40°C.***

4.4.3 Thermal limits in laboratory environment

The considerations on the effect of the radiation damage on the bulk leakage current do not apply in laboratory environment, where the scientific requirement is fulfilled at a higher operative temperature, given the low intrinsic leakage current of the SDDs. The operative range in laboratory is the same as in space, with the difference that a better performance is achieved at the same temperature, due to the lack of leakage current increase due to radiation damage. Operation at room temperature is also possible, with reduced performance. The non-operative temperature range is -60° C to +40° C also in the ground environment.

4.4.4 Temperature sensors

The response of the detectors is dependent on their temperature of operation. A monitoring of the operating temperature by using local temperature sensors is required; ***as is the case with the LAD instrument, these sensors are internal to the WFM-instrument, and are separate from the platform-provided temperature sensors that monitor temperatures for survival purposes.*** The data from the temperature sensors will be used to make onboard calibration of the WFM data (mainly ASIC gain and off-set, using look-up tables) and will be downloaded to ground as housekeeping to allow for the best data interpretation. Also the temperatures of the mechanical structure and in particular of the mask will be important for on-board and on-ground compensation of alignment shifts.

In principle, the proper location of the sensors should be as close as possible of the SDDs. A number of 2 sensors within the operating range of -100°C to +125°C and a sensitivity of 0.2-0.5 K^{-1} could be enough to monitor the detector plane temperature and to avoid the complexity of control them since they are a few number of sensors.

4.4.5 Heaters

As the WFM is expected to use passive cooling as a baseline, to meet the required operating temperature of <-23°C/-28°C, heaters may be required to prevent too low temperatures during non-operating phases (instrument switched-off) and/or to mitigate cooling in specific attitudes. A suitable placement of the heaters, a heater per SDD, may be in the detector tray since the SDDs are more critical elements of the unit. These survival heaters may be also used as operational heaters commanded by the BEE. Their basic function

would be stabilising the detector plane temperature in case of a new instrument pointing trying to keep internal alignment and stability as steady as possible. The estimated power for the heaters working in the operational mode could be 1W per camera. The required power for the heaters working in the survival mode will be provided by the spacecraft. Other heaters could be also needed for the BEE depending on their final location and their thermal behaviour.

4.5 Electrical interfaces and requirements

4.5.1 Instrument power distribution block diagram

Each WFM Unit (i.e., the set of 2 Cameras) will have its Power Supply Unit. Similar to the LAD, the power lines required by the WFM are:

Low Voltage (LV):	+/-3.3 V nominal (ASICs and FEE)
Medium Voltage (MV):	-100 V nominal (SDD voltage-divider bias)
High Voltage (HV):	-1300 V nominal (SDD drift fieldi voltage divider)
Digital Voltage (DVD):	+3.3V (TBC) nominal (Digital Electronics)
Analog Voltage (AVD):	+/-3.3V (TBC) nominal (Analogue Electronics).

A schematic view is given in the block diagram in the following figure.

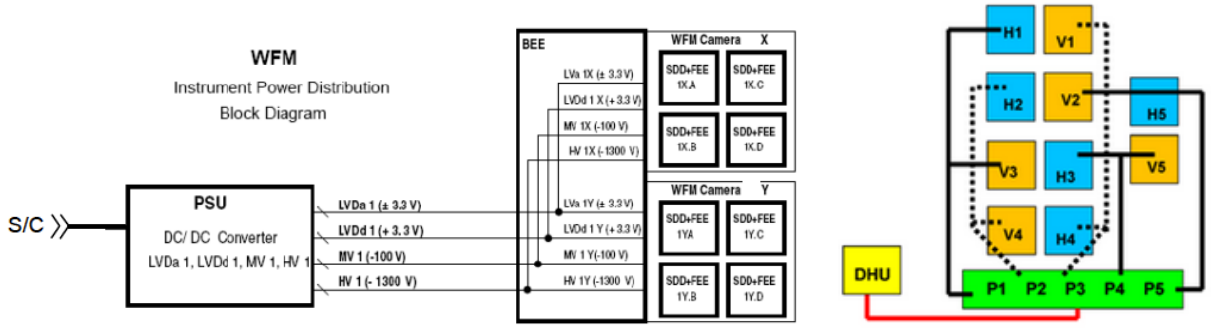

Figure 4-35: *Left panel:* Block diagram of the power distribution for each PSU of the WFM. *Right panel:* Redundancy scheme for the PSUs

4.5.2 Power budget

The power budget has changed with respect to the proposal, after the improvement in the WFM configuration.

Table 4-15: WFM power budget

			CBE [W]	CBE/0.7 (DC-DC efficiency) [W]	DMM @ 20% [W]	CBE + Margin [W]	NUMBER OF ITEMS
WFM			**63.76**	**91.09**	**18.22**	**109.30**	**1**
|							
	DHU + DFFT		15.60	22.29	4.46	26.74	1
5 x	BEE		2.00	2.86	0.57	3.43	5
5 x	UNIT		7.63	10.90	2.18	13.08	5
	|						
	2 x	CAMERA	3.82	5.45	1.09	6.54	10
		|					
		4 x Heaters	0.25	0.36	0.07	0.43	40
		4 x SDD	0.70	1.01	0.20	1.21	40
		HV	0.056	0.080	0.016	0.096	
		MV	0.001	0.0014	0.0003	0.002	
		LV	0.647	0.924	0.185	1.109	

4.5.3 Instrument modes duration

The WFM will normally always be in data taking mode, excluding the SAA passages, where the instrument will be in idle mode.

The Earth will during the orbit block part of the field of view of some of the WFM units, but the wide field of view of each camera will make the total blocking very brief and part of the sky will be visible. The Earth will block the cosmic diffuse X-ray background, which is the main contribution to the background in the WFM. Thus, the signal to noise ratio of an observation of a source will be higher while part of the field of view is blocked.

4.5.4 Telecommands

The WFM telecommands structure will follow the protocol specified by the spacecraft TM/TC system. In the general the telecommands will be divided classes according to their functionality.

- Load task parameters: set parameters
- Report task parameter: ask for a report packet on a specified parameter or parameter set
- Mode transitions: change the mode of the instrument, for example “enter science data taking” mode.

- Load memory: commands to enable the loading of values into memory, for example for onboard software code corrections
- Dump memory: commands to dump onboard memory locations to verify correct content
- Status information: information from the spacecraft system to be used by the WFM onboard software.

At the current stage the detailed TC list needs to be defined.

4.5.5 Status information

However, we can offer comments on the status information needed. The details depend on the architecture of the TC/TM system and how it is implemented: as a broadcast packet system, where relevant information is distributed on a regular time scale (for example 8 s) or as individual commands. Below is a (incomplete) list of information needed by the WFM onboard software from the spacecraft system. The indicated implementation is just an example to illustrate the functionality needed:

Pointing status/on-target flag: The WFM onboard software needs to know the pointing status of the AOCS in the form of an on-target flag (OTF) to indicate a stable pointing (within specifications), where image data can be accumulated.

Observation ID: Information to be used together with the on-target-flag to manage the accumulation of images. For example if the OTF changes to zero, while the observation ID remains constant, indicates that the loss of stable pointing could be temporary and that the ongoing image accumulation could be suspended until the OTF returns to 1. If the OTF goes to zero and the pointing ID changes (to zero during regular slew) then it would indicated that the current image should be terminated and prepared for final storage. A new pointing ID and a transition of OTF to 1 would indicate the start of a new pointed observation, where a new image accumulation could be started.

Entry into and exit from SAA: This information is needed to stop and start the image accumulation (and possibly switch off the detector HV). During SAA passage the noise will be very high and an image containing data from this high background period will be useless. Note: the SAA information may also be loaded from ground and kept internally in the WFM, if not provided from the spacecraft directly.

Imminent switch off: Information about an imminent instrument switch-off to enable the WFM to perform tasks needed (for example saving of data, storing of context data, mode changes etc.) in order to perform a graceful shut-down of the instrument

LAD TM usage information: It has been agreed that a mechanism should exist that will allow the WFM to use more TM in the case that the LAD will not use its maximum allocation (for example when the LAD is observing a very weak source). It is TBD if the flow of information (mass memory filling) will be routed through the spacecraft data handling system or directly from the LAD to the WFM.

4.5.6 Telemetry

4.5.6.1 Telemetry requirements

The normal, expected telemetry allocation for the WFM is assumed to be ~90 kbits/s averaged over one orbit. The selected data modes will ensure that this will normally be fulfilled without data gaps. The data modes will include compression based on the internal data structure. The actual amount of telemetry data generated can be predicted based on the count rates of the individual cameras and allow the onboard software to monitor the telemetry budget and take action (by changing to less expensive modes, with for example poorer energy or time resolution) in case of a predicted telemetry deficit.

It will be an advantage, if the WFM onboard software can be made aware of a possible higher available telemetry rate, if the LAD for example is not going to need its full allocation. This will enable a higher level of detail and flexibility in the analysis of the WFM data and a higher scientific return. These higher detail data will also be useful for some of the WFM calibration purposes.

The onboard software will employ a trigger mechanism to detect short transient events (new sources or changes in persistent sources with time scales less than ~300 s), where high resolution data are required and will be stored in photon-by-photon event mode (burst mode).

The data rates for the burst mode are summarized in Table 4-17 for one unit (2 cameras) for a set of assumptions about the sources seen by that unit. The typical rate will be the case of CXB+1 Crab source flux, where 1 trigger will produce ~2% of the tm budget for one orbit. The assumptions made in order to derive the data rates are described below.

Table 4-16: Data rate for the 1 WFM unit (2 cameras) in a 40 bit event-by-event mode as function of the point source flux in units of Crab (910 c/s before the mask, which is assumed to have a 25% transmission). The listed source flux is for the combined flux of sources in the unit field of view. The second column shows the data rate while in trigger mode. The third column shows the average "cost" to transmit the 300 s of data in order to compare with the WFM tm budget of 90 kbits/s

Total rate in 1 unit (2 cameras)	**Data rate for 40 bit event format**	**Average data rate over 1 orbit to transmit 300 s of data**
CXB	22 kbits/s	1.2 kbits/s
CXB + 1 Crab source	31 kbits/s	1.7 kbits/s
CXB + 10 Crab source	113 kbits/s	6.3 kbits/s
CXB + 30 Crab source	295 kbits/s	16.4 kbits/s
CXB + 100 Crab source	932 kbits/s	51.8 kbits/s

The requirement that the WFM is able to record the full information of the photon-by-photon mode for a 100 Crab transient lasting 5 minutes (300 s) will consume ~60% of the tm budget for one orbit. If we allow for the data to be stored for dumping over several orbits this requirement will not normally interfere with the normal operations of the WFM.

4.5.6.2 Telemetry description

4.5.6.2.1 Housekeeping telemetry

The housekeeping telemetry will contain all information relevant to the operational evaluation of the WFM.

- Analog data: voltages, currents, temperatures.
- Status data for the onboard software
- Detector count rates to monitor the detector performance.

The HK data is expected to be recorded on a 8 s time scale and require 1 kbits/s or less bandwidth.

The WFM Housekeeping (HK) consists of analogue HK (e.g., voltages, currents and temperatures) and digital HK (e.g., rate of events, dead-time counters,,...). Table 4-17 reports the analogue HK definition as well as the bandwidth requested for the on-ground download. Table 4-18 reports the digital HK definition as well as the bandwidth requested for the on-ground download.

Table 4-17: WFM analogue HK budget

Analog HK name	**# parameters**	**sampling time (s) in *fixed mode***	**# bits per sample**	**generation rate (kbps)**
ASICs bias current/voltage	448 (2 per ASIC)	16	12	0.84
Temperatures	80 (1 per SDD side)	16	12	0.06
HV bias current/voltage	40 (2 per SDD)	16	12	0.07
MV bias current/voltage	40 (2 per SDD)	16	12	0.07

DH & Power distr.	125	16	12	0.10
Mask and Structure	100	16	12	0.07
GRAND TOTAL (kbps)				**1.21**

Table 4-18: Digital HK definition as well as the bandwidth requested

Digital HK name	**# parameters**	**integration time (s)**	**# bits per sample**	**generation rate (kbps)**
Pipeline ratemeters	5 (10 per SDD side)	16	24	0.08
Rejected event deadtime	80 (1 per SDD side)	16	24	0.12
Good event deadtime	80 (1 per SDD side)	16	24	0.12
DH & Power distribution	250	16	16	0.25
GRAND TOTAL (kbps)				**0.57**

4.5.6.2.2 Science telemetry

The default science operating mode of the WFM will be image mode, when the LOFT spacecraft is in pointed mode, where 3 types of telemetry are collected in parallel:

1 Images (5 units, every 5 minutes, 8 energy bands, 25-80 kbits/s).
2 Science Ratemeters (5 cameras, 8 energy bands, 16 ms resolution, 9 kbits/s) .
3 Energy spectra (5 cameras, every 30 seconds, 100 eV bin, < 1 kbits/s) During slews and periods where the pointing is outside the specifications for pointed mode, the collection of images is suspended.
4 Science Ratemeters (5 units, 8 energy bands, 16 ms resolution, 9 kbits/s).
5 Energy spectra (5 units, every 30 seconds, 100 eV bin, < 1 kbits/s) During SAA passage all science data collection is suspended. In addition, an onboard trigger algorithm will run during pointed observations and may decide to transmit high resolution data (photon-by-photon or burst mode).
6 Trigger data (number of allowed triggers may be decided dynamically based on the available tm available, nominal 300 s of data per trigger, typical data load averaged over one orbit: 2-5 kbits/s for one trigger) If additional telemetry is available, for a shorter or longer period, one or more WFM units can be operated in the photon-by-photon mode.
7 30-100 kbits/s per unit, depending of the source flux in the field of view (this mode will be used for the payload validation and commissioning phases, and for some calibration activities). An electronic calibration mode will be used rarely to verify the performance of the detector system.

4.5.6.2.3 Assumptions for the description of telemetry rates

We assume the WFM to consist of 5 units, each consisting of two cameras. We assume the cosmic diffuse X-ray background, CXB to contribute 1100 c/s per detector unit (2200 c/s per unit) before absorption by the mask. We assume the Crab (as a reference source) to produce 455 c/s per camera (910 c/s per unit). We assume the mask to have an open fraction of 25%.

The exact rates will depend on the details of the mask and its manufacture: vignetting, support structure and the exact mask pattern, which may not be exactly 25% open. Therefore the given count rates should taking as a guideline only and may not exactly match numbers used in other parts of the WFM estimates, depending on the details accounted for.

We note that there may be times when a large fraction of the field of view of one unit will be occulted by the Earth (which at a 550 km orbit subtends a cone with radius ~66 degrees). This will result in a significantly reduced cosmic diffuse count rate.

Table 4-19: Count rates for the WFM 10 cameras, corresponding to the 5 units. CXB is the cosmic diffuse X-ray background

Source	1 camera Before the mask	1 unit Before the mask	**1 camera After 25% mask**	**1 unit After 25% mask**
CXB	1100 c/s	2200 c/s	**275 c/s**	**550 c/s**
1 Crab	455 c/s	910 c/s	**112 c/s**	**225 c/s**
CXB+ 1 Crab	1555 c/s	3100 c/s	**387 c/s**	**775 c/s**
CXB+10 Crab	5650 c/s	11300 c/s	**1412 c/s**	**2825 c/s**

4.5.6.2.4 Camera images

The normal mode of operations for the 5 WFM units will be the accumulation of images over a specified time and in a number of energy bands.

The telemetry allocation does not normally allow the transmission of information of photon-by-photon data and we accumulate images over a certain integration time, T. In order to maintain some energy information, the images will be accumulated in several energy bands, N_{Bands}. The number of pixels in the image depends on the spatial resolution of the detector. Let us denote the number of pixels in the X-direction by N_x, and in the Y-direction by N_y. The total number of pixels is then $N=N_x \times N_y$.

The task is then for each time interval T to transmit the number of counts in each pixel. This amounts to $N_i = N_x \times N_y \times N_{Bands}$ numbers for the i^{th} camera. If we have several camera units, $N_{cam,}$ the total is $N_{total} = N_x \times N_y \times N_{Bands} \times N_{cam}$. For $N_x = 2048$, $N_y = 32$, $N_{Bands} = 8$, and $N_{cam} = 10$ this is ~5.2 Mega-pixels per integration time, T.

With a high number of pixels per unit area the average number of counts per pixel may be low and the content may then be described using only a relatively low number of bits. Further, if the number of counts is lower than the total number of pixels, a significant number of pixels will not contain any counts. It may then be advantageous to transmit the distance from one filled pixel to the next and then encode the distances in the least possible number of bits. (For this purpose we treat the 2 dimensional image as a vector with length $N_x \times N_y$ elements).
If we assume N_{events} counts total and a Poisson distribution of counts in each pixel, then the average number of count per pixel is $<c> = N_{events} / N_{pixel}$, and the mean distance between two pixels containing a count will be $<\Delta s> = N_{pixel}/N_{events}$. Then the distribution of the values of Δs will be exponential:

$$N(\Delta s) = \exp\left(-\Delta s / \left\langle < \Delta s > \right\rangle\right)$$

For this distribution higher values of Δs become exceedingly rare. Less than 2% of the cases have 4 times the mean value, $<\Delta s>$. Thus we can code the values of Δs in $N_{bits}=Log_2(<\Delta s>\times 4)$ bits in >98% of the cases. The remaining cases are then coded by letting the maximum Δs value, $2^{N_{bits}}-1$, serve as a flag to indicate that the value in this case is describe in a following data word. The number of bits, O_{bits} used in the overflow word is for example $O_{bits}=16$. (Normally, a 2 stage overflow mechanism is implemented such that the normal, shorter overflow word can handle the common cases, while the second stage overflow word has a sufficient number of bits to handle pathological cases, like an image with 1 count in the first pixel and 1 count in the last pixel).

In general the distribution of pixel values may not be strictly Poissonian with the same mean value over the full detector. However, it is very easy to calculate the optimum value of number of bits to be used in the encoding in each case.

As an example, we note that for one unit with the CXB+10 Crab (which is a relatively high count rate, that will normally only be seen by cameras pointing towards the Galactic Center) we have ~850.000 counts in 300 seconds. This corresponds to only ~0.5 counts per pixel, if we have 8 energy bands with equal count rate, or a mean distance between filled pixels of ~2. We can thus code the distance in 4 bits in 98% of the cases. A detailed simulation shows that the bit rate for this encoding is 10.5 kbits/s.

The results of a detailed simulation of the bit rate for one WFM unit is shown in Figure 4-37 for 8 and 16 energy bands. We note that transmitting images in 16 energy bands does not require a significant additional telemetry. This is due to the fact that we are dealing with sparsely filled images. The telemetry required is proportional with the number of counts times the number of bits used to describe the distance between filled pixels. When the number of bands is doubled, the separation between events also doubles and one more bit is required per event.

When the average number of counts per pixel begins to approach ~0.5 there will be a significant number of pixels containing more than 1 count. In this case very many cases of Δs=0 will be found. It then becomes advantageous to code the Δs followed by the number of counts in each pixel, encoded in a few bits. An example of this combined Δs-Δh coding is shown in Figure 4-38; we see that for the baseline configuration, the optimum bit rate can be kept below 13 kbits/s for one unit up to a source flux of 30 Crab.

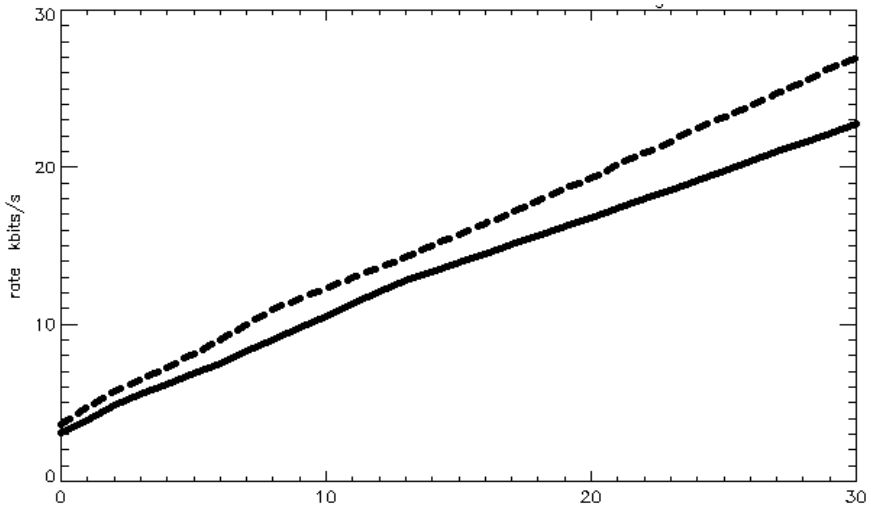

Figure 4-36: Bitrate for Δs encoded images from 1 unit in 8 and 16 (dotted line) energy bands with an integration time of 300 seconds. Source intensity in Crab units

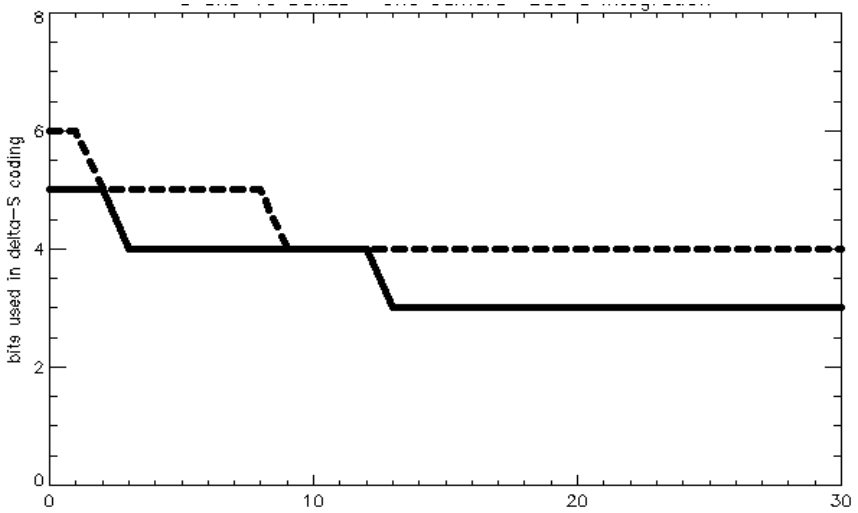

Figure 4-37: Number bits used in encoding Δs as function of count rate

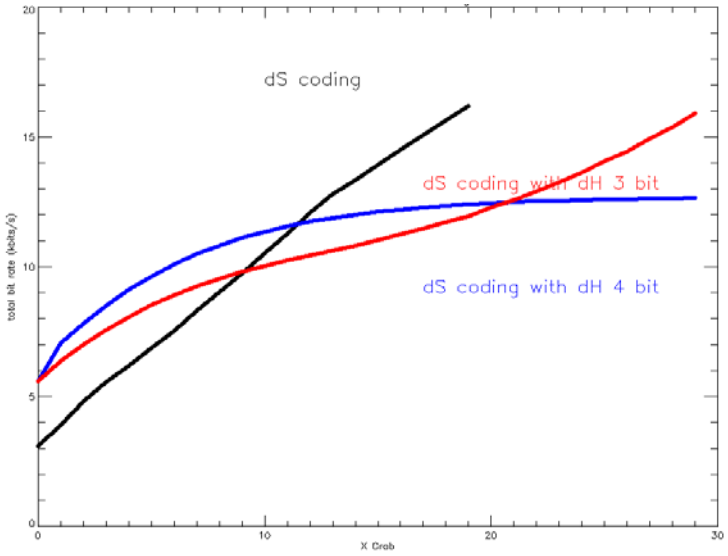

Figure 4-38: Bit rate for one unit as function of source flux for Δs coding (black), Δs coding + coding of pixel content, ΔH in 3 bits (red), and 4 bits (blue). We see that each of the three types of coding have a range of event rates where they are most efficient. Up to 30 Crab we can stay below a data rate of 13 kbits/s per unit

If we consider the extreme case of two units observing a 30 Crab source, while the 3 others observe a few Crab we see that the data rate will be about 40 kbits/s. We then need to consider some overhead for the tm packet headers, bringing the maximum image data rate to ~45 kbits/s, where the normal rate will be ~25 kbits/s.

4.5.6.2.5 Ratemeter data

In addition to the image data collected in normal data taking mode, we collect rate meter data. For each unit the total detector counts are recorded in several energy bands, N_{bands}. The time resolution is ΔT. The formula and table below indicate the required tm rate for rate meter data.

$$R_{ratemeter} = \frac{N_{bands} \times N_{bits} \times 4}{\Delta T / 1\,ms}\ kbits/s$$

If we choose 8 energy bands, we can normally, on average encode the rate meters with 4 bits per bin, we arrive at a required data rate of 9 kbits/s in a normal observing case.

The format includes compression in the sense that the number of bits used is optimized to the current count rate, and spikes and other features are accommodated with an overflow encoding. Therefore the rates given may vary depending on the detailed structure of the data to be transmitted.

Table 4-20: Average rate meter data rate as function of number of energy bands and time resolution. We assume 3 units to see background + 1 Crab of source flux each and 2 units see background + 10 Crab of source flux each.

	2 bands	**4 bands**	**8 bands**	**16 bands**
8 ms	5.4 kbits/s	8.7 kbits/s	16.4 kbits/s	25.1 kbits/s
16 ms	3.3 kbits/s	5.4 kbits/s	8.7 kbits/s	16.4 kbits/s
32 ms	1.8 kbits/s	3.1 kbits/s	5.4 kbits/s	8.7 kbits/s
64 ms	1.0 kbits/s	1.8 kbits/s	3.1 kbits/s	5.4 kbits/s

4.5.6.2.5.1 Spectral data

We assume the full detector energy spectra to be 512 bins (~100 eV resolution up to 30 keV). Very conservatively, if 16 bits are used for each bin and we have spectra for 5 units, the data rate is ≈1 kbits/s for an integration time of 30 s. This can normally easily be compressed by a factor of 2-3.

4.5.6.2.6 Photon-by-photon data – raw mode and trigger mode

The term photon-by-photon" or "event-by-event" data is used for the mode when detailed information about each detected photon is transmitted. The information is: position in X and Y, pulse height, PHA, which may or may not be corrected to an energy measure, E, and time information, T.

We may assume a raw event-by-event data format based of 48 bits per event (X,Y,PHA,T) with (12,6,10,20) bits, where the time resolution is 1 μs and T describes the time within 1 second. This raw format is used for ground testing and troubleshooting only.

For the trigger mode we use a more compressed format (which can be further optimized, if needed) with 40 bits per event (X,Y,E,ΔT) with (12,6,10,12) bits. Instead of providing an absolute time, we only calculate the time from the previous event, and with the expected background rate we can normally describe the ΔT with 12 bits, depending also on the time resolution that we need.
For one unit, and a 25% open mask:

$$Rate_{Back} = 0.25 \times 2200 \times 40\,bits = 26.4\,kbits/s$$
$$Rate_{Crab} = 0.25 \times 910 \times 40\,bits = 10.9\,kbits/s$$

4.5.6.2.7 Electronic calibration data

For verifying the performance of the detector and electronics an electronic calibration mode is foreseen. This will be used with regular interval for short periods of time.

4.5.6.2.8 Real Time Burst Alert Packages

The real time burst alert packages are not part of the regular telemetry as they are part of the LOFT Burst Alert System, which is designed to provide short alerts about new sources to ground based users in near real time. These packages are distributed from the WFM DHU to the OBDH for transmission trough the special VHF channel to a network of VHF ground receivers, which will cover as large as possible part of the LOFT orbit and relay the information.

Table 4-21: breakdown of data to be transmitted via the burst-alert system

Time	R.A.	Declination	Position error	Time scale	Camera information	Energy information	Quality flags
6 bytes	3 bytes	3 bytes	1 byte	1 byte	1 byte	1 byte	2 byte

The table indicates the most basic, bare bones, data that needs to be transmitted to ground concerning an onboard trigger. We see that this information is on the order of 100 bits. In addition some more detailed flags regarding the trigger may also be considered, which

could bring the message content to ~1kbits. It should also be noted that fast transmission is essential and that an initial alert message will then typically be followed by another packet with improved information.

4.5.7 Telemetry budget

The baseline WFM science telemetry consists of 3 types of binned data: detector images, detector rate meters, and detector spectra. The volume of all 3 of these data product can be adjusted by changing the parameters for the integration time, and for the two first types by changing the number of energy bands. The adjustment of these parameters can be applied dynamically based on the count rates and the filling factor of the WFM mass memory and on the information about the predicted LAD telemetry usage. The required binning parameters will also depend on the part of the sky, which is observed with the WFM, as the bright X-ray sources are not evenly distributed in the sky, but concentrated around the Galactic Center and along the Galactic plane. Therefore the WFM will always, on average, be able to stay within the allocated science tm budget. The mass memory will ensure that a temporary deficit can be carried over to the next ground station pass.

4.5.8 Electrical Interfaces

The WFM employs the same power bus and data line interfaces as the LAD.

4.6 Electromagnetic compatibility and electrostatic discharge requirements

4.6.1 Susceptibility requirements

4.6.1.1 Magnetic

The requirement of the SDDs with respect to magnetic fields (e.g., those from magneto-torquers) is that the deviation imposed to the drifting charge is smaller than the pitch of the charge collecting unit (the anode) or the detector position resolution, whatever is smaller. In the WFM, the tightest constraint derives from the position resolution in the anode direction, as high as 25 μm. The magnetic field causing a deviation of the order of 20% is $B_{\perp} < 40$ μT, where $B_{\perp}$ is the component of the external magnetic field orthogonal to the WFM detection plane, as derived by the following computation.

The magnetic field produces a displacement of the electron charge cloud in the SDDs due to the Lorentz force (Hall effect). For an electron in a semiconductor under a drift field [1](Lutz, 1999, p. 30), the angle between the electrostatic and magnetic force is given by $\tan\theta_n = \mu_n^H \cdot B$, where μ_n^H is the Hall mobility in low-doped silicon (1670 cm^2/Vs at room temperature) and B is the magnetic field. Taking into account the maximum displacement of 5 μm over the full length (35 mm), we obtain:

[1] [Lutz, 1999] Gerhard Lutz: ”Semiconductor Radiation Detectors. Device Physics”, Springer Verlag, Berlin, 1999, ISBN 978-3-540-71678-5

$$B < \frac{\tan\theta_n}{\mu_n^H} \approx \frac{\frac{5\mu m}{35mm}}{1670\frac{cm^2}{Vs}} = 855\,\mu T$$

At -30°C the Hall mobility increases by a factor ≈1.6, thus the maximum acceptable magnetic field is 535μT for the WFM. These are the requirements on the magnetic field component orthogonal to the plane defined by the WFM detection plane.

For comparison, the strength of the Earth magnetic field is up to ≈50μT, , while for typical magnetic torque actuators, at a distance of 1 m (the field scales as r-3), the magnetic field is up to 80μT, when the magnetic torquers are active. Thus the disturbance by the Earth magnetic field and the magneto-torquers are negligible.

4.6.1.2 Electrical

The SDD detectors are operated with the negative high voltage (nominally -1300 V) on the surface, to sustain the drift field. The negative high voltage may have some plasma susceptibility to the open space. In the WFM, the field of view is covered by the metal coded mask and thermal screen and the Be window. Based on previous experience from photo-multiplier supply voltages even exceeding 1300 V, plasma effects are not expected to take place in the closed, but ventilated space of the WFM camera.

4.6.1.3 ElectroStatic Discharges

The ASICs and SDDs are sensitive to the damage produced by electrostatic discharges (ESD), thus handling personnel has to be trained accordingly and must use proper grounding equipment (grounded hand-cuffs and conductive, grounded lab table work surfaces, electrically conductive bags, packing material and storage containers etc.) in order to prevent ESD.

4.7 Optical requirements

4.7.1 Straylight requirements

SDD detectors are sensitive to UV, Visible and IR radiation, causing an increase in the leakage current. The required attenuation at these frequencies is that it will not increase the leakage current of the detector by more than 0.5 pA/channel (volume: 145 μm x 35 mm x 450 μm) and therefore it will not impact significantly on the energy resolution and low energy discrimination threshold of the experiment. The light tight design of the detector tray including the Be-window will assure adequate protection against stray light.

4.7.2 Baffling requirements

The baffling against the diffuse X-ray cosmic radiation coming from outside the field of view is provided by the design of the collimator and the detector plane backshield.

4.8 Charged particle rejection requirements

The Silicon drift detectors operating in the WFM are 450 μm thick. The minimum ionizing particles release ~150 keV (MIP), on average. The upper amplitude discrimination

threshold set at 80 keV will therefore reject >95% of the particle-induced events. Taking into account that the WFM experiment background rate is largely dominated by the aperture background (that is, the photons from the CXB entering its wide field of view), there is no need for any additional particle rejection system.

4.9 Transportation, Handling, Cleanliness and Purging Requirements

4.9.1 Transportation requirements

For the transportation we put requirements on the temperature, that has to be kept within the non-operative range (-60° C / +40 ° C TBV), and the humidity, below 30%(TBC).

When transporting the LOFT instrumentation, care has to be taken not to expose it to strong shocks and vibrations and high thermal gradients. In any case, shock recorders have to be mounted on the container case in order to verify the shock history during transportation.

4.9.2 Handling requirements

There are no specific handling requirements, which exceed the usual care to be taken while handling space-borne X-ray detectors within an experimental environment. The ASICs and SDDs are sensitive to the damage produced by electrostatic discharges (ESD), thus handling personnel has to be trained accordingly and must use proper equipment in order to avoid ESD.

4.9.3 Cleanliness requirements

The WFM instrumentation requires a cleanliness level corresponding to a class 100,000 or better.

4.9.4 Purging requirements

The WFM SDDs are marginally hygroscopic, but only when in operation, i.e. when the HV power supply is on. Low humidity (<TBD%) environment should be ensured during ground operation.

4.10 Ground and flight operations requirements

The LOFT-WFM operations requirements are summarized in this section. They will be updated as additional information is provided by the prime (ESA).

4.10.1 Ground and pre-flight operation

Ground and pre-flight operations (RD13, “Calibrations”) will include:

- Software will be developed to ensure easy access to instrument performance interfaces, i.e. via ground test interfaces.
- On-going verification of instrument.
- On-going calibration of the instrument

- Support Integration of the instrument onto the spacecraft
- Support the prime in terms of performance verification (LOFT-WFM + S/C).

4.10.2 Launch and Ascent Phase

Launch and ascent phase activities will include:

- Provide technical support and advice to the prime as required. There is no requirement to power the LAD or WFM during launch or ascent, so no critical items are foreseen.

4.10.3 Instrument Commissioning Phase

Instrument Commissioning Phase activities will include:

- Verify nominal performance following launch
- Perform post-launch calibration of the instrument.
- Evaluate and test performance constraints (offset pointing etc.).
- Verify correlations between WFM camera orientation and ACS system.

4.10.4 Flight operations

Flight operations activities will include:

- Planning of instrument operations and calibration campaigns
- Support of the MOC in the commanding of the instrument.
- Support Science Data Centere in transient detection, identification and TOO alerts.
- Coordinate the creation of the scientific products, their archiving and distribution to the scientific community
- Monitor instrument health and respond to changes.

4.11 Deliverable Models and GSE

At the present time this is very generic. The LOFT WFM development programme is composed of the following models:

- BreadBoard Model (BB) (development)
- Structural Thermal model (STM)
- Engineering Model (EM)
- Qualification Model (QM)
- Flight Model (FM)
- Flight Spares (FS).

4.11.1 Breadboard Model

The LOFT-WFM breadboard model will be used for the early verification/validation of equipment. It will provide sufficient information (proof of concept/model correlation) to enable the progression of the project to the next, more representative model(s): Engineering model (EM) and Structure Thermal Model (STM).

It is planned that where possible the breadboard model will be manufactured from standard-off-the-shelf components. However, in some instances this might not be possible (minimum order quantities and specialist fabrication constraints).

Current planning indicates that the LOFT-WFM breadboard model will include:

- Detector
  - SDD
- Electronics
  - ASIC (proof of concept including performance)
  - BEE
  - DHU
  - PSU
- Software
  - Most critical components (instrument control) including):
    - data compression
    - data time stamping
    - trigger algorithm
- Structure
  - Mask fabrication and suspension.
  - Support structure stability
  - Thermal blanket mounting
  - Fabrication techniques (early validation of concepts)
  - Correlation of models (thermal and stability).

Validation programme: There is no formal test programme associated with the breadboard equipment.
Deliverable status: The LOFT-WFM breadboard is a non-deliverable piece of equipment).

4.11.2 Structural Thermal Model

The LOFT-WFM STM will be used for the verification/validation of structure/thermal related equipment. It is foreseen that this model consist of just one representative LOFT-WFM unit plus mass dummies for the remaining four units in the assembly.

The STM will be manufactured from standard off the shelf components wherever possible (heaters will be used to simulate the thermal dissipation of electronics units).
Validation programme: STM equipment will be subjected to a test programme as defined in Table 4-22.
Deliverable status: The LOFT-WFM STM is a deliverable piece of equipment and will be delivered to the prime contractor (ESA).

4.11.3 Engineering Model

The engineering model will be the first 'all-up' verification of the LOFT-WFM design (all systems – although not a complete WFM assembly). The following elements are foreseen as part of the EM programme:

- 1 x complete camera mechanics including mask, collimator and detector frame.
- 1 x detector tile with ASICs
- 1 x BEE
- 1 x DHU
- 1 x PSU.

Validation programme: EM equipment will be subjected to the test programmes defined in Table 4-22.
Deliverable status: The LOFT-WFM EM is a non-deliverable piece of equipment.

4.11.4 Qualification model

The LOFT-WFM QM will be used for the qualification of the LOFT-WFM design. It is not realistic to manufacture the entire LOFT-WFM assembly and as such only a subset of equipment will be manufactured, i.e. sufficient for model correlation and proof of testing.
Current planning is that the QM will include the following pieces of equipment:

- 1 x WFM assembly support structure with thermal control hardware.

(Note: we have 5 different, unique structures)

- 1 x complete, functional and integrated Camera
- 9 x Camera mass and power/thermal dummies
- 1 x BEE
- 1 x DHU
- 1 x PSU.

Validation programme: QM equipment will be subjected to a qualification level test programme (Table 4-22).
Deliverable status:
The LOFT-WFM QM is a non-deliverable piece of equipment.
Additional consideration: The QM elements may be considered for re-use as a flight spares.

4.11.5 Flight model

The LOFT-WFM FM is the final deliverable instrument.
The FM will include the following pieces of equipment:

- 5 x WFM support structures with thermal control hardware.
- 10 x complete Cameras
- 5 x BEE
- 2 x DHU (1 for cold redundancy)
- 2 x PSU (1 for cold redundancy).

Validation programme: FM equipment will be subjected to acceptance level test programmes (Table 4-22).
Deliverable status: The LOFT-WFM FM is a deliverable piece of equipment and will be delivered to the Prime (ESA).

4.11.6 Flight spare model

It is conceivable that QM equipment could be refurbished and reused as the flight spare. However, if this is not acceptable (Prime/ESA) then a set of spares will be maintained; in addition to the following pre-assembled/calibrated items (i.e. sufficient for the timely replacement of large failed equipment (< 1 month TBC):

- 1 x Camera
- 5 x Support Structures (all different)
- 1 x BEE
- 1 x DHU
- 1 x PSU.

4.11.7 Verification Strategy

The LOFT-WFM verification strategy is summarized in the following table.

Table 4-22: LOFT-WFM Instrument verification strategy; A = Analysis; T = Test; TQ = Test at qualification level; TA = Test at acceptance level

Test	Model				
	STM	EM	QM	FM	FS
Physical properties	**A,T**	**-**	**A,T**	**A,T**	**A,T**
Functional & performance	**-**	**T**	**T**	**T**	**T**
Humidity	(not applicable)				
Leak	(applicable only on sealed / pressurized items)				
Pressure	(applicable only on sealed / pressurized items)				
Acceleration	**-**	**-**	**-**	**A**	**-**
Sinusoidal vibration	**T_Q**	**-**	**T_Q**	**T_A**	**T_A**
Random vibration	**T_Q**	**-**	**T_Q**	**T_A**	**T_A**
Acoustic	(spacecraft level)				
Shock[3]	**-**	**-**	**T**	**-**	**-**
Corona & arcing					
Thermal vacuum	**T**	**-**	**T_Q**	**T_A**	**T_A**
Thermal cycling	**T**	**-**	**T_Q**	**T_A**	**T_A**
EMC/ESD	**-**	**T**	**T**	**T**	**-**
Life	(tested at equipment level only, where required)				

4.11.8 Ground support equipment

Although the LOFT instruments are still in an early stage of development, preliminary tests on representative samples are ongoing. The GSE developed for these prototypes, as well as the experience gathered in previous space programs conducted by several institutes in the Consortium, will be the basis for the design of the WFM GSE. The small number of

instruments and the large modularity simplify the design and development of the GSE. The following Ground Support Equipment (GSE) is foreseen for the LOFT-WFM program:

4.11.8.1 EGSE

- General electronics systems support equipment (power, conditioning, etc.)
- EGSE to command and monitor the operational parameters of the electronics systems
- Local EGSE: Providers of sub-systems will provide subsystem simulators for interface testing at various levels of integration within the WFM (e.g. ASIC to BEE, BEE to DHU).
- Software development system - sufficient for the development of algorithms and scripts (in advance of more representative hardware being made available from the prime)
- Spacecraft simulator (note. it is expected that this - consortium manufactured S/C simulator - will be replaced at a later date by the S/C prime
- Data analysis tools.

4.11.8.2 MGSE

- Detector manufacture tools: sufficient for the assembly/dis-assembly and alignment of individual detectors
- Alignment GSE for all levels of LOFT-WFM alignment, including:
    - Detector tiles in detector planes.
    - Detector planes relative to mask frames
    - Inter-alignment of separate WFM cameras
- Transportation equipment (e.g. dolly's)
- Purge GSE + sufficiently clean gas supply (LOFT-WFM cleanliness)
- Shipping containers.

4.11.8.3 OGSE

- Optical performance (alignment verification) GSE
- Detector calibration GSE.

4.11.8.4 Facilities

The following calibration facilities have been identified for the LOFT-WFM programme.
Panther (Germany), Leicester (UK), Palermo (Italy), INTA (Spain).
Additional work will be performed during the assessment phase in order to identify alternative (additional) facilities.